# Palynology and calcareous nannofossil biostratigraphy of the Turonian – Coniacian boundary: the proposed boundary stratotype at Salzgitter-Salder, Germany and its correlation in NW Europe

Ian Jarvis[1], Martin Pearce[1,2], Tobias Püttmann[3], Silke Voigt[4], Irek Walaszczyk[5]

[1]Department of Geography, Geology and the Environment, Kingston University London, Kingston upon Thames KT1 2EE, UK
[2]Evolution Applied Limited, 33 Gainsborough Drive, Sherborne, Dorset DT9 6DS, UK
[3]Geological Survey of North Rhine-Westphalia, De-Greiff-Str. 195, 47803 Krefeld, Germany
[4]Institute of Geosciences, Goethe University Frankfurt, Altenhöferallee 1, 60438 Frankfurt, Germany
[5]Faculty of Geology, University of Warsaw, Żwirki i Wigury 93, 02-089 Warszawa, Poland

**Abstract**

New palynological and calcareous nannofossil records are presented for the Turonian–Coniacian boundary section at Salzgitter-Salder, Germany, the candidate Coniacian GSSP. The proposed base of the Coniacian Stage is the base of Bed 46, the first appearance datum level of *Cremnoceramus deformis erectus*, which is coincident with a $\delta^{13}C$ minimum at the top of the Navigation carbon isotope event. Palynological assemblages are dominated by organic walled dinoflagellate cysts (dinocysts). Stratigraphic ranges, abundances, species richness, diversity, and assemblage composition data are reported for 137 dinocyst and 119 nannofossil taxa. Dinocyst assemblages are dominated by the peridinioid cyst *Palaeohystrichophora infusorioides* and the gonyaulacoid cysts of *Spiniferites* spp. Dinocyst records, events and zonations are assessed. An uppermost Turonian *P. infusorioides* abundance minimum occurs within the Navigation event, and a marked influx and acme of the taxon with other peridinioid cysts occurs in the lower Coniacian (the *P. infusorioides* Event). The highest occurrence of *Cyclonephelium membraniphorum* is recorded at the base of the Coniacian. Correlation of the *P. infusorioides* Event between Germany, Czech Republic and England is demonstrated. This event represents a productivity pulse,

attributed to water-mass reorganisation accompanying early Coniacian eustatic sea-level rise. The nannofossils *Biscutum constans*, *Kamptnerius magnificus* and *Zeugrhabdotus noeliae*, potential cool water indicators, display maximum relative abundances immediately below and above the stage boundary. An increased abundance of *Marthasterites furcatus* characterises the lowest Coniacian, and a coeval but more extended acme of the species occurs elsewhere. *Helicolithus turonicus* has its highest occurrence in the lower Coniacian *Cremnoceramus walterdorfensis hannovrensis* Zone.

**Keywords**

Turonian - Coniacian boundary; Coniacian GSSP; dinoflagellate cysts; calcareous nannofossils; palynology; carbon isotope stratigraphy

## 1 Introduction

The Salzgitter-Salder Quarry section of northern Germany was first proposed as a potential GSSP (Global Boundary Stratotype Section and Point) for the Coniacian Stage more than 35 years ago by Birkelund et al. (1984) and Wood et al. (1984), and subsequently promoted by the Coniacian Working Group (Kauffman et al., 1996), with the Turonian – Coniacian boundary being defined by the first appearance datum (FAD) of the inoceramid bivalve *Cremnoceramus rotundatus* (*sensu* Tröger *non* Fiege), subsequently referred to *Cremnoceramus deformis erectus* (Meek) (see Walaszczyk and Cobban, 1998, 2000; Walaszczyk and Wood, 1998). However, further study of the inoceramid biostratigraphy suggested the presence of two small hiatuses in the boundary interval (Walaszczyk and Wood, 1998; Wood et al., 2004). These apparently missing intervals were documented in the stratigraphically restricted river-cliff succession at Słupia Nadbrzeżna in central Poland, another Coniacian GSSP candidate section. Consequently, a composite Coniacian basal boundary stratotype, composed of the Salzgitter-Salder and the Słupia Nadbrzeżna sections, was proposed by Walaszczyk and Wood (2008; see also Walaszczyk et al., 2010). This concept, well-received initially at the meeting of the International Commission on Stratigraphy during the Oslo Geological Congress in 2008, was eventually declined, due to changes of requirements for GSSPs.

Subsequently, a number of alternative Turonian – Coniacian boundary sections have been investigated (e.g. Walaszczyk et al., 2012; Ifrim et al., 2014; Cooper et al., 2017), but none of these have proved to be more suitable than Salzgitter-Salder. Importantly, new records from Salzgitter-Salder demonstrate that *C. d. erectus* appears slightly lower than previously documented which, in combination with new high-resolution carbonate carbon-isotope ($\delta^{13}C_{carb}$) data (Voigt et al., 2020), offer a revised correlation to Słupia Nadbrzeżna that removes the need to invoke hiatuses in the Salzgitter-Salder succession. Consequently, Salzgitter-Salder is again being formally proposed as the preferred candidate Coniacian GSSP (Walaszczyk et al. submitted), with three supporting auxiliary sections: (1) Słupia Nadbrzeżna (central Poland); (2) the Střeleč railway cut, adjacent to Střeleč Quarry (Bohemia, Czech Republic); and (3) El Rosario, Sierra del Carmen National Park (Coahuila, Mexico).

In this paper we present results of new palynological and calcareous nannofossil studies of the Turonian – Coniacian boundary interval at Salzgitter-Salder that offer improved resolution of the biostratigraphy of the stage boundary in the candidate GSSP and its potential for regional to global correlation. Results are compared to previous work on Salzgitter sections (Salzgitter-Salder Quarry and the Salzgitter-Beddingen Konrad 101 borehole), and published studies of the Turonian – Coniacian boundary in NW Europe. We define a new organic walled dinoflagellate cyst (dinocyst) biostratigraphic marker event in the lower Coniacian *Cremnoceramus walterdorfensis hannovrensis* Zone: an influx and acme of *Palaeohystrichophora infusorioides* (*P. infusorioides* Event), and more generally a peak in peridinioid / gonyaulacoid (P/G) cyst ratios, following a P/G minimum in the uppermost Turonian *Mytiloides herbichi* Subzone. Stratigraphic changes in dinocyst and calcareous nannofossil assemblages spanning the Turonian – Coniacian boundary are interpreted to reflect significant palaeoenvironmental change in the northern European epicontinental sea, and have potential for stratigraphic correlation on a wider scale.

## 2 Study section

The abandoned limestone quarry of Salzgitter-Salder (52.1244°N 10.3278°E), formerly operated by Fels-Werke Peine Salzgitter GmbH and now owned by the Stiftung Naturlandschaft, is located in the Lower Saxony Basin of northern Germany (Fig. 1), 50 km SE of Hannover. The quarry is situated approximately 2 km south of the city of Salzgitter, on the NE section of Lichtenberg Ridge, 600 m south of Salder village and the A39 motorway. The site is now part of the Harz Braunschweiger Land Ostfalen UNESCO Geopark (https://geopark-hblo.de/en/locations/geopoints/salder-quarry/).

Salzgitter-Salder Quarry is located on the steeply dipping (c. 70° NNE) southern limb of the asymmetrical Lesse Syncline, and exposes approximately 220 m of middle Turonian – lower Coniacian strata (Wood and Ernst, 1998; Wiese et al., 2004a). Regionally, Turonian – early Campanian sedimentation was affected by tectonic inversion and salt migration that generated significant synsedimentary thickness variation, with distinct areas of high

**Fig. 1.** Late Cretaceous palaeogeography of Europe showing the location of the Salzgitter-Salder candidate Coniacian GSSP and other major sections discussed in this paper. White filled symbols are sections with $\delta^{13}C_{org}$ profiles that are used for correlation purposes in this paper. Modified from Blakey (2012).

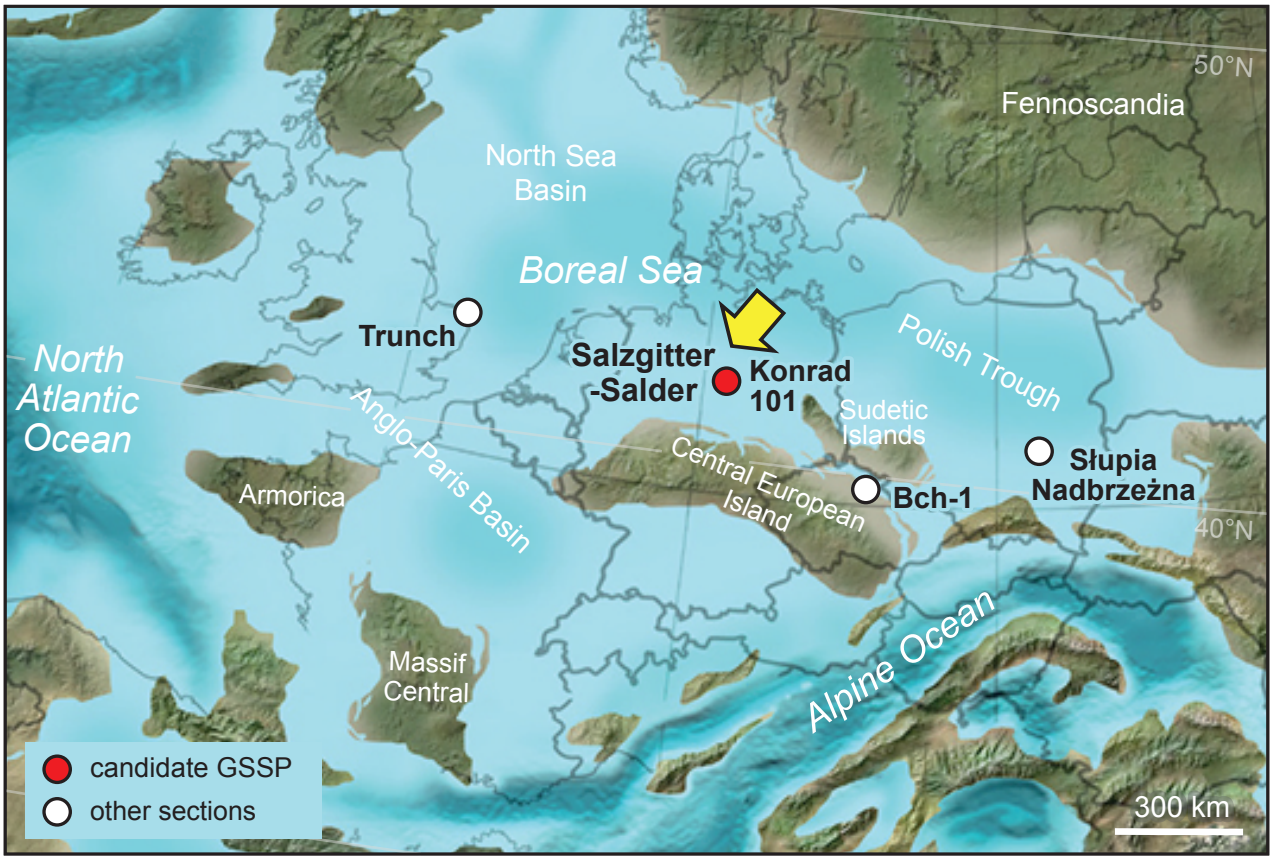
50°N
Fennoscandia
North Sea
Basin
Boreal Sea
Trunch
Salzgitter
-Salder
Konrad
101
Polish Trough
North
Atlantic
Ocean
Anglo-Paris Basin
Sudetic
Islands
Central European
Island
Słupia
Nadbrzeżna
Bch-1
Armorica
40°N
Massif
Central
Alpine Ocean
candidate GSSP
other sections
300 km

subsidence or uplift resulting in locally expanded or condensed successions, respectively (Voigt et al., 2008).

Sedimentation within the Lesse Syncline was influenced by the rising Broistedt salt dome to the north, and the contemporaneously subsiding Hohenassel-Salzgitter marginal trough to the south (Baldschuhn and Kockel, 1998). As a result, Turonian facies pass within a distance of around 6 km from soft calcisphere-rich chalk successions to the north, into expanded sections of marly limestone to the south (Mutterlose et al., 1998). The section at Salzgitter-Salder thus presents an abnormally thick but relatively indurated (a product of its greater burial depth, cf. Voigt and Hilbrecht, 1997) Turonian – Coniacian boundary succession. The average compacted sedimentation rate for the upper Turonian is 8.5 cm $kyr^{-1}$, calculated using GTS2020 ages for the base upper Turonian (base *Inoceramus perplexus* Zone, 91.0 Ma) and base Coniacian (FAD of *C. d. erectus* 89.4 Ma; Gradstein et al., 2020 p. 1038).

The stage boundary interval at Salzgitter-Salder lies within the upper Turonian – lower Coniacian Erwitte Formation (Niebuhr et al., 2007; Wiese et al., 2007) which is characterized by dm-scale regularly bedded marls, marly limestones and limestones, comprised of coccolith lime-mudstones to calcisphere-foraminiferal wackestones. The Erwitte Formation, top of the Upper Plänerkalk Subgroup, is constituted by 2 members at Salzgitter-Salder: Grauweiße Wechselfolge ("grey-white alternation" - interbedded marls and limestones; Ernst et al., 1979); and Upper Limestone (oberer Plänerkalkstein). The Turonian – Coniacian boundary section studied here (Figs. 2, 3) spans the upper half of the Grauweiße Wechselfolge and lower half of the Upper Limestone (Wood et al., 1984; Wood and Ernst, 1998).

The section at Salzgitter-Salder and its constituent fossils have been studied for more than half a century (Bräutigam, 1962; Ernst and Schmid, 1975; Ernst et al., 1979, 1983; Rasemann, 1984; Wood et al., 1984, 2004; Dahmer and Ernst, 1986; Dahmer et al., 1986; Ernst and Wood, 1995; Kauffman et al., 1996; Voigt and Hilbrecht, 1997; Walaszczyk and Wood, 1998; Wiese and Kröger, 1998; Wood and Ernst, 1998; Wiese, 1999; Sikora et al., 2004; Wiese et al., 2004a, b; Lees, 2008; Walaszczyk et al., 2010). Exposure has deteriorated progressively since quarrying ceased in 1992 (Fig. 2), but remains moderately

**Fig. 2.** Field photograph of the Turonian – Coniacian boundary section of the Erwitte Formation exposed in the eastern wall of Salzgitter-Salder Quarry in 1996 (modified from Voigt et al., 2020). The succession consists of interbedded limestones, marly limestones and marls: numerals are the bed numbers of Wood et al. (1984); see Fig. 3 for bed thicknesses. Exposure quality has degraded substantially over the last 25 years, but the boundary interval remains accessible and readily sampled. The yellow dashed line at the base of Bed 46 marks the proposed stage boundary horizon: the first appearance datum (FAD) of the inoceramid bivalve *C. d. erectus* (Voigt et al., 2020). Placement of the 100 kyr cycles follows Voigt et al. (2020), based on cyclostratigraphic analysis of carbon and oxygen stable-isotope data and lithology. The fourth cycle (dashed white line) is derived using lithological criteria only. Filled circles indicate the stratigraphic position of samples collected for palynology. The levels of key dinocyst, nannofossil and planktonic foraminifera events (see text) are indicated.

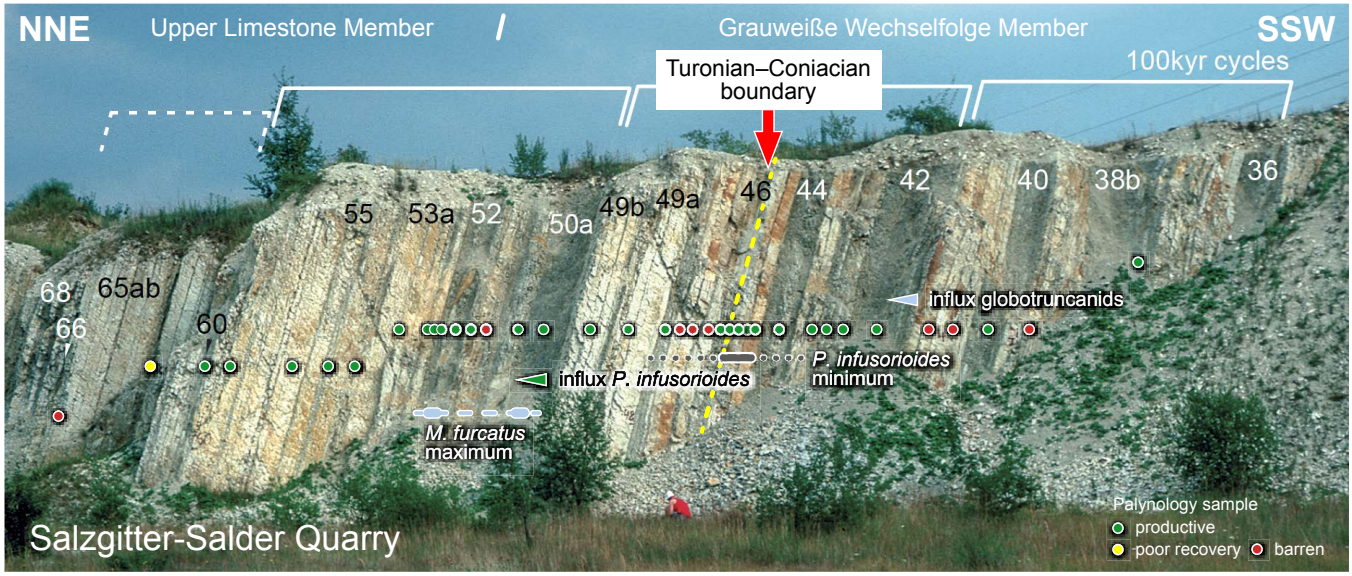
NNE
Upper Limestone Member
Grauweiße Wechselfolge Member
SSW
100kyr cycles
Turonian–Coniacian boundary
68
66
65ab
60
55
53a
52
50a
49b
49a
46
44
42
40
38b
36
influx globotruncanids
influx P. infusorioides
P. infusorioides minimum
M. furcatus maximum
Salzgitter-Salder Quarry
Palynology sample
productive
poor recovery
barren

**Fig. 3.** Stratigraphy, stable-isotope profiles and cyclicity of the Turonian – Coniacian boundary succession at Salzgitter-Salder. Members are subunits of the Erwitte Formation, Upper Plänerkalk Group (Niebuhr et al., 2007). Bed numbers and lithostratigraphic log modified from Wood et al. (1984) and Wood and Ernst (1998), with location of palynology (green, yellow, red 'traffic light' arrow scheme) and calcareous nannofossil samples (pale blue arrows) for this study. Records of stratigraphically significant macrofossil occurrences (compiled from Wood et al., 1984; Kauffman et al., 1996; Walaszczyk and Wood, 1998; Wood and Ernst, 1998; Walaszczyk et al., 2010; Čech and Uličný, 2020; Voigt et al., 2020), with key lowest and highest occurrence datum levels, are inoceramids (black symbols and names), echinoids (brown), and ammonites (purple). *Cww* = *Cremnoceramus walterdorfensis walterdorfensis*, *Cci* = *Cremnoceramus crassus inconstans*. Note multiple beds with *Mytiloides herbichi* in the upper Turonian, and the Turonian – Coniacian boundary defined by the first appearance datum (FAD) of *Cremnoceramus deformis erectus* in Bed 46. Isotope data from Voigt and Hilbrecht (1997) and Voigt et al. (2020). Carbon isotope events (CIEs, green and beige horizontal bars) modified from Jarvis et al. (2006, 2015), Pearce et al. (2020) and Voigt et al. (2020). Named positive $\delta^{13}C_{carb}$ CIEs are green, the negative Navigation Event is cream with options 1 and 2 of Voigt et al. (2020) indicated by the darker vs. lighter colours (see Voigt et al., 2020 and text). Key planktonic foraminifera (dark blue symbols and names; after Peryt in Walaszczyk et al., 2010), nannofossil (medium blue) and dinocyst (green) marker datum levels (Voigt et al., 2020 and this study) are indicated. The entire succession lies within Upper Cretaceous nannofossil zones UC9c / CC13 (see text). 100 kyr progradational cycles derived from spectral analysis of $\delta^{13}C_{carb}$ and $\delta^{18}O_{carb}$ curves and lithology (cycles 1 – 3) or lithology alone (cycle 4; after Voigt et al., 2020). FS = flooding surface.

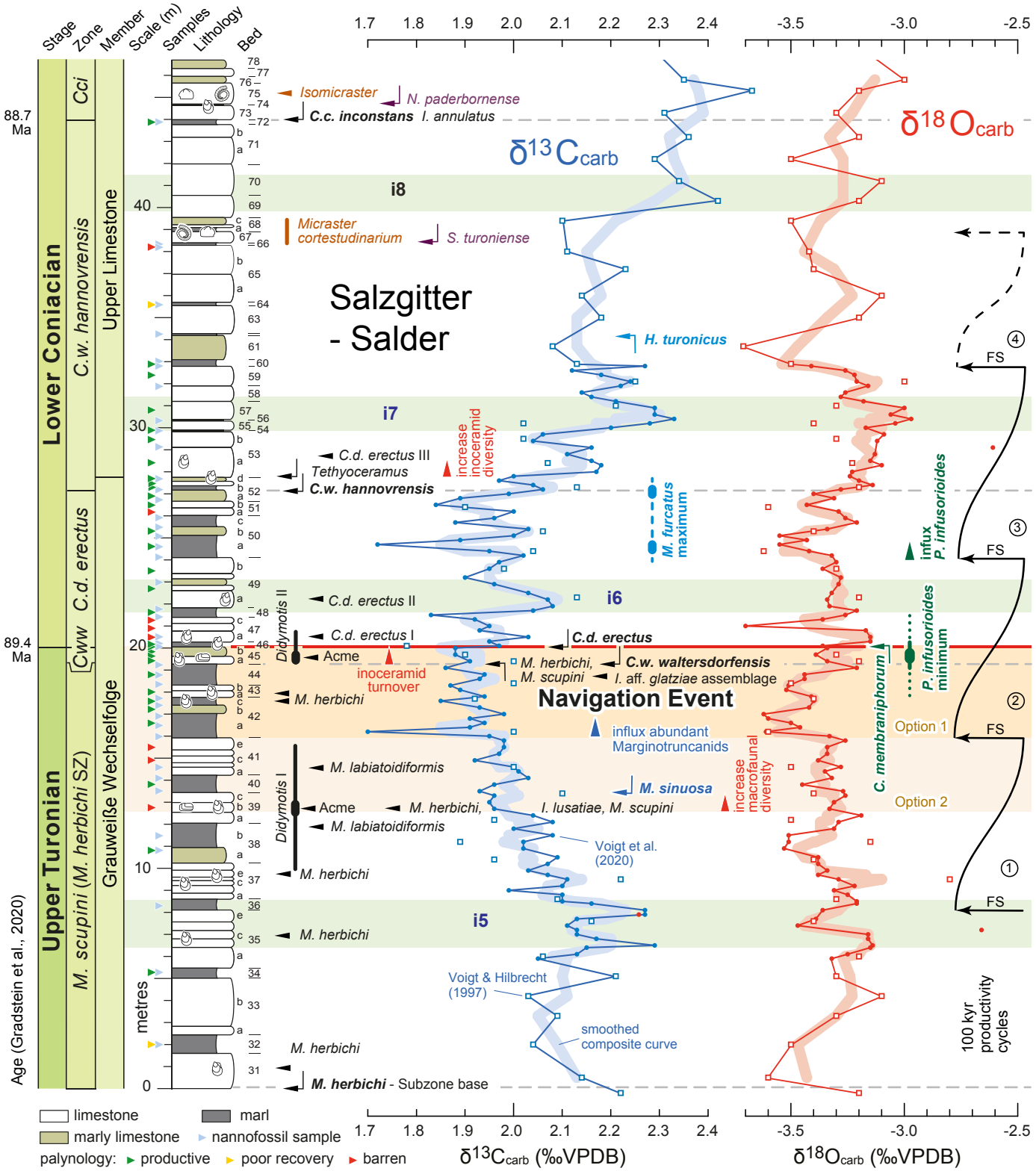
Stage
Zone
Member
Scale (m)
Samples
Lithology
Bed
Lower Coniacian
Upper Turonian
Cci
C.w. hannovrensis
C.d. erectus
Cww
M. scupini (M. herbichi SZ)
Upper Limestone
Grauweiße Wechselfolge
88.7 Ma
89.4 Ma
Age (Gradstein et al., 2020)
metres
Isomicraster
N. paderbornense
C.c. inconstans
I. annulatus
Micraster cortestudinarium
S. turoniense
Salzgitter - Salder
δ13Ccarb
δ18Ocarb
i8
i7
i6
i5
H. turonicus
C.d. erectus III
Tethyoceramus
C.w. hannovrensis
increase inoceramid diversity
M. furcatus maximum
C.d. erectus II
Didymotis II
C.d. erectus I
Acme
C.d. erectus
inoceramid turnover
M. herbichi, M. scupini
C.w. waltersdorfensis
I. aff. glatziae assemblage
Navigation Event
M. herbichi
influx abundant Marginotruncanids
M. labiatoidiformis
Didymotis I
M. sinuosa
increase macrofaunal diversity
I. lusatiae, M. scupini
Voigt et al. (2020)
Voigt & Hilbrecht (1997)
smoothed composite curve
influx P. infusorioides
P. infusorioides minimum
C. membraniphorum
Option 1
Option 2
FS
100 kyr productivity cycles
M. herbichi - Subzone base
limestone
marl
marly limestone
nannofossil sample
palynology: productive poor recovery barren
δ13Ccarb (‰VPDB)
δ18Ocarb (‰VPDB)

good across the boundary interval. The section yields abundant macrofossils (Rasemann, 1984; Wood and Ernst, 1998), notably inoceramid bivalves, common echinoids and brachiopods, and sparse ammonites, principally heteromorphs. Recently, new faunal records were provided by Čech and Uličný (2020), and a high-resolution carbon stable-isotope curve with revised biostratigraphic data for the Turonian – Coniacian boundary interval have been presented by Voigt et al. (2020).

The stratigraphy of the Turonian – Coniacian boundary interval at Salzgitter-Salder is illustrated in the field photograph (Fig. 2), and summarised in Fig. 3, compiled from Wood et al. (1984), Kauffman et al. (1996), Walaszczyk and Wood (1998), Wood and Ernst (1998), Walaszczyk et al. (2010), Čech and Uličný (2020) and Voigt et al. (2020). The lithological log and numbered bed stratigraphy follow Wood et al. (1984) and Wood and Ernst (1998). The section studied here extends from the base of Bed 31 (base *M. herbichi* Subzone, *Mytiloides scupini* Zone) upwards (from 136.5 m height on the log of Wood and Ernst, 1998) to Bed 78 (lower *Cremnoceramus crassus inconstans* Zone). Key macrofossil datum levels (principally inoceramids and *Didymotis* bivalves: black lettering and symbols) including abundance levels, named events, and lowest and highest occurrences are shown in Fig. 3, along with calcareous nannofossil (pale blue), planktonic foraminifera (medium blue) and dinocyst (green) markers.

A new high-resolution (20 – 25 cm, 3 kyr) time-series for carbonate carbon ($\delta^{13}C_{carb}$) and oxygen ($\delta^{18}O_{carb}$) stable isotopes through Turonian – Coniacian boundary interval (Beds 35 – 60) at Salzgitter-Salder was presented by Voigt et al. (2020). This refined the earlier metre-scale sampling of Voigt and Hilbrecht (1997) to better resolve the chemostratigraphy of the stage boundary interval at Salzgitter-Salder (Fig. 3). Of particular importance is the characterisation of the $\delta^{13}C_{carb}$ minimum and inflection point that occurs close to the stage boundary. This negative excursion, which is consistently observed in $\delta^{13}C$ profiles globally, both from carbonate and organic matter (Jenkyns et al., 1994; Jarvis et al., 2006, 2015; Takashima et al., 2010, 2019; Wendler, 2013; Joo and Sageman, 2014), was named the Navigation carbon isotope event (CIE) by Jarvis et al. (2006), who concluded that the base of the Coniacian, as defined by the FAD of *C. d. erectus*, falls at the top of the negative excursions defining the event. This occurs in Bed 46 at Salzgitter-Salder (Fig. 3), as initially

indicated by the low-resolution data of Voigt and Hilbrecht (1997) and now confirmed by the new high-resolution study of Voigt et al. (2020). Bed 46 is a 30-cm-thick unit of soft marl, characterised by abundant *Cremnoceramus waltersdorfensis waltersdorfensis* (Andert) and the first rare *C. deformis erectus*; some sponge fragments occur in the lower part of the bed.

The base of the Navigation CIE is less clearly defined, and two options were proposed by Voigt et al. (2020; Fig. 3). For wider correlation purposes the downwards step in $\delta^{13}C_{carb}$ values at the base of Bed 39b was selected (Voigt et al., 2020 Option 2), coincident with the acme level of the *Didymotis* I Event, an influx of inoceramids and a general increase in faunal diversity (Wood et al., 1984). Voigt et al. (2020) additionally defined three minor positive $\delta^{13}C_{carb}$ excursions in the boundary section, designated as CIEs i5 – i7 (Fig. 3) which were demonstrated to be of regional correlation value. We additionally recognise a higher positive excursion, i8 (Fig. 3), based on the low-resolution $\delta^{13}C_{carb}$ profile of Voigt and Hilbrecht (1997).

Spectral analysis of the high-resolution $\delta^{13}C_{carb}$ and $\delta^{18}O_{carb}$ time series has revealed the presence of three 100 kyr short-eccentricity cycles (Figs. 2, 3). These correspond to asymmetric lithological cycles that start with a dominance of marls, and continue upwards with progressive shift towards thicker limestone-dominated beds. A fourth cycle can be recognized based on lithological criteria alone. These cycles were interpreted by Voigt et al. (2020) to reflect increasing carbonate productivity and shallowing-upwards.

## 3 Methods

Field sampling was undertaken by reference to the lithological logs and numbered bed stratigraphy of Wood et al. (1984) and Wood and Ernst (1998). Samples were collected from the 42-m succession through the upper Turonian – lower Coniacian boundary section (Figs. 2, 3), from Bed 32 close to the base of the *M. herbichi* Subzone (*M. scupini* Zone) to Bed 72 at the top of the *C. w. hannovrensis* Zone. Sample spacing for palynology (43 samples) varied from >1 m in the bottom 15 m and top 10 m of the section, to 20 – 40 cm across the stage boundary (Fig. 3). A separate suite of 41 samples, with similarly varying

sampling resolution, was taken from the marl-rich beds for analysis of the calcareous nannofossils through the same interval.

### *3.1 Palynology*

For palynology, approximately 200 g of fresh grey rock was collected in the field following the removal of any yellow-coloured surficial layers, judged to represent superficial weathering (oxidation). Samples were crushed to medium gravel size, rinsed with tap water, air dried, and picked to remove any remaining discoloured material. Weighed (40 g) samples were processed by Palynological Laboratory Services (PLS, Anglesey, UK). Samples were treated with HCl and HF to remove the carbonate and silicate matrix, and the organic residue was concentrated with a 15 µm sieve mesh using the method of Lignum (2009), modified from Lignum et al. (2008), 'Company B' methodology. Samples were spiked with *Lycopodium clavatum* spore tablets (Department of Geology, Lund University) to enable the determination of palynomorph absolute abundances. Oxidation was not required.

Palynology slides were analysed with a Leica DM1000 LED microscope with x63 and x100 oil-immersion objectives. A full count was reached when 200 identified dinocysts (excluding spores and pollen, acritarchs and unidentified specimens) were recorded. A dinocyst specimen was recorded if over 50% of an individual was observed. Operculae and loisthocyst (cysts with no attached operculum; Sarjeant et al., 1987) fragments were recorded but only used to indicate the presence of a species if the loisthocyst was not included in the count (see Pearce et al., 2020). Subsequently, whole slides were visually scanned for the presence of additional taxa. These were recorded as present (crosses on range chart Fig. 4) but were not included in the numerical count data. Absolute palynomorph abundances were determined using a *Lycopodium* spike method (Pearce et al., 2003). A species list and full taxonomic citations are provided in Appendix A. Full palynological counts are documented in Supplementary data Table 1.

### *3.2 Calcareous nannofossils*

Marl-rich samples collected for nannofossil analysis were processed following the standard method of Perch-Nielsen (1985). Smear slides were analysed with an Olympus BH-2 light-

microscope (magnification of 1250x) by screening at least three traverses with medium particle density. Taxonomy and biostratigraphy follow Burnett et al. (1998), with modifications from Lees (2008) and the Nannotax3 database (Young et al., 2020). Sample material and smear slides are stored in the collection of the Geological Survey of North-Rhine Westphalia (GD NRW), Germany.

The preservation of nannofossils is classified into three categories, simplified from Roth (1978): *Poor preservation* (P): assemblages of mostly robust taxa, that are fragmented or affected by secondary calcite overgrowth. *Moderate preservation* (M): nannofossil assemblages are dominated by robust taxa, delicate coccoliths are commonly affected by fragmentation or re-crystallization. *Good preservation* (G): nannofossil assemblages are diverse, the coccoliths are rarely affected by fragmentation or overgrowth with fragile structures commonly preserved. Due to the generally low abundance of coccoliths in the studied material, the abundance of a species recorded in each sample is classified as follows: Very rare (VR): only 1–2 specimens present; rare (R): 3–5 specimens present; common (C): 5–19 specimens present; abundant (A): >20 specimens per sample. A species list and full taxonomic citations are provided in Appendix B. All nannofossil records are documented in Supplementary data Table 2.

## 4 Palynology results and discussion

Palynomorph preservation through the Turonian – Coniacian boundary interval at Salzgitter-Salder is generally poor, occasionally moderate. A range chart showing the relative abundance of representative dinocyst taxa is presented in Fig. 4, and selected stratigraphically important and distinctive species are illustrated in Fig. 5. A full count was obtained for 33 samples, 2 showed poor recovery (Beds 32 and 64), and 8 were technically barren (all were limestones exhibiting signs of weathering; Fig. 4). Assemblages are overwhelmingly dominated by dinocysts with respect to species richness, and both relative and absolute abundance; these are associated with common algal remains and rare acritarchs (Supplementary data Table 1). Terrestrial palynomorphs are very rare to absent.

**Fig. 4.** Dinocyst range chart showing the relative abundance of representative taxa from the Turonian – Coniacian boundary interval at Salzgitter-Salder. Dark green bars and gradient shaded vertical columns are gonyaulacoid dinocysts, red ornaments represent peridinioid cysts, grey ornaments are cysts of uncertain taxonomic affinity. Relative abundances of accessory taxa are multiplied x3, as indicated, to better visualize stratigraphic trends. Horizontal coloured bars are carbon isotope events (see Fig. 3 and text for detail). Small black crosses indicate a species presence where this fell outside the quantitative count. Note the dominance of *P. infusorioides* and *Spiniferites* species and the inverse correlation of the former taxon with *S. ambigua*. The highest record of *C. membraniphorum* is from the base of Bed 46, the base of the Coniacian, consistent with the highest persistent occurrence of the species elsewhere in NW Europe (Pearce et al., 2020). Samples yielding an anomalously high absolute abundance of dinocysts (>3000 dpg), Beds 45b and 52d, are highlighted by stars. The interval with a low relative abundance of *P. infusorioides* at the Turonian – Coniacian boundary and the level of influx in the lower Coniacian are highlighted.

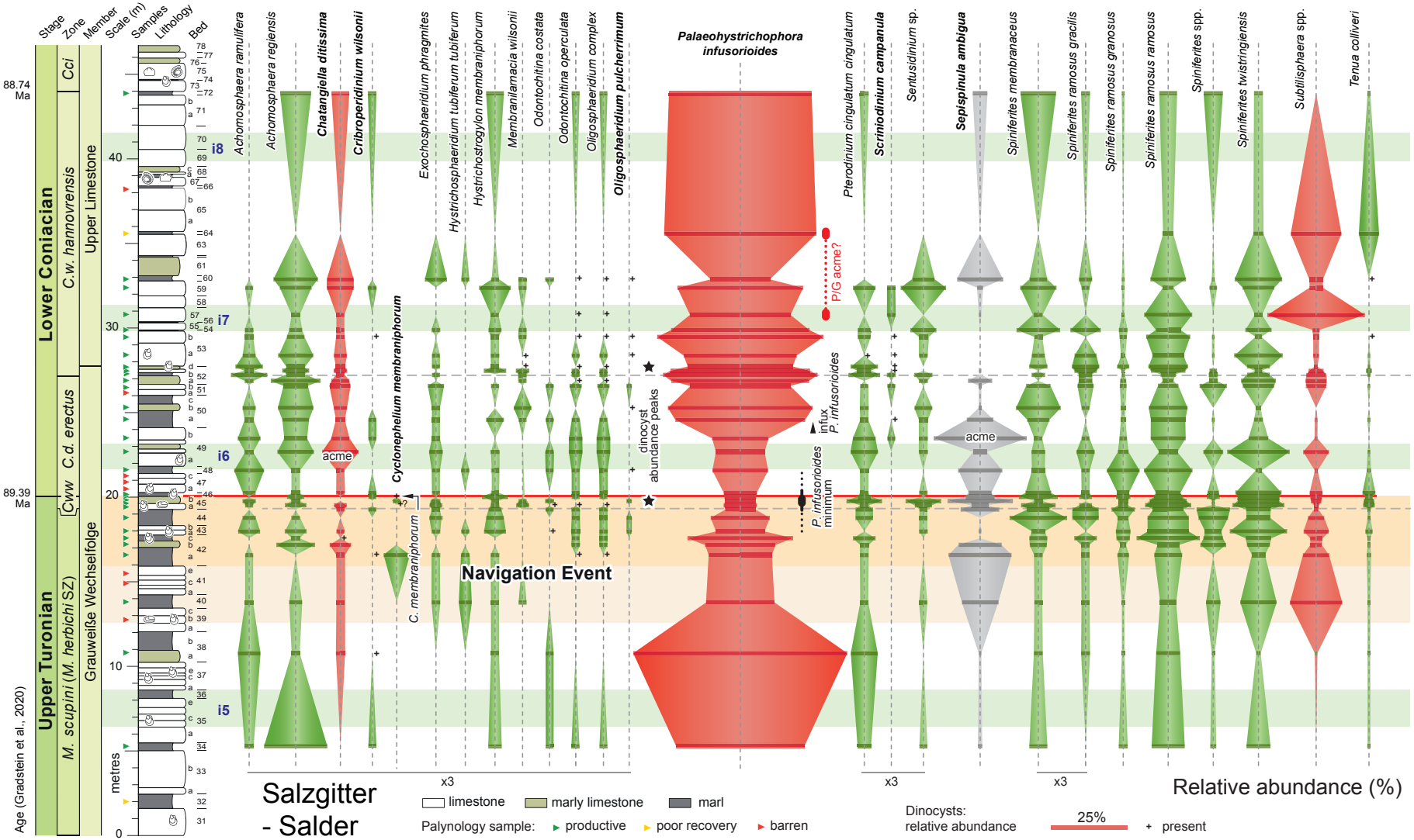
Stage
Zone
Member
Scale (m)
Samples
Lithology
Bed
Lower Coniacian
Upper Turonian
C.w. hannovrensis
C.d. erectus
M. scupini (M. herbichi SZ)
Cci
Cww
Upper Limestone
Grauweiße Wechselfolge
88.74 Ma
89.39 Ma
Age (Gradstein et al., 2020)
metres
i8
i7
i6
i5
Achomosphaera ramulifera
Achomosphaera regiensis
Chatangiella ditissima
Cribroperidinium wilsonii
Cyclonephelium membraniphorum
C. membraniphorum
Exochosphaeridium phragmites
Hystrichosphaeridium tubiferum tubiferum
Hystrichostrogylon membraniphorum
Membranilamacia wilsonii
Odontochitina costata
Odontochitina operculata
Oligosphaeridium complex
Oligosphaeridium pulcherrimum
Palaeohystrichophora infusorioides
dinocyst abundance peaks
P/G acme?
P. infusorioides influx
P. infusorioides minimum
Pterodimium cingulatum cingulatum
Scriniodinium campanula
Sentusidinium sp.
Sepispinula ambigua
Spiniferites membranaceus
Spiniferites ramosus gracilis
Spiniferites ramosus granosus
Spiniferites ramosus ramosus
Spiniferites spp.
Spiniferites twistringiensis
Subtilisphaera spp.
Tenua colliveri
acme
Navigation Event
x3
Salzgitter - Salder
limestone
marly limestone
marl
Palynology sample:
productive
poor recovery
barren
Dinocysts: relative abundance
25%
present
Relative abundance (%)

A total of 137 dinocyst, 6 acritarch, 6 prasinophyte, 11 spore and 8 pollen taxa were identified (Appendix A; Supplementary data Table 1), together with fungal hyphae and spores, a colonial marine alga (*Palambages morulosa*), chlorophyte (*Pediastrum*) and zygnemataceous zygospore (*Ovoidites*), microforaminiferal test linings, and undifferentiated zooclasts. In addition, a conspicuous *incertae sedis*, typically recorded from relatively low-latitude Upper Cretaceous successions, including Mauritania (offshore), Pakistan, Peru and Saudi Arabia (P. Dodsworth, pers. comm., 2020), and Brazil (M. Pearce, pers. obs.) is recorded at Saltzgitter-Salder. Despite its rarity, the first published photograph of a specimen (to our knowledge) is provided here (Fig. 5E).

Palynomorph assemblages from the Turonian – Coniacian boundary interval at Salzgitter-Salder are characterised predominantly by long-ranging dinocyst taxa (Fig. 4), but sporadic records of stratigraphically significant species occur. These are discussed in Section 4.3.2. Despite a high species richness, the range chart (Fig. 4) illustrates the overwhelming dominance of *Palaeohystrichophora infusorioides* (Fig. 5F) through most of the succession, together with high numbers of *Sepispinula ambigua* (Fig. 5J; we follow Pearce et al., 2020 in considering this species a senior synonym of the type species of *Sepispinula* and therefore, a confident taxonomic combination), *Spiniferites* taxa (e.g. Fig. 5L), and *Subtilisphaera* spp (Fig. 5M). The absolute abundances of these dominant taxa are illustrated in Fig. 6, and more general assemblage parameters are plotted in Fig. 7.

## *4.1 Palynological abundance*

The average absolute abundance of palynomorphs in the Salzgitter-Salder Turonian – Coniacian boundary succession is ~1400 palynomorphs per gram (ppg), but with considerable sample-to-sample variation (standard deviation 950 ppg) and no clear systematic stratigraphic trend (Fig. 7). Palynomorph abundance peaks, dominated by dinocysts, are observed in top Turonian Bed 45b where the assemblage is characterised by *S. ambigua* and *Spiniferites* spp., and at the top of the Grauweiße Wechselfolge in Bed 52d with a flood abundance of *P. infusorioides* and *Spiniferites ramosus ramosus* (Figs. 5L, 6).

**Fig. 5.** Stratigraphically important and distinctive species from the Turonian – Coniacian boundary interval, Salzgitter-Salder. **A**. *Canningia glomerata* Fensome et al., 2019b, Bed 52c. **B**. *Chatangiella ditissima* (McIntyre, 1975) Lentin and Williams, 1976, Bed 52c. **C**. *Chatangiella islae* Pearce et al., 2019, Bed 60 (middle). **D**. *Cyclonephelium membraniphorum* Cookson and Eisenack 1962, Bed 52c. **E.** *Incertae sedis*, Bed 52c. **F**. *Palaeohystrichophora infusorioides* Deflandre, 1935, Bed 38a. **G**. *Psaligonyaulax deflandrei* Sarjeant, 1966, Bed 52c. **H**. *Raetiaedinium truncigerum* (Deflandre, 1937) Kirsch, 1991, Bed 53a. **I**. *Scriniodinium campanula* Gocht, 1959, Bed 52c. **J**. (gracile) *Sepispinula ambigua* (Deflandre, 1937) Masure in Fauconnier and Masure, 2004, Bed 49b. **K**. *Spiniferites porosus* (Manum and Cookson, 1964) Harland, 1973, Bed 50a. **L**. *Spiniferites ramosus* subsp. *ramosus* (Ehrenberg, 1837) Mantell, 1854. Bed 52c. **M**. *Subtilisphaera* spp., Bed 59 (middle). **N**. *Surculosphaeridium longifurcatum* (Firtion, 1952) Davey et al., 1966, Bed 40 (middle). **O**. *Trichodinium castanea* Deflandre, 1935 ex Clarke and Verdier, 1967, Bed 52c. Scale bars are 20 µm.

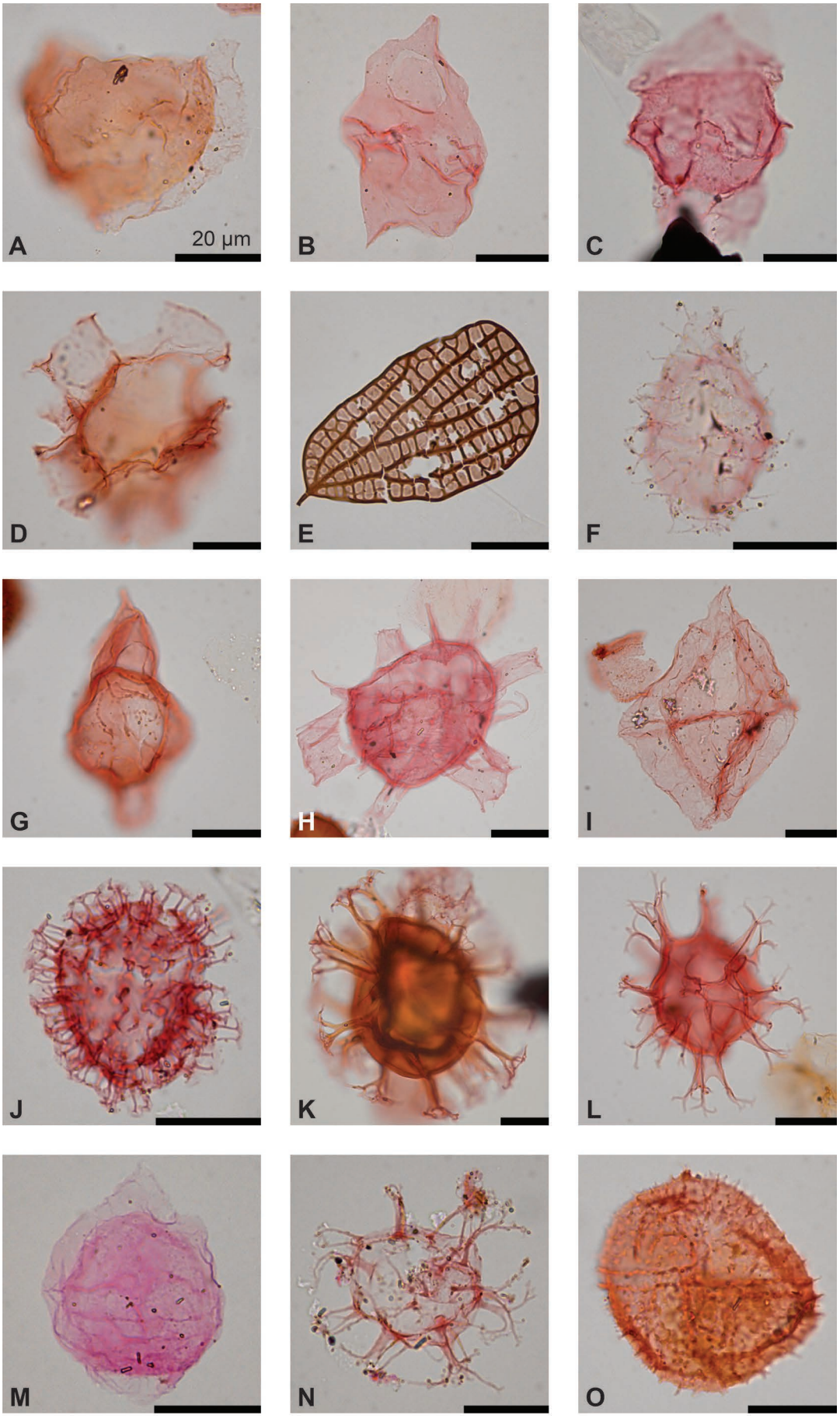
A
20 µm
B
C
D
E
F
G
H
I
J
K
L
M
N
O

**Fig. 6.** Absolute abundance plot for dominant dinocyst taxa from the Turonian – Coniacian boundary interval at Salzgitter-Salder. Dark green bars and gradient shaded vertical columns are gonyaulacoid dinocysts, red ornaments represent peridinioid cysts, grey ornaments are cysts of uncertain taxonomic affinity. Selected key palynological datum levels are indicated. Dpg = dinocysts per gram.

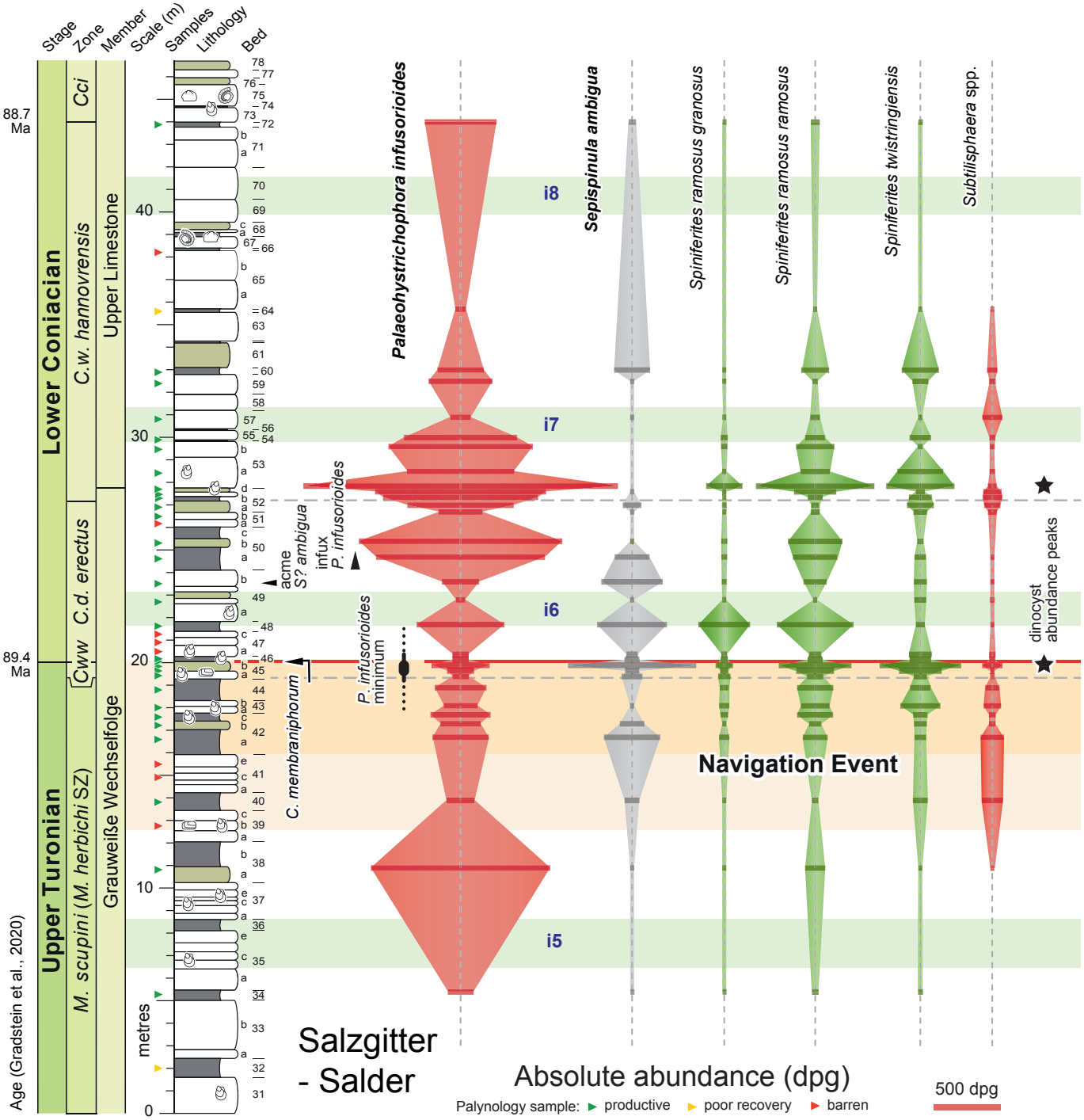
Stage
Zone
Member
Scale (m)
Samples
Lithology
Bed
88.7 Ma
89.4 Ma
Lower Coniacian
Upper Turonian
Cci
C.w. hannovrensis
C.d. erectus
Cww
M. scupini (M. herbichi SZ)
Upper Limestone
Grauweiße Wechselfolge
Age (Gradstein et al., 2020)
metres
0
10
20
30
40
Palaeohystrichophora infusorioides
Sepispinula ambigua
Spiniferites ramosus granosus
Spiniferites ramosus ramosus
Spiniferites twistringiensis
Subtilisphaera spp.
i8
i7
i6
i5
acme S? ambigua
influx P. infusorioides
P. infusorioides minimum
C. membraniphorum
dinocyst abundance peaks
Navigation Event
Salzgitter - Salder
Absolute abundance (dpg)
Palynology sample: productive poor recovery barren
500 dpg

**Fig. 7.** Palynomorph abundance and dinocyst assemblage parameter plots for the Turonian – Coniacian boundary interval at Salzgitter-Salder. P/G ratio = species number of peridinioid / gonyaulacoid cysts; C-H / S-P ratio = *Circulodinium* - *Heterosphaeridium / Spiniferites* - *Palaeohystrichophora* ratio. Red and yellow curves highlight coherent trends in P/G ratio and Shannon diversity, respectively, across the Turonian – Coniacian boundary. Fisher's α diversity correlates well with species richness; Shannon diversity correlates inversely to the P/G ratio. The boundary interval is characterised by *P. infusorioides* and P/G ratio minima, a dinocyst abundance peak, followed by coincident C-H / S-P ratio and Shannon diversity maxima along with the HO of *C. membraniphorum*. Selected key palynological datum levels are indicated.

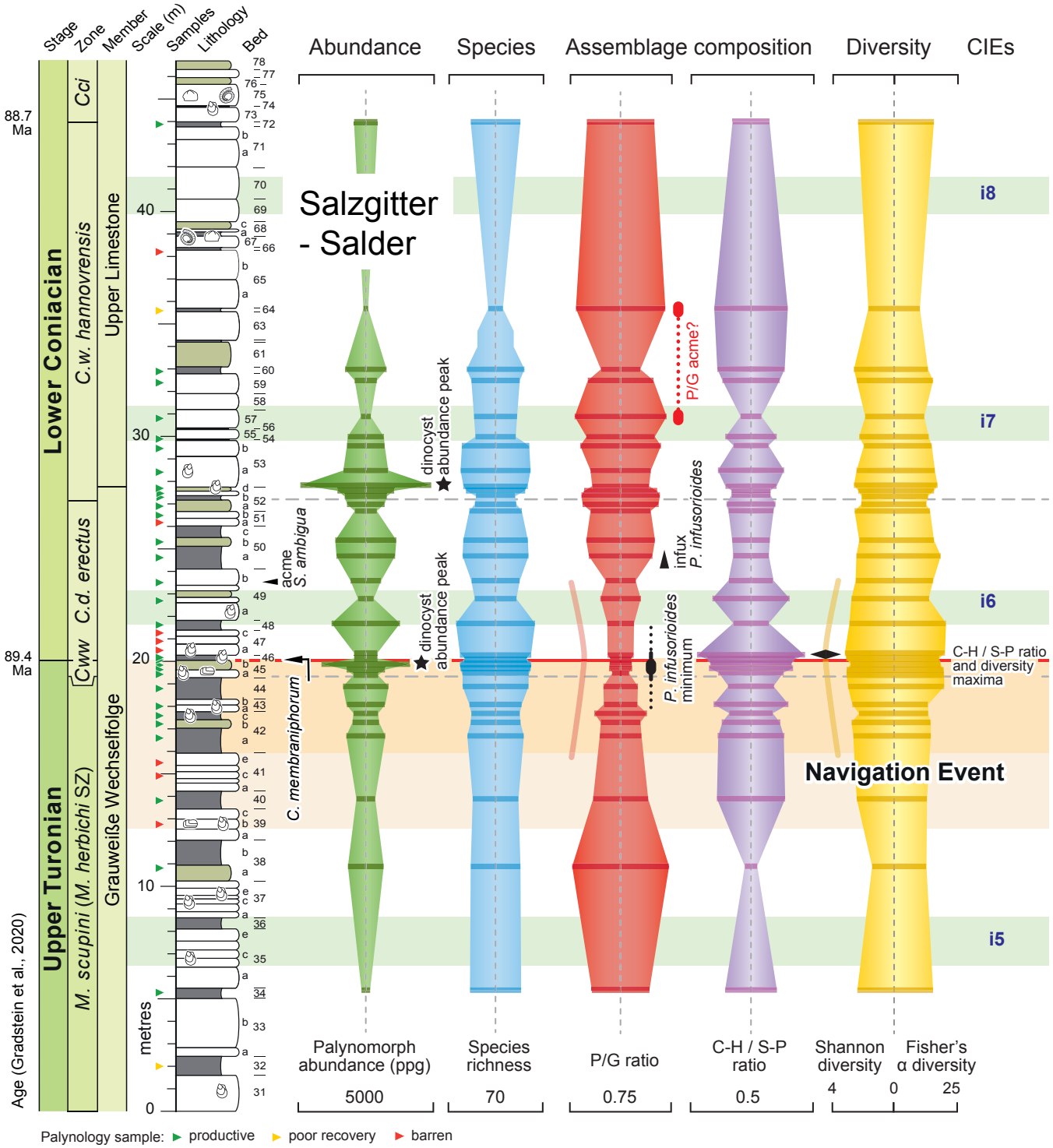
Stage
Zone
Member
Scale (m)
Samples
Lithology
Bed
Abundance
Species
Assemblage composition
Diversity
CIEs
88.7 Ma
89.4 Ma
Lower Coniacian
Upper Turonian
Cci
C.w. hannovrensis
Cww
C.d. erectus
M. scupini (M. herbichi SZ)
Upper Limestone
Grauweiße Wechselfolge
Salzgitter - Salder
i8
i7
i6
i5
dinocyst abundance peak
dinocyst abundance peak
P/G acme?
acme S. ambigua
influx P. infusorioides
P. infusorioides minimum
C. membraniphorum
C-H / S-P ratio and diversity maxima
Navigation Event
Age (Gradstein et al., 2020)
metres
Palynomorph abundance (ppg)
Species richness
P/G ratio
C-H / S-P ratio
Shannon diversity
Fisher's α diversity
5000
70
0.75
0.5
4
0
25
Palynology sample: productive poor recovery barren

### *4.2 Dinocyst species richness and diversity*

Dinocyst species richness in productive samples from Salzgitter-Salder varies from 29 to 59 taxa with an average of 42 taxa, with a cyclic pattern but no systematic trend (Fig. 7). Maximum species richness is observed in lower Coniacian Bed 48. Fisher's α diversity (Fisher et al., 1943) closely follows dinocyst species richness ($R^2$ = 0.617), while the Shannon index (Shannon, 1948) displays a more damped long-term trend (Fig. 7). Both diversity indexes exhibit broad peaks spanning stage boundary Beds 44 – 48, with a Shannon diversity (*H*) maximum of 3.22 (Fisher's α = 17.5) in Bed 46 at the base of the Coniacian. The Shannon index correlates inversely with the peridinioid/gonyaulacoid (P/G) ratio ($R^2$ = 0.882; Fig. 7), with *P. infusorioides* dominating the P-cyst component. A maximum in the *Circulodinium* - *Heterosphaeridium / Spiniferites* - *Palaeohystrichophora* (C-H/S-P) assemblage ratio (cf. Pearce et al., 2003, 2009; Prince et al., 2008) coincides with the Shannon diversity maximum.

Terrestrial assemblages are poorly represented, typically < 3% of the total assemblage, with a species richness in productive samples of only 1 to 6 taxa (Supplementary data Table 1), and no clear stratigraphic trends.

### *4.3 Dinocyst biostratigraphy of the Turonian – Coniacian boundary - Salzgitter-Salder Quarry and the Konrad 101 core*

Palynomorph assemblages through the Turonian – Coniacian boundary interval at Salzgitter-Salder are dominated by long-ranging Cretaceous dinocyst taxa, but of particular note is the highest occurrence (HO) of *Cyclonephelium membraniphorum*, a significant biostratigraphic marker (Pearce et al., 2020), at the base of Bed 46, coincident with the base of the Coniacian (Fig. 4). Records of other potentially significant species in the Salzgitter-Salder boundary section are considered below, and are compared to results from a previous low-resolution palynological study of the boundary section in the quarry (Sikora et al., 2004) and those from the nearby Konrad 101 borehole at Salzgitter-Beddingen (Prössl, 1990).

Sikora et al. (2004) analysed a small (undisclosed) number of samples from Beds 35 – 63 in Salzgitter-Salder Quarry. A "low-diversity" organic-walled dinoflagellate cyst (dinocyst)

assemblage strongly dominated by *P. infusorioides* was noted. A correlation diagram to Wagon Mound New Mexico indicated the positions of 5 dinocyst datum levels at Salzgitter-Salder (Sikora et al., 2004 fig. 19), but no range chart was provided and no specimens were described or figured. The significance of Sikora et al.'s (2004) datum levels is critically assessed below (Section 4.6).

### 4.3.1 Salzgitter-Beddingen Konrad 101 borehole

The Konrad 101 borehole was drilled in 1985 at the former Konrad iron mine in Salzgitter-Beddingen (52.1702°N 10.4185°E), 8 km NE of Salzgitter-Salder Quarry (Prössl, 1990; Niebuhr et al., 2001). The 1001.75 m deep borehole cored a 615 m thick Cretaceous section, and terminated in the uppermost Middle Jurassic (middle Bajocian; Gerardi, 1986); the top of the core sampled a Turonian – Coniacian boundary section. Palynological analysis of the Cretaceous section of the Konrad 101 cored borehole at an average spacing of 5 m by Prössl (1990; 131 samples) provides some of the most comprehensive information on dinocyst ranges for the Hauterivian – lower Coniacian of northern Germany available to date, and this has become a widely cited source (e.g. Nøhr-Hansen, 1996; Torricelli, 2000; Prauss, 2001; Williams et al., 2004; Prince et al., 2008; Svobodová et al., 2011; Masure et al., 2013; Olde et al., 2015a; Dodsworth and Eldrett, 2019; Estebenet et al., 2019; Tahoun and Ied, 2019; Ibrahim et al., 2020; Pearce et al., 2020).

The stratigraphic framework for the Prössl (1990) study of Konrad 101 was based on assigning ages to geophysical markers in downhole logs with little independent biostratigraphic calibration. Detailed study of macrofossils and lithofacies in the Upper Cretaceous section of the Konrad 101 core has shown subsequently that the original stratigraphic framework required substantial revision (Niebuhr et al., 2001). Of particular significance to the present work, Prössl (1990) assigned the limestones at the top of the core (11 – 61 m) to the "upper Turonian", with the base "middle Turonian" at 133 m and the base "lower Turonian" at 164 m. New records of *Cremnoceramus deformis* group inoceramids in the core (Niebuhr et al., 2001) demonstrate that the upper section (11 – ~29.5 m) is Coniacian, and further inoceramid records and associated lithostratigraphy (Fig. 8) place the substage bases at: upper Turonian, 116 m; middle Turonian, 140 m; with the Cenomanian – Turonian boundary at 162.4 m.

The revised stratigraphy of the Konrad 101 borehole (Fig. 8) significantly impacts the stratigraphic ranges reported for dinocyst taxa by Prössl (1990), particularly in relation to the Turonian – Coniacian boundary events discussed here. Comparison of thicknesses for upper Turonian – Coniacian stratigraphic units in the Salzgitter-Salder (Wood and Ernst, 1998) and Konrad 101 (Niebuhr et al., 2001) sections yields 43 m vs. 19 m for the Grauweiße Wechselfolge Member, and 61 m vs. 32 m for the *M. scupini* Zone, respectively, indicating that Salzgitter-Salder section is approximately twice the thickness of that in the borehole. Prössl (1990) analysed 6 samples between 14.89 – 42.24 m depth, spanning the Turonian – Coniacian boundary interval: 4 samples from the Grauweiße Wechselfolge and 2 from the Upper Limestone (Fig. 8). These provide a comparison to records from our high-resolution study at Salzgitter-Salder, although the two lowest Grauweiße Wechselfolge and highest Upper Limestone samples from the Konrad 101 core fall outside the stratigraphic interval sampled in this study (Figs. 8, 9).

Palynological records from the Konrad 101 borehole provide important information on the ranges of taxa in the Cretaceous of Lower Saxony (Prössl, 1990). However, most samples from the top Cenomanian – uppermost middle Turonian (166.4 – 125.5 m) in the core were barren. One low-recovery sample was obtained at the top of the lower Turonian (140.43 m), 1.4 m below the Weiße Grenzbank (Niebuhr et al., 2001), and a second originated from the summit of the middle Turonian (Fig. 8, 118.8 m). The barren interval corresponds to Rotpläner facies (Söhlde Formation), brownish to red flaser-bedded limestones and thin red marls, with poor preservation of organic matter (Niebuhr et al., 2007; Wiese, 2009b). Palynologically productive samples from the Söhlde Formation originated solely from subordinate intervals of white bedded limestone. It is noted also that the lower two-thirds of the upper Turonian in Konrad 101, which yielded a lower species richness and relative abundance of dinocysts (Figs. 8, 9), includes beds redeposited by sediment gravity flow processes (allochthonite facies of Niebuhr et al., 2001). The highest allochthonite occurs immediately above the $T_F$ marl, at the base of the *M. scupini* Zone (Fig. 8; Niebuhr et al., 2001).

**Fig. 8.** Stratigraphy of the middle Turonian – Coniacian interval in the Konrad 101 borehole, Salzgitter-Beddingen, dinocyst species richness and P/G ratio. Stratigraphy follows Niebuhr et al. (2001), with palynological data and dinocyst zonation from Prössl (1990). Significant dinocyst events are indicated. Note that grey coloured events with open symbols are estimated positions derived from correlation to Salzgitter-Salder (Fig. 4); they were not resolved by the low-resolution sampling of Konrad 101. Grey text and projected positions of carbon stable-isotope events are similarly based on litho- and biostratigraphic correlation to Salzgitter-Salder (cf. Voigt and Hilbrecht, 1997; Voigt et al., 2020; this study). MTu = middle Turonian; LCo = lower Coniacian; *M. striat. – M. labiat.* = *M. striatoconcentricus – M. labiatoidiformis*; *Cremnoc.* = *Cremnoceramus*; Wech. = Wechselfolge. [1] Dinocyst zones and subzones after Olde et al. (2015a); [2] Dinocyst zonation after Prössl (1990). The estimated stratigraphic extent of the Salzgitter-Salder study section (outlined by light blue square) is shown for comparison.

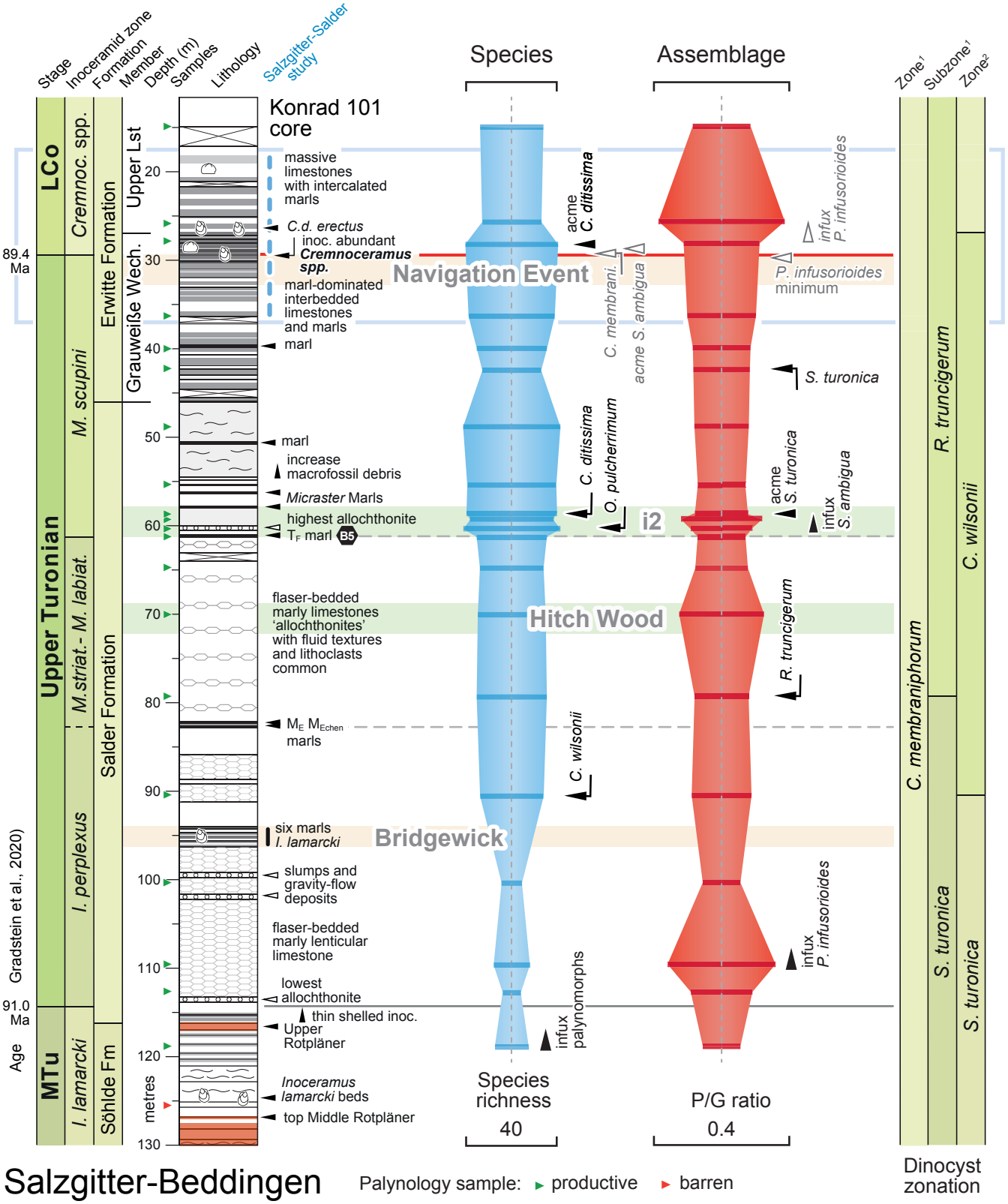
Stage
Inoceramid zone
Formation
Member
Depth (m)
Samples
Lithology
Salzgitter-Salder study
Species
Assemblage
Zone¹
Subzone¹
Zone²
Konrad 101 core
LCo
Upper Turonian
MTu
Cremnoc. spp.
M. scupini
M.striat.- M. labiat.
I. perplexus
I. lamarcki
Erwitte Formation
Salder Formation
Söhlde Fm
Upper Lst
Grauweiße Wech.
89.4 Ma
91.0 Ma
Age
Gradstein et al., 2020)
metres
massive limestones with intercalated marls
C.d. erectus
inoc. abundant Cremnoceramus spp.
marl-dominated interbedded limestones and marls
marl
marl
increase macrofossil debris
Micraster Marls
highest allochthonite
T_F marl B5
flaser-bedded marly limestones 'allochthonites' with fluid textures and lithoclasts common
M_E M_Echen marls
six marls I. lamarcki
slumps and gravity-flow deposits
flaser-bedded marly lenticular limestone
lowest allochthonite
thin shelled inoc.
Upper Rotpläner
Inoceramus lamarcki beds
top Middle Rotpläner
Navigation Event
Hitch Wood
Bridgewick
i2
acme C. ditissima
C. membrani.
acme S. ambigua
C. ditissima
O. pulcherrimum
C. wilsonii
infux palynomorphs
P. infusorioides infux
P. infusorioides minimum
S. turonica
acme S. turonica
infux S. ambigua
R. truncigerum
infux P. infusorioides
Species richness
40
P/G ratio
0.4
C. membraniphorum
R. truncigerum
C. wilsonii
S. turonica
S. turonica
Dinocyst zonation
Salzgitter-Beddingen
Palynology sample: productive barren

**Fig. 9.** Dinocyst range chart showing the relative abundance of representative taxa from the middle Turonian – Coniacian interval in the Konrad 101 borehole, Salzgitter-Beddingen. Stratigraphy revised after Niebuhr et al. (2001) with dinocyst zones of Prössl (1990). Dinocyst ranges and relative abundance from Prössl (1990) with updated taxonomic assignments (Appendix A). Based on examination of the plates, *Achomosphaera triangulata* of Prössl (1990) is re-identified as *Spiniferites ramosus*. Dark green bars and gradient shaded vertical columns are gonyaulacoid dinocysts, red ornaments represent peridinioid cysts, grey ornaments are cysts of uncertain taxonomic affinity. See Fig. 8 for lithological information and abbreviations.

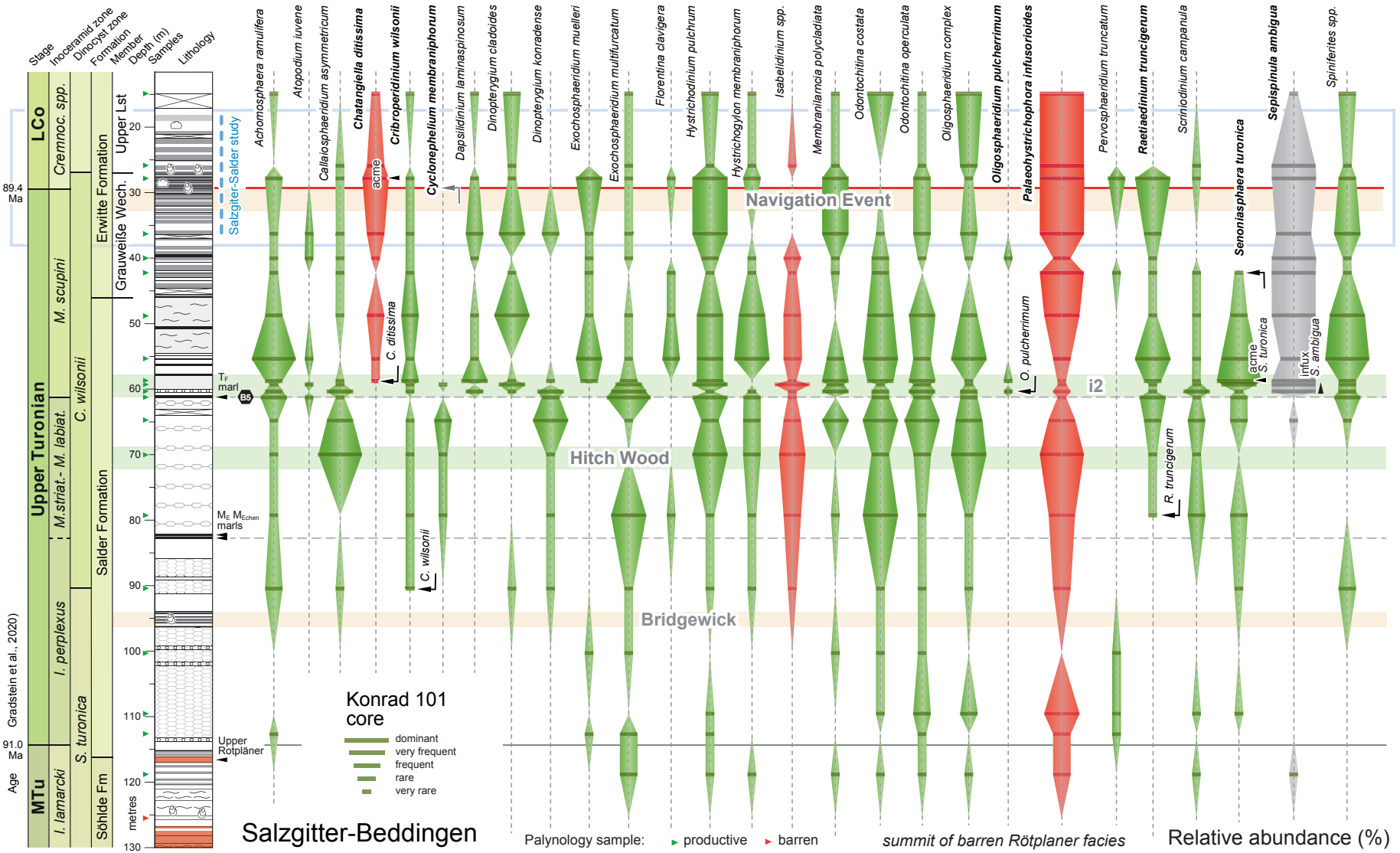
Stage
Inoceramid zone
Dinocyst zone
Formation
Member
Depth (m)
Samples
Lithology
Age
Gradstein et al., 2020)
MTu
LCo
Upper Turonian
I. lamarcki
I. perplexus
M.striat.- M. labiat.
M. scupini
Cremnoc. spp.
S. turonica
C. wilsonii
Söhlde Fm
Salder Formation
Erwitte Formation
Upper Lst
Grauweiße Wech.
89.4 Ma
91.0 Ma
metres
20
30
40
50
60
70
80
90
100
110
120
130
Salzgiter-Salder study
TF marl
B5
ME MEchen marls
Upper Rotpläner
Achomosphaera ramulifera
Atopodium iuvene
Callaiosphaeridium asymmetricum
Chatangiella ditissima
acme
C. ditissima
Cribroperidinium wilsonii
C. wilsonii
Cyclonephelium membraniphorum
Dapsilidinium laminaspinosum
Dinopterygium cladoides
Dinopterygium konradense
Exochosphaeridium muelleri
Exochosphaeridium multifurcatum
Florentina clavigera
Hystrichodinium pulchrum
Hystrichogylon membraniphorum
Isabelidinium spp.
Membranilarnacia polycladiata
Odontochitina costata
Odontochitina operculata
Oligosphaeridium complex
Oligosphaeridium pulcherrimum
Palaeohystrichophora infusorioides
O. pulcherrimum
Pervosphaeridium truncatum
Raetiaedinium truncigerum
R. truncigerum
Scriniodinium campanula
Senoniasphaera turonica
acme
S. turonica
Sepispinula ambigua
influx
S. ambigua
Spiniferites spp.
Navigation Event
Hitch Wood
Bridgewick
i2
Konrad 101 core
dominant
very frequent
frequent
rare
very rare
Salzgitter-Beddingen
Palynology sample:
productive
barren
summit of barren Rötplaner facies
Relative abundance (%)

### 4.3.2 Late Turonian dinocyst event stratigraphy: appraisal for Salzgitter

Pearce et al. (2020) erected a new dinocyst event stratigraphy for the Cenomanian – lowermost Campanian of NW Europe, and differentiated between evolutionary inception and extinction levels (first appearance datum, FAD; last appearance datum, LAD) versus regional lowest (LO) and highest (HO) recorded occurrences in sections. Event ages were calculated, included those derived using the GTS2020 base Turonian age of 89.4 Ma (Gradstein et al., 2020 table 1.2, 1038).

Six dinocyst biostratigraphic datum levels were identified from the latest Turonian by Pearce et al. (2020, GTS2020 ages for reference): (1) FAD of *Senoniasphaera filoreticulata* (89.81 Ma, NW Europe); (2) reappearance *Oligosphaeridium pulcherrimum* (89.77 Ma, N Hemisphere); (3) HO of persistent *Cyclonephelium membraniphorum* (89.57 Ma, NW Europe); (4) LAD of *Stephodinium coronatum* (89.53 Ma, N Hemisphere); (5) HO of persistent *Senoniasphaera turonica* (89.52 Ma, NW Europe); (6) LAD of *Sentusidinium devonense* (89.41 Ma, NW Europe). No early Coniacian markers were proposed; the next significant dinocyst event occurs in the middle Coniacian: LO of persistent *Heterosphaeridium verdieri* (87.46 Ma, NW Europe). The applicability of this event stratigraphy to the Salzgitter sections is as follows:

(1) *Senoniasphaera filoreticulata* was recorded from a single sample at Salzgitter-Salder (top Bed 45), at the top of the Turonian Stage in the section. This is consistent with a latest Turonian FAD, but occurs somewhat higher than the expected FAD level. The species was not listed by Prössl (1990) or by Sikora et al. (2004).

(2) *Oligosphaeridium pulcherrimum* occurs sparsely through the upper Turonian – lower Coniacian boundary interval at Salzgitter-Salder (Fig. 4). The species was not reported by Sikora et al. (2004). In the Konrad 101 core, Prössl (1990) recorded the species consistently through the Hauterivian to low upper Albian, an absence above, then a reappearance in the lower part of the *M. scupini* Zone (Fig. 9). This lies stratigraphically below our study interval at Salzgitter-Salder, and coincides with the dinocyst reappearance event of Pearce et al. (2020).

(3) *Cyclonephelium membraniphorum* (Fig. 5D) occurs sporadically at the summit of the upper Turonian at Salzgitter-Salder and has its HO at the base of Bed 46 (Fig. 4), i.e. immediately above the base Coniacian. The species was not recorded by Sikora et al. (2004). In Konrad 101 the species occurs in the upper Albian and then appears again in the upper Turonian *Mytiloides striatoconcentricus* to lower *M. scupini* zones (Fig. 9; Prössl, 1990). The HO at Salzgitter-Salder is therefore significant, and is discussed further below (Section 4.5.1).

(4) Neither we nor Sikora et al. (2004) have recorded *Stephodinium coronatum* from the boundary interval at Salzgitter-Salder. The species occurs consistently in the Aptian to upper Cenomanian of Konrad 101 but is absent above (Prössl, 1990), so the HO does not correspond to the LAD event of Pearce et al. (2020), which cannot be recognised in Lower Saxony.

(5) We record a single specimen of *Senoniasphaera* sp. from top Turonian Bed 45a at Salzgitter-Salder; the genus was not mentioned by Sikora et al. (2004). The LO of *Senoniasphaera turonica* lies at the top of the lower Turonian in Konrad 101, within the largely barren interval. It occurs consistently through the upper Turonian, with a HO in the lower Grauweiße Wechselfolge, stratigraphically below the base of our sampling interval at Salzgitter-Salder (Fig. 9; Prössl, 1990). The taxon is unrecorded from the Coniacian in Lower Saxony. This HO is somewhat below the level of the HO of persistent *S. turonica* datum defined by Pearce et al. (2020) which was placed between the i5 and Navigation CIEs.

(6) *Sentusidinium devonense* has not been recorded at Salzgitter-Salder or in Konrad 101, although we note the presence of *Sentusidinium* spp. throughout the boundary section at the former site, with a HO in lower Coniacian Bed 60 (Fig. 4).

### *4.4 Relative abundance trends*

The most prominent feature on the palynological range chart for Salzgitter-Salder is the dominance and large amplitude stratigraphic variation seen in the relative abundance of *P.*

*infusorioides* (Fig. 4), which constitutes up to 70% of the total dinocyst assemblage. The long-term relative abundance of *P. infusorioides* initially falls upwards through the sample interval to a minimum of ~10% in beds 45 and 46 (Bed 47 yielded no palynomorphs) spanning the Turonian – Coniacian boundary ("*P. infusorioides* minimum" in Figs. 2–4, 6, 7). The species abundance then rises to higher values of 30 – 50% from Bed 50a upwards (influx *P. infusorioides* in Figs. 2–4, 6, 7). *Sepispinula ambigua* has a loosely inverse relative abundance relationship with *P. infusorioides* and has an acme in Bed 49b (31% of the assemblage).

Sikora et al. (2004) previously noted the overwhelming dominance of *P. infusorioides* in palynological assemblages from the Turonian – Coniacian boundary succession at Salzgitter-Salder. In the Konrad 101 core, *P. infusorioides* is present in most samples from the basal lower Cenomanian upwards (Prössl, 1990), with a dominance (together with *S. ambigua*) in the upper middle – lower upper Cenomanian and then again through the upper Turonian – lower Coniacian boundary succession (Fig. 9). Sampling from the Konrad 101 core did not include the interval of the *P. infusorioides* minimum observed at Salzgitter-Salder, and the low-resolution sampling and semi-quantitative nature of the data from the former site precludes detailed comparison of trends across the stage boundary interval.

## *4.5 Dinocyst zonations*

In addition to the late Turonian dinocyst events identified by Pearce et al. (2020), previous authors have proposed zonation schemes for the Turonian – Coniacian boundary interval.

### 4.5.1 *Cyclonephelium membraniphorum* and the *C. membraniphorum* Zone

The HO of *C. membraniphorum* (Fig. 5D) is recorded at the base of the Coniacian at Salzgitter-Salder (Figs. 3, 4). This corresponds well to the highest persistent occurrence (HO pers) recorded by Pearce et al. (2003, 2020), and provides the only significant dinocyst species LO or HO identified from the boundary interval at Salzgitter-Salder. Foucher (1971, 1975, 1976, 1980), Costa and Davey (1992) and Prince et al. (2008) similarly placed the HO of *C. membraniphorum* at the top of the Turonian in France and southern England. It is notable that Kirsch (1991) did not observe the species in his study of the Coniacian –

Maastrichtian of the Alps, southern Germany. Similarly, the species is unrecorded from Coniacian or younger sediments in Kansas and Texas (Scott et al., 2018; Dodsworth and Eldrett, 2019), despite being common below. However, records from elsewhere (Foucher, 1983; Williams and Bujak, 1985; Mohr and Gee, 1992; Schiøler, 1992) led Pearce et al. (2020) to propose a late Coniacian LAD for *C. membraniphorum*.

Olde et al. (2015a) described the dinocyst biostratigraphy of the Turonian – lower Coniacian of the Bch-1 core in the Bohemian Cretaceous Basin of the Czech Republic (Fig. 10) and reviewed published data from four English Chalk localities. The Czech site is situated 400 km SE of Salzgitter-Salder. From their study, Olde et al. (2015a) proposed a *C. membraniphorum* interval Zone for the Turonian (revised from the original definition of Clarke and Verdier, 1967), the base of which was defined by HO of common *Litosphaeridium siphoniphorum* (intra-upper Cenomanian). The zone comprises a: (1) lower unnamed division (Cenomanian – Turonian boundary interval); (2) *Senoniasphaera turonica* Subzone, base marked by the LO of common *S. turonica* (lower Turonian – mid-middle Turonian); and (3) *Raetiaedinium truncigerum* Subzone, base marked by the LO of persistent *R. truncigerum* (mid-middle Turonian – lower Coniacian).

The HO of common *C. membraniphorum* was placed in the uppermost Turonian, below the Navigation CIE by Olde et al. (2015a fig. 6). The base of the overlying lower Coniacian *O. pulcherrimum* Zone (cf. Williams, 1977), *S. rotundata* (now *C. glomerata*) Subzone, was defined by the LO of common *Oligosphaeridium pulcherrimum.* This species occurs sporadically in very low numbers through the Salzgitter sections (Figs. 4, 9), so the sampled intervals at Salzgitter-Salder and in the Konrad 101 core (Fig. 8) may not include the *O. pulcherrimum* Zone, the base of which approximates to the base of the *C. c. inconstans* Zone in Bch-1 (Fig. 10).

The *C. membraniphorum* Zone sensu Olde et al. (2015a) was adopted by Dodsworth and Eldrett (2019) for the Cenomanian – lower Coniacian of the US Western Interior, defined as the interval "*From the first sample stratigraphically above the LO of common* Litosphaeridium siphoniphorum *(base of zone) to the higher of either the LO of* Cauveridinium membraniphorum *or the LO of* Isabelidinium magnum *(top of subzone)*"; LO

refers to last occurrence in this context. Dodsworth and Eldrett (2019) recognised that *C. membraniphorum* had not been recorded above the Turonian in the Cretaceous Western Interior Seaway to date, and therefore used the alternate HO of *I. magnum* to make the Zone more widely applicable. Subzones were revised (based on the absence of *Raetiaedinium truncigerum* in the Turonian) to include, from base to summit: *Adnatosphaeridium tutulosum*, *Isabelidinium magnum*, *Senoniasphaera turonica,* and *S. rotundata* interval subzones, to match the assemblage compositions in North America.

Despite the inability to identify the top of the *C. membraniphorum* Zone at Saltzgitter-Salder (given the absence of common *Oligosphaeridium pulcherrimum*, or any specimens of *Isabelidinium magnum*), the highest occurrence of *C. membraniphorum* appears to be consistent with the bulk of published records for a highest persistent or common occurrence at the top of the Turonian.

### 4.5.2 *Senoniasphaera turonica* and the *S. turonica* Subzone

The lowest occurrence of *Senoniasphaera 'rotundata'* has been widely used as a marker for the Turonian (Foucher, 1980, 1981; Tocher and Jarvis, 1987, 1994, 1995; Jarvis et al., 1988a, b; FitzPatrick, 1995; Lamolda and Mao, 1999; Dodsworth, 2000). Subsequent taxonomic revision (Pearce et al., 2003, 2011) differentiated two main species of *Senoniasphaera* in the Turonian: *S. turonica* (= *S. rotundata alveolata* of Pearce et al., 2003, 2009; Prince et al., 2008); and *S. rotundata* (= *S. rotundata rotundata*), with the former representing the older Turonian species. Recently, *S. rotundata rotundata* has been reassigned to *Canningia glomerata* (Fensome et al., 2019b; Fig. 5A).

Foucher (1981) erected a "*Senonisphaera rotundata* Zone", defined by the LO of *S. 'rotundata'*, (= *S. turonica*), for the middle – upper Turonian of Europe (a top was not considered). Prössl (1990) proposed a "*Craspeodinium turonicum* Zone" [sic] (= *S. turonica*) from the LO of the index species to the LO of *Cribroperidinium wilsonii* for the "lower to mid-middle Turonian" of the Lower Saxony Basin, based on his records from the Konrad 101 core (Fig. 9). This is recalibrated here as top lower Turonian – low upper Turonian (Fig. 9; cf. Niebuhr et al., 2001). Olde et al. (2015a) defined a *S. turonica* Subzone for the lower – middle Turonian. A lower to middle Turonian influx also occurs in North America, where the

event defines the base of the *S. turonica* interval Subzone of Dodsworth and Eldrett (2019), and Pearce et al. (2020) proposed the LO of common *S. turonica* as a lower Turonian NW European event marker.

*Senoniasphaera* abundances vary considerably between sections, but an acme of *S. turonica* occurs consistently in the upper Turonian (*Plesiocorys* (*Sternotaxis) plana* echinoid Zone; *Subprionocyclus neptuni* ammonite Zone) of English Chalk successions (FitzPatrick, 1995; Pearce et al., 2003, 2020; Olde et al., 2015a). A comparable event can be seen in the Konrad 101 core (Fig. 9; Prössl, 1990). The HO of persistent *S. turonica* represents an uppermost Turonian NW European datum level (Pearce et al., 2020), although the species is again recorded from the upper Coniacian – Santonian in the Anglo-Paris Basin of southern England (Prince et al., 2008; as *Senoniasphaera rotundata* subsp. *alveolata*). It is notable, however, that the species has not been recorded from the Coniacian – Maastrichtian in the Alps, southern Germany (Kirsch, 1991).

*Senoniasphaera turonica* has not been identified from the Turonian – Coniacian boundary section at Salzgitter-Salder, but ranges up into the lower Grauweiße Wechselfolge Member (upper *M. scupini* Zone) in the Konrad 101 core (Fig. 9; Prössl, 1990). Its HO thus lies stratigraphically immediately below our study interval in the Quarry. A *S. turonica* acme in the basal *M. scupini* Zone a short distance below the HO of the species in Konrad 101, is comparable with records for the acme top in southern England (FitzPatrick, 1995; Pearce et al., 2003; Olde et al., 2015a), although the species continues to be persistent up to the Navigation CIE in the Trunch borehole of eastern England, where it has a high lower Coniacian HO (Pearce et al., 2020 fig. 6).

### 4.5.3 *Cribroperidinium wilsonii* and the *C. wilsonii* Zone

Prössl (1990) erected a *Acanthaulax wilsonii* (= *Cribroperidinium wilsonii*) Interval Zone for the “upper Turonian” of the Lower Saxony Basin based on his Konrad 101 records. The range of the species in the core is now revised to: low upper Turonian (upper *I. perplexus* Zone) to lower Coniacian (Fig. 9). *Cribroperidinium wilsonii* similarly occurs in low numbers throughout the sampled interval at Salzgitter-Salder (Fig. 4). A Turonian LO is consistent with records from southern Germany and Denmark (Kirsch, 1991; Schiøler, 1992). The LO of

*C. wilsonii* has been recorded in the top Turonian for the Bch-1 borehole (Olde et al., 2015a, b).

The LO of *C. wilsonii* is observed in the lower upper Turonian (base *P. (S.) plana* Zone) above the Bridgewick CIE of the Trunch borehole, with a lowest common occurrence above the Hitch Wood CIE in the mid-upper Turonian (Pearce et al., 2020). There it becomes increasingly common through the mid- to upper Coniacian, confirming its importance as a significant component of Coniacian dinocyst assemblages. *Cribroperidinium wilsonii* continues through the Santonian – lower Campanian at Trunch, becoming less abundant upwards. The species ranges from upper Albian – Campanian in southern England (Prince et al., 1999, 2008; Lignum, 2009; Pearce et al., 2020).

The upper Turonian LO of *C. wilsonii* documented in the Konrad 101 and Trunch boreholes, may provide a regional marker in northern Germany and other North Boreal areas, but lies below the Turonian – Coniacian boundary interval studied at Salzgitter-Salder.

## *4.6 Stratigraphic significance of other dinocyst taxa: a critical appraisal*

A number of other taxa recorded at Salzgitter have been considered to be stratigraphically significant.

### 4.6.1 *Chatangiella granulifera*

Sikora et al. (2004) noted a LO of *Chatangiella granulifera* in Bed 47 at Salzgitter-Salder. We record the consistent presence of the species from Bed 45a upwards. The species was not identified by Prössl (1990). *Chatangiella granulifera* has a FAD in the earliest Turonian according to Costa and Davey (1992), and was proposed as a subzonal marker for the lower Turonian by Nøhr-Hansen et al. (2020). The species ranges up into the Campanian – Maastrichtian (Mao and Mohr, 1992). It is not considered to have stratigraphic significance for the Turonian – Coniacian boundary.

### 4.6.2 *Dapsilidinium laminaspinosum*

Sikora et al. (2004) highlighted a HO of *Dapsilidinium laminaspinosum* in Bed 54 at Salzgitter-Salder and noted that it has a lower Coniacian HO. The species occurs rarely; our HO is from Bed 52a (Supplementary data Table 1). Prössl (1990) recorded its presence to the top of the section in Konrad 101 (Fig. 9); here the taxon occurs throughout the Barremian – lower Coniacian. The species occurs in low numbers throughout the Cenomanian – lower Campanian section in eastern England (Pearce et al., 2020), so the HO recorded in the Lower Saxony sections is not considered to be significant.

### 4.6.3 *Florentinia clavigera*

Sikora et al. (2004) noted a HO of "Turonian index" *Florentinia clavigera* in basal Coniacian Bed 47 at Salzgitter-Salder. We record the species sporadically in the upper Turonian and lower Coniacian of the section (Supplementary data Table 1); the species ranges down into the mid-upper Turonian *M. striatoconcentricus* Zone at Konrad 101 (Fig. 9; Prössl, 1990) but is absent from older strata. The taxon certainly ranges up into the Coniacian.

### 4.6.4 *Oligosphaeridium pulcherrimum*

Olde et al. (2015a, b) recorded the First Common Occurrence (FCO) and an acme of *Oligosphaeridium pulcherrimum* in the lower Coniacian (at the 'Beeding' CIE; base of their *O. pulcherrimum* Zone, *S. rotundata* (now *Canningia glomerata*) Subzone) in the Bch-1 borehole, that was considered to be stratigraphically significant. This is above the sampled intervals at Salzgitter-Salder (Voigt et al., 2020 fig. 6) and in the Konrad 101 borehole (Prössl, 1990), where the species occurs sporadically through the sampled upper Turonian – Coniacian sections (Figs. 4, 9). The reappearance of the species at the base of the *M. scupini* Zone (equivalent level to the i2 CIE) in Konrad 101 (Fig. 9), marginally lower than at Trunch (LO at i3), is consistent with the dinocyst reappearance event of Pearce et al. (2020).

### 4.6.5 *Oligosphaeridium totum totum*

Sikora et al. (2004) recorded an HO of *Oligosphaeridium totum totum* at the base of the Coniacian in Bed 47 at Salzgitter-Salder and stated that this taxon has a characteristic upper Turonian HO. We have not observed this species in the section. *Oligosphaeridium totum*

*totum* is typically found in the Lower Cretaceous (e.g. Århus, 1991; Nøhr-Hansen, 1993; Torricelli, 2000; Oboh-Ikuenobe et al., 2007; Pestchevitskaya and Nikitenko, 2019), with some authors documenting it as ranging up to the late Cenomanian (e.g. Dodsworth et al., 2020), no younger. We consider the Sikora et al. (2004) records to be erroneous or based on reworked specimens.

### 4.6.6 *Raetiaedinium truncigerum*

Sikora et al. (2004) highlighted a reappearance of *Raetiaedinium truncigerum* in lower Coniacian Bed 53 at Salzgitter-Salder, but we record it in small numbers throughout the boundary interval (Fig. 5H; Supplementary data Table 1). In the Konrad 101 core the species has a well-defined LO within the upper Turonian low *M. striatoconcentricus* Zone (Fig. 9), and is then recorded in the majority of samples upwards into the lower Coniacian (Prössl, 1990). The LO in Konrad 101 corresponds well with the upper Turonian LO of persistent *R. truncigerum* event of Pearce et al. (2020).

The FAD of *Raetiaedinium truncigerum* occurs in the middle Turonian, evidenced by records from the Bch-1 core (Olde et al., 2015a, b; Pearce et al., 2020). The FAD and local LO thus lie below the stage boundary interval. The species ranges into the Campanian in England and southern Germany (Kirsch, 1991; Williams et al., 1993; Prince et al., 1999; Pearce et al., 2020).

### 4.6.7 *Scrinodinium campanula*

*Scrinodinium campanula* (Fig. 5I) has been reported to have a Coniacian top (Stover et al., 1996). Generally, this species is most consistently present in Turonian and older sediments (Clarke and Verdier, 1967; Costa and Davey, 1992; FitzPatrick, 1995). The taxon occurs consistently in low numbers in the lower Coniacian at Salzgitter-Salder (Fig. 4; Beds 49b–59, upper *C. d. erectus* – lower *C. w. hannovrensis* zones); Sikora et al. (2004) highlighted a HO of *S. campanula* in Bed 54, consistent with our record of its HO in Bed 59. Prössl (1990) documented the species occurring throughout the Lower and Upper Cretaceous section at Konrad 101 with a HO in his penultimate sample, towards the base of the Upper Limestone Member (Fig. 9), consistent with records at Salzgitter-Salder. Olde et al. (2015a, b) similarly

recorded *S. campanula* only from the lowest Coniacian of Bch-1 in the Bohemian Cretaceous Basin (the species was not observed in the Turonian). However, none of these studies sampled a significant range of Coniacian or younger strata.

*Scrinodinium campanula* occurs sporadically through the Cenomanian – Santonian of the Trunch borehole (Pearce et al., 2020). Its range certainly extends into the upper Santonian (Williams and Bujak, 1985; Prince et al., 1999, 2008; Pearce et al., 2020), as recorded in southern Germany by Kirsch (1991). The LAD of *S. campanula* in the Northern Hemisphere was suggested to be in the mid-late Santonian by Pearce et al. (2020), who designated this as one of their stratigraphically significant dinocyst events.

### *4.7 Correlation of NW European Turonian – Coniacian boundary sections and the* P. infusorioides *Event*

Turonian – Coniacian boundary sections in NW Europe that have yielded dinocyst assemblages containing abundant peridinioid cysts similar to Salzgitter (i.e. *Spiniferites* – *Palaeohystrichophora* assemblages, cf. Pearce et al., 2003, 2009; Prince et al., 2008) are located in the Bohemian Cretaceous Basin of the Czech Republic (Bch-1 borehole; Olde et al., 2015b) and in the southern North Sea basin of eastern England (Trunch borehole; Pearce et al., 2020). Elsewhere, including the candidate GSSP references section at Słupia Nadbrzeżna in central Poland (Olde et al., 2016), and sections in the Anglo-Paris Basin of southern England (Clarke and Verdier, 1967; FitzPatrick, 1995; Pearce et al., 2003; Prince et al., 2008), assemblages are commonly dominated by gonyaulacoid cysts and a *Circulodinium* – *Heterosphaeridium* (C–H) assemblage of Pearce et al. (2003) and Prince et al. (2008).

The C–H assemblage (typified by the assemblage from the Banterwick Barn borehole in southern England, Pearce et al., 2003) is characterised by a low diversity and is dominated by areoligeracean dinocysts; it is considered to be representative of more proximal palaeoenvironments situated closer to a shoreline. This is in direct contrast to the S–P assemblage that comprises a significantly higher diversity, with dinocyst taxa typical of more distal settings. An additional feature of the C–H assemblage is the apparent absence of cyst-producing heterotrophic dinoflagellates, given the conspicuous absence of *P. infusorioides*.

This appears to be specific to European chalk sections where terrestrial runoff was likely minimal, resulting in relatively oligotrophic and stable near-shore palaeoenvironments unable to support a heterotrophic community. As a result, sites containing the C–H assemblage cannot be compared to the S–P assemblage at Saltzgitter-Salder.

### 4.7.1 Bohemian Cretaceous Basin Bch-1 borehole

The relative abundances of dinocyst taxa through the Turonian – Coniacian boundary interval at Bch-1 are plotted together with the inoceramid biostratigraphy, $\delta^{13}C_{carb}$ and $\delta^{13}C_{org}$ isotope curves in Fig. 10. Assemblages are dominated by *P. infusorioides*, *S. ambigua*, *S. ramosus ramosus* and, towards the top of the section, *S. longifurcatum* (Olde et al., 2015a, b). A prominent acme of *P. infusorioides* in the lower Coniacian occurs at 71.5 m depth, where it represents 85% of the dinocyst assemblage. This lies in the lower half of the *C. w. hannovrensis* Zone according to the recently recalibrated biostratigraphy (Fig. 10; Čech and Uličný, 2020). A minimum, with *P. infusorioides* constituting only 1% of the assemblage, occurs at 97.5 m in Bch-1; this corresponds to the $\delta^{13}C_{org}$ minimum and the lower of two $\delta^{13}C_{carb}$ minima that constitute the Navigation Event (Voigt et al., 2020), at the base of the *Didymotis* I, II interval in the *M. herbichi* Subzone (Fig. 10). Thus, at both Salzgitter and Bch-1, a *P. infusorioides* minimum is developed at the level of the Navigation Event, across the stage boundary at Salzgitter-Salder and within the lower part of the CIE at Bch-1.

*Sepispinula ambigua* shows a major increase in relative abundance in the mid-upper Turonian uppermost *M. striatoconcentricus – M. labiatoidiformis* to basal *M. scupini* zones in both the Konrad 101 and Bch-1 cores (Fig. 9; Olde et al., 2015b fig. 7), and continues as a major component of the assemblages upwards into the basal *C. w. hannovrensis* Zone (Fig. 10). Above this, it declines rapidly to constitute only a minor component of the assemblage from the base of the *C. c. inconstans* Zone, which contains an acme of *S. longifurcatum* (Fig. 5N) and increasing abundances upwards of *S. ramosus ramosus*. A broadly inverse relationship is observed between the relative abundances of *P. infusorioides* and *S. ambigua* at Bch-1 (Fig. 11), and to a lesser extent in the Salzgitter-Salder (Fig. 4) and Konrad 101 plots (Fig. 9). *Spiniferites* spp. are particularly abundant in the basal *M. scupini* Zone in Bch-1, and in the mid-*C. c. crassus* Zone (not sampled in Germany).

**Fig. 10.** Stratigraphy and dinocyst range chart showing the relative abundance of representative taxa from the upper Turonian – lower Coniacian interval in the Bch-1 borehole, Czech Republic. Stratigraphy after Čech and Uličný (2020) with $\delta^{13}C_{org}$ profile from Uličný et al. (2014) and $\delta^{13}C_{carb}$ after Jarvis et al. (2015). Dinocyst records and key palynological marker levels from Olde et al. (2015a, b). Dark green bars and gradient shaded vertical columns are gonyaulacoid dinocysts, red ornaments represent peridinioid cysts, grey ornaments are cysts of uncertain taxonomic affinity. Relative abundances of accessory taxa are multiplied x5 for clarity, as indicated. Note the *P. infusorioides* minimum within the top Turonian Navigation CIE, and a well-defined acme of the species immediately above the i7 CIE in the lower *C. w. hannovrensis* Zone. *Cww*, *Cremnoceramus walterdorfensis walterdorfensis*; *Cde*, *C. deformis erectus*; *Cci*, *C. crassus inconstans*; *Ifg*, *Inoceramus frechi / I. globbosus*; *Mh*, *Mytiloides herbichi*; g, glauconite; ph, phosphate; Q, quartz.

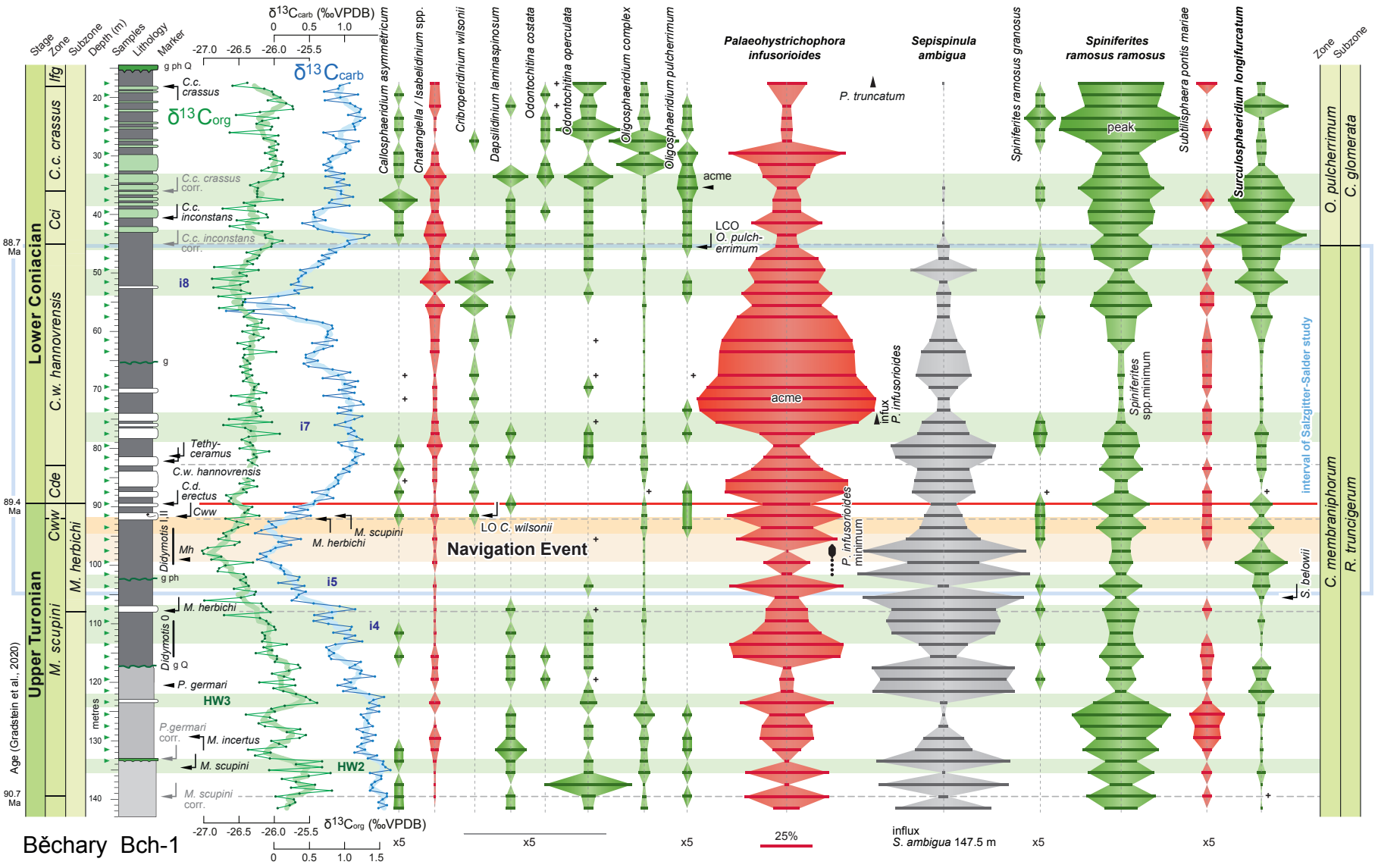
Stage
Zone
Subzone
Depth (m)
Samples
Lithology
Marker
δ13Ccarb (‰VPDB)
δ13Ccarb
δ13Corg
δ13Corg (‰VPDB)
Callosphaeridium asymmetricum
Chatangiella / Isabelidinium spp.
Cribroperidinium wilsonii
Dapsilidinium laminaspinosum
Odontochitina costata
Odontochitina operculata
Oligosphaeridium complex
Oligosphaeridium pulcherrimum
Palaeohystrichophora infusorioides
Sepispinula ambigua
Spiniferites ramosus granosus
Spiniferites ramosus ramosus
Subtilisphaera pontis mariae
Surculosphaeridium longifurcatum
Zone
Subzone
Lower Coniacian
Upper Turonian
lfg
C.c. crassus
Cci
C.w. hannovrensis
Cde
Cww
M. herbichi
M. scupini
C.c. crassus
C.c. crassus corr.
C.c. inconstans
C.c. inconstans corr.
i8
i7
i5
i4
HW3
HW2
Tethy-ceramus
C.w. hannovrensis
C.d. erectus
Cww
Didymotis I
Didymotis 0
Mh
M. herbichi
M. scupini
P. germari
P.germari corr.
M. incertus
M. scupini
M. scupini corr.
Navigation Event
LO C. wilsonii
acme
LCO O. pulch-errimum
P. truncatum
peak
Spiniferites spp.minimum
P. infusorioides influx
P. infusorioides minimum
S. belowii
interval of Salzgitter-Salder study
O. pulcherrimum
C. glomerata
C. membraniphorum
R. truncigerum
88.7 Ma
89.4 Ma
90.7 Ma
Age (Gradstein et al., 2020)
metres
x5
25%
influx S. ambigua 147.5 m
Běchary Bch-1

The increases in relative numbers of *Surculosphaeridium longifurcatum* in the lower Coniacian is also observed in the Banterwick Barn borehole (UK; Pearce et al., 2003). Here, the event occurs at 31.74 m in the mid-*M. cortestudinarium* Zone, mid-way between the Beeding Event and Light Point CIEs of Jarvis et al. (2006), and appears to be synchronous in Bch-1.

### 4.7.2 Southern North Sea Basin Trunch borehole

The relative abundances of dinoflagellate taxa through the Turonian – Coniacian boundary interval in the Trunch borehole are plotted together with the echinoid biostratigraphy, inoceramid records and $\delta^{13}C_{carb}$ isotope curve in Fig. 11. Assemblages are dominated by *P. infusorioides* and *S. ramosus ramosus* (Pearce et al., 2020). A prominent acme of *P. infusorioides* in the lower Coniacian is documented at 426 m depth, where it represents 47% of the dinocyst assemblage. This occurs in the lower half of the *Micraster cortesudinarium* Zone. A minimum with *P. infusorioides* constituting only 1% of the assemblage occurs at 432.4 m; this lies within $\delta^{13}C_{org}$ minimum and the lower $\delta^{13}C_{carb}$ negative excursion that constitute the Navigation Event (Jarvis et al., 2006; Pearce et al., 2020).

By contrast to Salzgitter and Bch-1, *S. ambigua* is generally absent above the Cenomanian at Trunch, within which it comprises a major component of the assemblage (Pearce et al., 2020 fig. 6). It is recorded in small numbers in uppermost Turonian samples from 433.0 and 433.3 m, but here it is associated with an assemblage of other typically Cenomanian taxa and is therefore considered to be reworked (Fig. 11). Cenomanian specimens of *S. ambigua* from Trunch and other European sites (i.e. Aksudere, Crimea, Dodsworth, 2004 pl. 2 fig. 3; Eastbourne, UK, Pearce et al., 2009 pl. v fig. 10) are characteristically robust forms. Their high numbers and subsequent disappearance were used by Pearce et al. (2020) as a stratigraphic marker for the latest Cenomanian. Specimens of *S. ambigua* from the upper Turonian and lower Coniacian at Salzgitter-Salder are noticeably gracile (see Fig. 5J) and appear to possess a larger number of processes. Further study of these morphogroups may result in their formal differentiation as separate species. Prössl (1990, plate 13, fig. 6) figured a specimen of *S. ambigua* that resembles the robust morphotype, but the stratigraphic position of the specimen was not given.

**Fig. 11.** Stratigraphy and dinocyst range chart showing the relative abundance of representative taxa from the upper Turonian – lower Coniacian interval in the Trunch borehole, eastern England. Macrofossil records from Wood et al. (1994); carbon isotope values and events after Jarvis et al. (2006) and Pearce et al. (2020). The section provides the data used to construct the upper Turonian – lower Coniacian portion of the English Chalk $\delta^{13}C_{carb}$ reference curve of Jarvis et al. (2006) and Cretaceous global reference curve of Cramer and Jarvis (2020). The 'i3' CIE of Jarvis et al. (2006) was split into i3 and i4 and an additional i5 CIE was recognised by Pearce et al. (2020). Stratigraphically significant dinocyst lowest (LO) and highest occurrences (HO), and acme levels are indicated; pers. = persistent, reapp. = reappearance. Dark green bars and gradient shaded vertical columns are gonyaulacoid dinocysts, red ornaments represent peridinioid cysts. Note the *P. infusorioides* minimum within the top Turonian Navigation CIE, an influx above, and a well-defined acme of the species immediately above the Beeding CIE and the LO of *C. w. hannovrensis*.

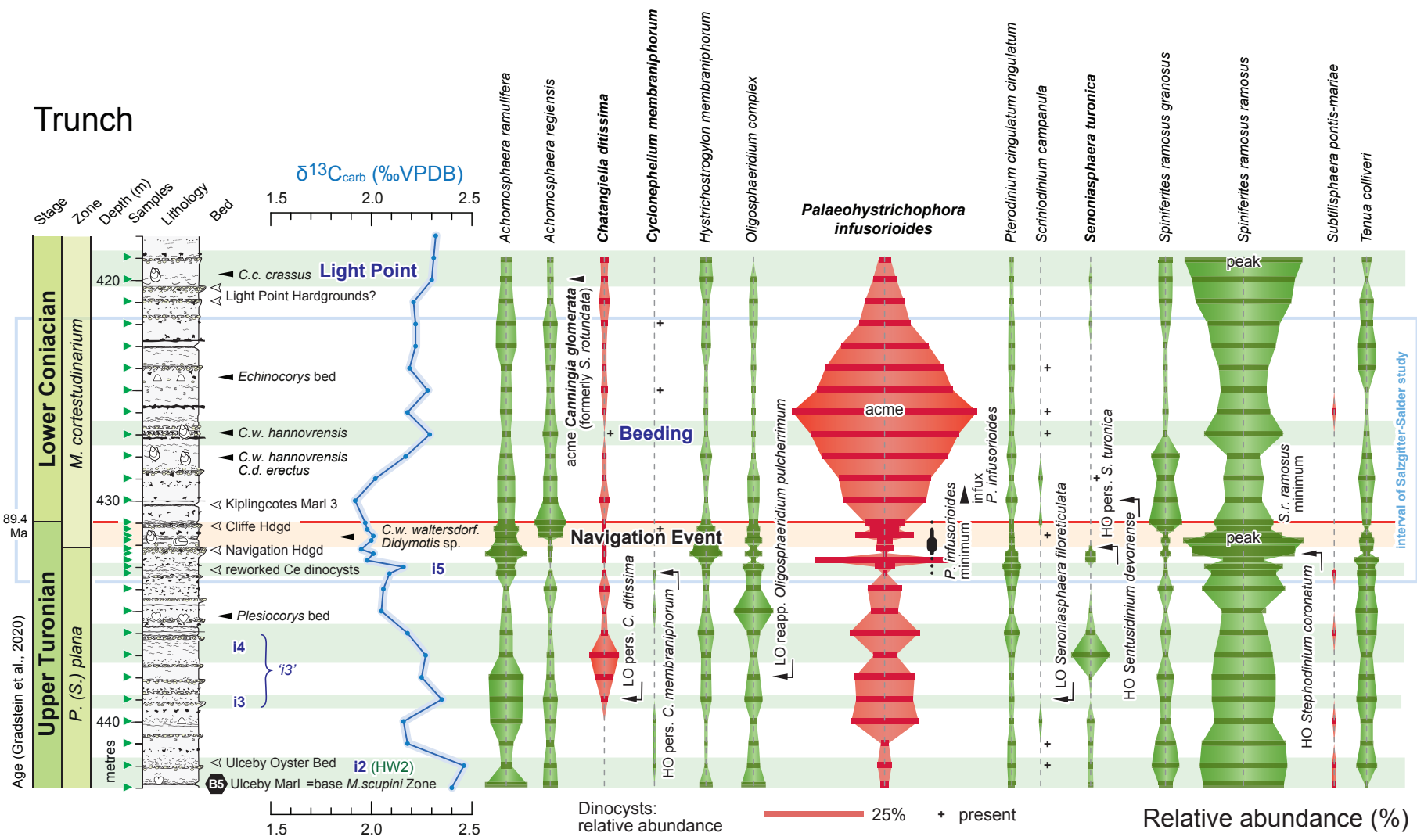
Trunch
Stage
Zone
Depth (m)
Samples
Lithology
Bed
δ13Ccarb (‰VPDB)
1.5
2.0
2.5
Lower Coniacian
M. cortestudinarium
Upper Turonian
P. (S.) plana
Age (Gradstein et al., 2020)
89.4 Ma
420
430
440
metres
C.c. crassus
Light Point
Light Point Hardgrounds?
Echinocorys bed
C.w. hannovrensis
C.w. hannovrensis
C.d. erectus
Kiplingcotes Marl 3
Cliffe Hdgd
Navigation Hdgd
reworked Ce dinocysts
C.w. waltersdorf.
Didymotis sp.
i5
Plesiocorys bed
i4
'i3'
i3
Ulceby Oyster Bed
i2 (HW2)
B5
Ulceby Marl =base M.scupini Zone
Achomosphaera ramulifera
Achomosphaera regiensis
Chatangiella ditissima
Cyclonephelium membraniphorum
Hystrichostrogylon membraniphorum
Oligosphaeridium complex
Palaeohystrichophora infusorioides
Pterodinium cingulatum cingulatum
Scriniodinium campanula
Senoniasphaera turonica
Spiniferites ramosus granosus
Spiniferites ramosus ramosus
Subtilisphaera pontis-mariae
Tenua colliveri
acme Canningia glomerata (formerly S. rotundata)
Beeding
Navigation Event
LO pers. C. ditissima
HO pers. C. membraniphorum
LO reapp. Oligosphaeridium pulcherrimum
acme
P. infusorioides minimum
influx P. infusorioides
LO Senoniasphaera filoreticulata
HO pers. S. turonica
HO Sentusidinium devonense
peak
peak
S.r. ramosus minimum
HO Stephodinium coronatum
interval of Salzgitter-Salder study
Dinocysts: relative abundance
25%
+ present
Relative abundance (%)

### 4.7.3 Placement of the Turonian – Coniacian boundary

Lower Saxony Basin sections at Salzgitter are correlated to the Bch-1 and Trunch boreholes in Fig. 12. The correlation is pinned to the base Coniacian defined by the FAD of *C. d. erectus* at Salzgitter-Salder (Voigt et al., 2020) and the LO at Bch-1 (Čech and Uličný, 2020), but the taxon has not been recorded in the Trunch section.

The base of the Coniacian at Trunch was placed at the $\delta^{13}C_{carb}$ minimum at 430 m depth in the core, immediately above Kiplingcotes Marl 3 by Pearce et al. (2020; see Fig. 11). Placement of the stage boundary was constrained by records of *C. w. walterdorfensis* and *Didymotis* sp. in the beds at 431 – 432 m (Wood et al., 1994; Pearce et al., 2020) between the Cliffe and Navigation Hardgrounds, confirming a latest Turonian age, and identification of the isotope minimum. The LO of *C. w. hannovrensis* is at 428 m (Fig. 11). Elsewhere in southern England, the LO of *C. w. walterdorfensis* occurs 70 cm above the Navigation Hardground at Dover, Kent and immediately above the Navigation Marls at Downley, Hampshire (Wood et al., 2004). The LO of *C. d. erectus* is recorded 50 cm below the Cliffe Hardground equivalent at the latter site, with the LO of *C. w. hannovrensis* a short distance above the hardground; this correlates to some distance below Kiplingcotes Marl 3 in northern England (Wood et al., 2004, fig. 2).

Lithostratigraphic correlation of Chalk marker beds between southern, eastern, and northern England is not straightforward (Pearce et al., 2020), but if the marker beds have been correctly identified in the Trunch succession, they indicate that the base Coniacian would be better placed 1 m lower, around the Cliffe Hardground at 431 m in the Trunch borehole (Fig. 12), as suggested previously by Jarvis et al. (2006). The single low $\delta^{13}C_{carb}$ value above, used as the stage boundary marker by Pearce et al. (2020), may correspond to an outlier above the longer-term minimum, as seen in the new high-resolution isotope record at Salzgitter-Salder (Voigt et al., 2020). Here a shift to consistently rising $\delta^{13}C_{carb}$ values begins at the base of the *C. w. hannoverensis* Zone (Fig. 3), above a slightly elevated but erratic plateau interval spanning the *C. d. erectus* Zone. Recognition of the i6 CIE within the plateau interval at Salzgitter-Salder provides a means of better identifying the position

**Fig. 12.** Correlation of Turonian – Coniacian boundary sections and the *P. infusorioides* event. Macrofossil zone abbreviations as in Fig. 10. P/G is the peridinioid / gonyaulacoid ratio with P-cysts overwhelmingly dominated by *P. infusorioides*. Coloured horizontal bands indicate the proposed CIE correlation constrained by macrofossil biostratigraphy; options 1 and 2 of Voigt et al. (2020) for the Navigation Event are indicated by the darker vs. lighter colours (see Fig. 3). The Konrad 101 P/G profile is rescaled to match the Salzgitter-Salder heights (calibrated to the $T_F$ Marl, base Grauweiße Wechselfolge Member (GW) and base Coniacian); P/G values derived from the semiquantitative relative abundance data of Prössl (1990), arbitrarily scaled to Salzgitter-Salder. Data sources: **Bch-1**, $\delta^{13}C_{carb}$ (Jarvis et al., 2015), CIEs (Uličný et al., 2014; Jarvis et al., 2015; Čech and Uličný, 2020), macrofossils (Čech and Uličný, 2020), P/G ratio (Olde et al., 2015a, b); **Salzgitter-Salder**, $\delta^{13}C_{carb}$ and CIEs (Voigt and Hilbrecht, 1997; Voigt et al., 2020) with 'Peaks +2 to +4' of Wiese (1999), macrofossils (Ernst et al., 1983; Wood et al., 1984; Voigt and Hilbrecht, 1997; Wiese, 2009a; Čech and Uličný, 2020; Voigt et al., 2020), P/G ratio (this study); **Konrad 101**, P/G ratio (Prössl, 1990; this study); **Trunch**, $\delta^{13}C_{carb}$ curve and CIEs (Jarvis et al., 2006; Pearce et al., 2020; this study), macrofossils (Morter et al., 1975; Wood et al., 1994), P/G ratio (Pearce et al., 2020).

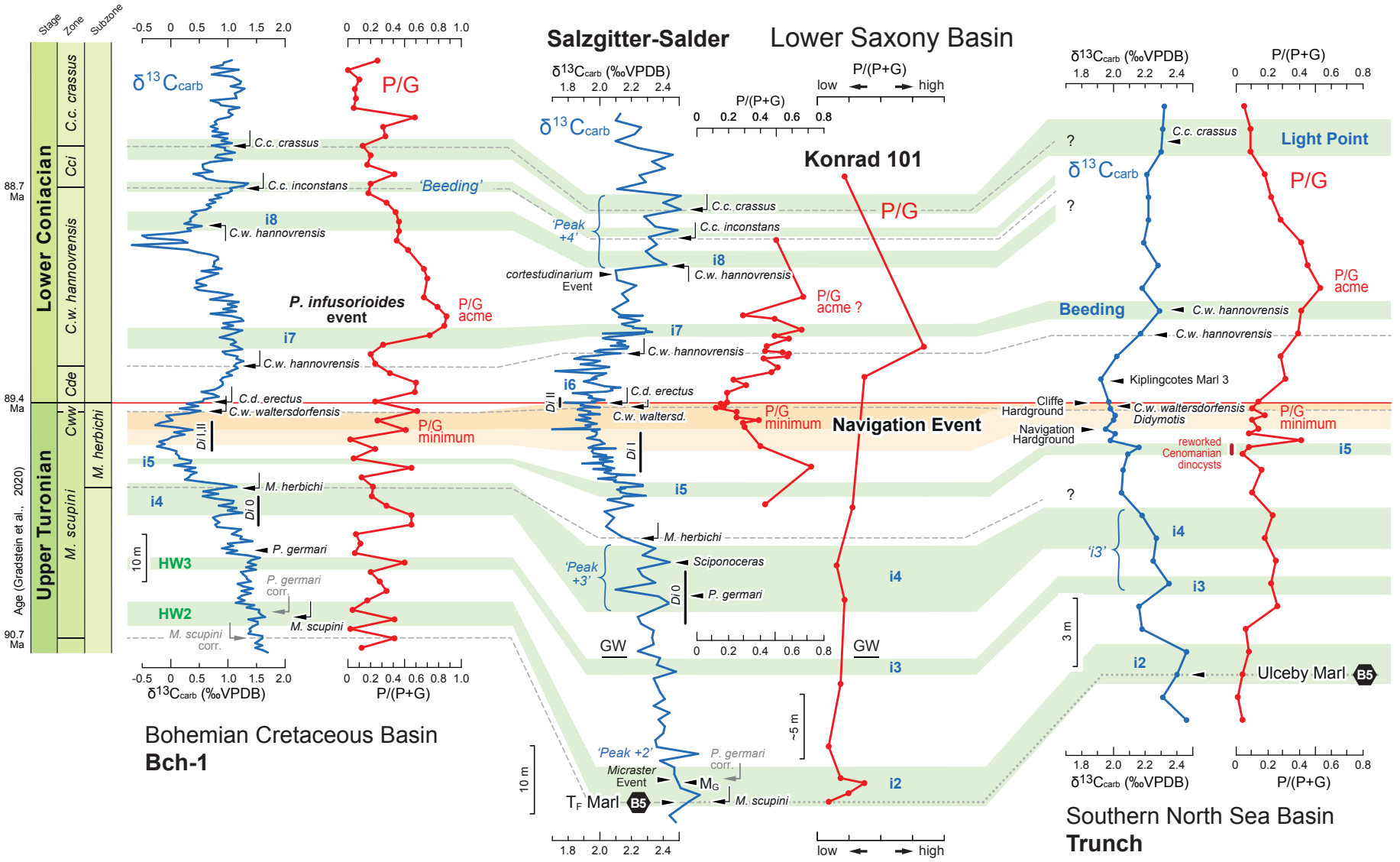
Stage
Zone
Subzone
Lower Coniacian
Upper Turonian
C.c. crassus
Cci
C.w. hannovrensis
Cde
Cww
M. scupini
M. herbichi
88.7 Ma
89.4 Ma
90.7 Ma
Age (Gradstein et al., 2020)
δ13Ccarb
P/G
C.c. crassus
C.c. inconstans
'Beeding'
i8
C.w. hannovrensis
P. infusorioides event
P/G acme
i7
C.w. hannovrensis
C.d. erectus
C.w. waltersdorfensis
Di I,II
P/G minimum
i5
M. herbichi
i4
Di 0
10 m
HW3
P. germari
P. germari corr.
HW2
M. scupini
M. scupini corr.
δ13Ccarb (‰VPDB)
P/(P+G)
Bohemian Cretaceous Basin
Bch-1
Salzgitter-Salder
Lower Saxony Basin
Konrad 101
'Peak +4'
cortestudinarium Event
P/G acme ?
Di II
C.w. waltersd.
Navigation Event
Di I
'Peak +3'
Sciponoceras
GW
~5 m
'Peak +2'
Micraster Event
P. germari corr.
MG
TF Marl
B5
low
high
Light Point
Beeding
Kiplingcotes Marl 3
Cliffe Hardground
Navigation Hardground
Didymotis
reworked Cenomanian dinocysts
'i3'
3 m
i2
Ulceby Marl
Southern North Sea Basin
Trunch

of the stage boundary. A higher resolution isotope study at Trunch is required to further address this issue.

### 4.7.4 Bio- and chemostratigraphic correlation of Salzgitter-Salder to Bch-1

Numerous and relatively continuous inoceramid records are available from Salzgitter-Salder and Bch-1 that enable a more precise placement of inoceramid zone boundaries than in the English Chalk (Walaszczyk et al., 2010; Uličný et al., 2014; Čech and Uličný, 2020; Voigt et al., 2020). However, correlation the German and Czech sections is complicated by the erratic isotope signature of the uppermost Turonian – Coniacian interval within the Bch-1 core (Fig. 11). Here $\delta^{13}C_{carb}$ falls below 0‰ in some intervals, compared to values around 2‰ at Salzgitter-Salder, Trunch and in most other European sections (e.g. Jenkyns et al., 1994; Wiese, 1999; Stoll and Schrag, 2000; Jarvis et al., 2006; Wilmsen et al., 2019). This points to a significant and variable diagenetic overprint in Bch-1, likely caused by the addition of organic-derived carbonate cements in the relatively carbonate-poor sediments (<40% $CaCO_3$; Jarvis et al., 2015).

Despite concerns regarding diagenesis effecting $\delta^{13}C_{carb}$ values, near-coincidence of major peaks and troughs in the companion $\delta^{13}C_{org}$ profiles for Bch-1 (Fig. 10) support the preservation of a primary chemostratigraphic signal. Minor disparities between the correlations of isotope events by different authors remain (e.g. compare Čech and Uličný, 2020; Voigt et al., 2020). Our preferred correlation is shown in Fig. 12. Of note is the offset between the LO of *C. d. erectus* reported by Čech and Uličný (2020) and the onset of the $\delta^{13}C_{carb}$ rise marking the top of the Navigation CIE. This revises the previous placement of the LO, which was based on regional correlation to other sections (Uličný et al., 2014; Jarvis et al., 2015; Olde et al., 2015b), where the LO and isotope shift were considered to be coincident. It is notable that at Střeleč Quarry, a candidate GSSP auxiliary section in the Bohemian Cretaceous Basin, a shift to rising $\delta^{13}C_{org}$ values occurs exactly at the LO of *C. d. erectus* (Čech and Uličný, 2020), which is consistent with records from the adjacent Střeleč core.

### 4.7.5 Bio- and chemostratigraphic correlation of Salzgitter-Salder to Trunch

Correlation of the upper Turonian between Salzgitter-Salder and Trunch is achieved using the $T_F$ Marl which coincides with the base *M. scupini* Zone. This marl is interpreted to be a bentonite (Bräutigam, 1962; Ernst et al., 1979; Wray, 1995; B5 of Jarvis et al., 2006; Fig. 12) that is correlative to the Ulceby Marl in northern England and the Lewes Marl in southern England, based on biostratigraphy and chemostratigraphy employing the rare-earth element and trace-element geochemistry of marl seams (Wray, 1995, 1999; Wray et al., 1996; Wray and Wood, 1998). The immediately overlying CIE was termed i2 by Jarvis et al. (2006) which is correlated here to the HW2 CIE of Uličný et al. (2014) at Bch-1 (Fig. 12). A proposed correlation of other uppermost Turonian CIEs is shown in Fig. 12.

The base of the Coniacian is placed at the Cliffe Hardground at Trunch (Section 4.7.3). Correlation within the lower Coniacian is more difficult. Comparison between Salzgitter-Salder and Bch-1 shows significant differences in the shape of the $\delta^{13}C_{carb}$ profiles due to diagenetic overprinting at the latter locality (Section 4.7.4), but the correlation is well constrained by detailed inoceramid biostratigraphy (Fig. 12). For Trunch there is good correspondence in the values and shape of the $\delta^{13}C_{carb}$ curve compared to Salzgitter-Salder but the $\delta^{13}C_{carb}$ data from Trunch lack stratigraphic resolution, and inoceramid records are limited. However, the Trunch isotope stratigraphy is important because the carbon isotope profile for the mid-upper Turonian to low middle Coniacian from the core was used by Jarvis et al. (2006) to construct their English Chalk composite curve, which continues to provide a major international reference (Cramer and Jarvis, 2020).

The carbon isotope stratigraphy of the lower Coniacian (approximating to the English *Micraster cortestudinarium* Zone) hinges on the recognition and correlation of two positive isotope excursions: the Beeding and the Lightpoint events (Jarvis et al., 2006). Above these, the next CIE, a stepped rise defining the East Cliff Event, occurs within the lower part of the middle Coniacian (*Micraster coranguinum* Zone). The Beeding CIE was defined by Jarvis et al. (2006 p. 582) as "*A positive $\delta^{13}C$ excursion of + 0.5‰ to maximum values of 2.1‰ occurs around the level of the Beeding Hardground at Dover*". This was constrained biostratigraphically by the LO of "*Cretirhynchia" subplicata* (Datum 32; a M.

cortestudinarium Zone marker species, Simon and Owen, 2001), below, and the LO of *Cremnoceramus schloenbachi* (Böhm) (Datum 33; = *C. crassus* Walaszczyk and Wood, 1998) with *C. inconstans woodsi* (Fiege) in the *Cremnoceramus* band, above (Bailey et al., 1983; Jarvis et al., 2006, fig. 7; Prince et al., 2008, fig. 2). Although defined at Dover, the $\delta^{13}C_{carb}$ data used for the English composite curve were derived from the correlative interval at Trunch because the section there is more expanded.

Biostratigraphic placement of the Beeding Event at Trunch is constrained by two beds yielding *C. w. hannovrensis*, one coincident with the $\delta^{13}C_{carb}$ maximum and the other 1 m below (Figs. 11, 12; Wood et al., 1994). The lower bed and LO of *C. w. hannovrensis* has also yielded "*C.*? *rotundatus*" (i.e. *C. d. erectus*), which points to the Beeding CIE lying within the lower *C. w. hannovrensis* Zone. Based in these records and comparison of the isotope profile shapes and values indicates that the Beeding CIE correlates to i7 at Salzgitter-Salder, as originally suggested by Jarvis et al. (2006 fig. 8) and Voigt (in Walaszczyk et al., 2010). A record of *C. c. crassus* (= *Cremnoceramus* ex gr. *schloenbachi* (Böhm) of Wood et al., 1994) within the interval of the Light Point CIE around 419 – 420 m at Trunch place this with the *C. c. crassus* Zone (Fig. 11). This zone lies at the top of the Salzgitter-Salder section and above the level of our sampling from the Quarry. No detailed correlation is possible given the limitations of the Trunch data (Fig. 12).

The correlation of the Beeding CIE to i7 has not been universally adopted. Uličný et al. (2014), Olde et al. (2015b), Jarvis et al. (2015) and Voigt et al. (2020) equated the Beeding CIE to the marked coincident $\delta^{13}C_{org}$ and $\delta^{13}C_{carb}$ peaks immediately above the LO of *C. c. inconstans* at Bch-1 and to the top of 'Peak +4' of Wiese (1999) at Salzgitter-Salder (Fig. 12). This was based on a single record of *C. c. inconstans* from the level of the Hope Gap Hardground at Dover, immediately below the Beeding CIE (Bailey et al., 1983). The maximum value of the $\delta^{13}C$ peak defining the Beeding Event (data derived from Jenkyns et al., 1994) occurs between the Hope Gap and Beeding Hardgrounds at Dover. This is correlated to nodular chalks yielding *C. w. hannovrensis* at 427 m depth in the Trunch borehole (Fig. 11; Jarvis et al., 2006, fig. 7; Pearce et al., 2020). The records of *C. c. inconstans* and *C. w. hannovrensis* at equivalent stratigraphic levels at Dover and Trunch could potentially place the Beeding CIE within the basal *C. c. inconstans* Zone around the

level of the *Isomicraster* Event (Bed 75 at Salzgitter-Salder; cf. Walaszczyk and Wood, 1998, fig. 6). However, the inoceramid data from Trunch and $\delta^{13}C_{carb}$ correlation between Salzgitter-Salder and Trunch (Fig. 12) points to the Beeding CIE lying within the lower *C. w. hannovrensis* Zone and not the *C. c. inconstans* Zone.

### 4.7.6 An early Coniacian P/G ratio acme and the *P. infusorioides* Event

The dinocyst data presented here offer additional criteria to characterize and correlate Turonian – Coniacian boundary sections. A prominent common feature of the dinocyst distribution charts (Figs. 4, 10, 11) is a general dominance of *P. infusorioides* through most of the succession, with a minimum within the beds constituting the Navigation Event and a broad acme within the lower Coniacian.

*Palaeohystrichophora infusorioides* stands out as the main peridinioid dinocyst (P-cyst) in an assemblage otherwise dominated by gonyaulacoid cysts (G-cysts). Stratigraphic and spatial variation in dinocyst assemblage composition is commonly expressed by comparing changes in the relative proportions of these two major groups of dinocyst. The P/G ratio, obtained by the equation P/G = nP/(nP + nG), where n is the number of specimens counted, P are peridinioid (or protoperidinioid) dinocysts and G are gonyaulacoid dinocysts (Powell et al., 1992; Eshet et al., 1994; de Vernal and Marret, 2007; Pearce et al., 2009; Prauss, 2015; Tahoun et al., 2018; Amenábar et al., 2020; Leandro et al., 2020), is generally regarded as a proxy for nutrient availability and palaeoproductivity (Powell et al., 1992; Eshet et al., 1994). Recently, the P/G ratio was used by Tahoun et al. (2018) to define stratigraphic dinocyst "ecological zones" in a monotonous mid-Cenomanian to Campanian carbonate succession in Egypt.

In addition to *Palaeohystrichophora*, the principal peridinioid genera in the Turonian – Coniacian boundary interval of our study sections are *Chatangiella*, *Isabelidinium*, and *Subtilisphaera* (Appendix A; Supplementary data Table 1; Figs. 4, 9–11). A dominance of peridinioid cysts, principally *P. infusorioides*, with a minimum in the P/G ratio immediately below the Turonian – Coniacian stage boundary, followed by a marked influx and acme in the lower Coniacian is a common feature in eastern England, the Czech Republic and

northern Germany (Fig. 12). The question remains whether the well-developed influxes of *P. infusorioides* and P/G ratio acmes at Salzgitter-Salder, Bch-1 and Trunch are synchronous.

Based on available inoceramid bivalve records and the $\delta^{13}C_{carb}$ profiles from the three sections (Fig. 12), a good match can be achieved that places the P/G acme and a *P. infusorioides* Event consistently within the basal *C. w. hannovrensis* Zone. Assigning the Beeding Event to the *C. c. inconstans* Zone based on the single record of *C. c. inconstans* at Dover (Bailey et al., 1983) generates a significant temporal offset in the timing of the acme. It is notable that Wood et al. (2004) revised many previously published inoceramid species identifications from England, casting doubt on some earlier records. Testing the placement of the acme and *P. infusorioides* Event at Dover rather than the correlative section at Trunch is not possible because sections in East Kent yield C-H assemblages with only sparse *P. infusorioides* and other peridinioid taxa throughout the upper Turonian and Coniacian (FitzPatrick, 1992; Prince et al., 2008).

The isochronous nature of the early Coniacian P/G ratio acme and *P. infusorioides* Event needs to be tested further with the study of additional sections, re-examination of available inoceramid material, and acquisition of new biostratigraphic data and a higher resolution $\delta^{13}C_{carb}$ profile for Trunch. On balance, however, a synchronous basal *C. w. hannovrensis* Zone age is proposed here, making the P/G ratio acme and *P. infusorioides* Event consistent lower Coniacian markers.

### *4.8 Dinocyst events and late Turonian – early Coniacian palaeoenvironmental change*

The changing dinocyst assemblages observed through the upper Turonian – lower Coniacian in northern Germany, Czech Republic and eastern England reflect the response of the Late Cretaceous phytoplankton to long-term palaeoenvironmental change. This can be expressed by changes in the P/G ratio, P-cysts being dominated by *P. infusorioides,* and the *Circulodinium* - *Heterosphaeridium / Spiniferites* - *Palaeohystrichophora* (C-H/S-P) ratio. These indexes enable easier comparison of trends between assemblages with varying species compositions.

The P/G ratio is generally regarded as a proxy for nutrient availability and palaeoproductivity (Powell et al., 1992; Eshet et al., 1994; de Vernal and Marret, 2007; Pearce et al., 2009; Prauss, 2015; Tahoun et al., 2018; Amenábar et al., 2020; Leandro et al., 2020), based on observations of the distribution of living protoperidinioid dinoflagellates and their cyst records in associated sediments (e.g. Reichart and Brinkhuis, 2003). Application of the P/G ratio to the geologic record assumes that extinct species of dinoflagellates generating P-cysts would have had the same heterotrophic habit as the living dinoflagellate genus *Protoperidinium*, while G-cysts would have originated from dinoflagellates with a phototrophic or mixotrophic behaviour (Sluijs et al., 2005; de Vernal and Marret, 2007; Esper and Zonneveld, 2007).

Protoperidinioid dinoflagellate species feed mainly on diatoms and other phytoplankton, so high relative abundances of P-cysts characterize areas of high organic productivity driven by an elevated concentration of dissolved nutrients in surface waters, such as upwelling zones, inner shelf environments, and estuaries (Powell et al., 1990; Sluijs et al., 2005; de Vernal and Marret, 2007). By contrast, a high relative abundance of G-cysts suggests nutrient-poor outer shelf or open ocean waters. However, it is known that some modern peridinioid dinoflagellates are phototrophic autotrophs (Dale and Fjellså, 1994; Sluijs et al., 2005) and no consensus exists on which Cretaceous peridinioid dinocysts are associated with heterotrophic dinoflagellates, which complicates the interpretation of the P/G ratio. However, evidence suggests (e.g. Eshet et al., 1994; Reichart and Brinkhuis, 2003), as also pointed out by Pearce et al. (2009), that although the inclusion of some peridinioid cysts from phototrophic dinoflagellate species in such a ratio will modify the palaeoenvironmental signal, it will not obscure it.

It is clear that environmental changes evidenced by changing dinocyst assemblage compositions, like those expressed by the P/G ratio, may not be synchronous on a regional to global scale. Nonetheless, such changes may generate reliable stratigraphic marker events. For example, a pulse and subsequent abundance peaks of the Boreal G-cyst *Cyclonephelium compactum–membraniphorum* morphological plexus in the upper Cenomanian of mid-latitude sites, are interpreted to be associated to transient cooling and water mass reorganisation during the Plenus Cold Event, and show a high degree of regional

synchroneity (Eldrett et al., 2014, 2017; Van Helmond et al., 2014, 2016), despite the plexus persisting as a major constituent of assemblages during subsequent warming (Dodsworth et al., 2020).

The dominant P-cyst (and dominant dinocyst in many parts of the Turonian – Coniacian boundary sections studied), *P. infusorioides*, has previously been interpreted to have predominated at offshore sites of upwelling in Late Cretaceous epicontinental seas lacking significant terrestrial influence (Gedl, 2007; Pearce et al., 2009), or to be associated with episodes of increased runoff and supply of land-derived nutrients, with reduced salinity and stratified water masses (e.g. Van Helmond et al., 2014; Tahoun et al., 2018). In Bch-1, high relative abundances of *P. infusorioides* generating high P/G ratios through the lower Turonian – lower Coniacian (Olde et al., 2015b) occur consistently in intervals with the lowest terrestrial/marine palynomorph (T/M) ratios. Terrestrial palynomorphs are minor constituents throughout the Turonian – Coniacian boundary interval at Salzgitter-Salder. There, the only three samples with slightly elevated T/M ratios, associated with pulses of fungal hyphae in beds 44, 51b and 60 (Supplementary data Table 1), show similar or lower P/G ratios than adjacent samples. Terrestrial palynomorphs are unrecorded from many samples at Trunch and they show no association with the P/G ratio peak.

It is concluded that an increased terrestrial nutrient supply was unlikely to have been the mechanism driving phases of enhanced productivity at any of our Turonian – Coniacian boundary study sites. This is perhaps surprising for Bch-1, given the site's palaeogeographic position in close proximity to the Central European and Sudetic Islands (Fig. 1), and a greater terrestrial influence, reflected by higher non-carbonate and higher terrestrial palynomorph contents than any of the other study sites. The *P. infusorioides* Event and P/G acme is therefore interpreted to reflect a regional productivity pulse driven by upwelling and period of ocean current reorganisation, which was likely associated with latest Turonian – earliest Coniacian sea-level fall and subsequent Coniacian transgression (Hancock and Kauffman, 1979; Haq, 2014; Uličný et al., 2014).

## 5 Calcareous nannofossils results and discussion

Lees (2008) recorded calcareous nannofossils throughout the entire section of Salzgitter-Salder, and at particularly high-resolution from beds 35 to 53. Recovered assemblages were moderately rich taxonomically (species richness typically 30 – 40), reasonably well preserved, and stratigraphically comparable to other coeval sections (see Lees, 2008, fig. 6). This is fully consistent with our records. By contrast, Sikora et al. (2004, p.225) had concluded previously that "*Nannofossils are consistently rare to very rare and poorly preserved throughout the Salzgitter-Salder section, making meaningful biostratigraphic zonation very difficult*". Most samples were reported to contain 10 or fewer taxa, which is in contrast to a median of 36 different species observed per sample in this study (see Appendix B, Supplementary data Table 2).

The preservation of nannofossils in our studied samples from beds 32 – 72, spanning the stage boundary interval at Salzgitter-Salder, varies from poor (14 samples), through moderate (24 samples), to good (3 samples). The occurrences of selected nannofossils are plotted in Fig. 13 and illustrated in Fig. 14. Nannofossil abundances are relatively low in all samples. The presence of *Broinsonia parca expansa* (lowest occurrence in nannofossil-zone UC9a; Fig. 14D) together with *Marthasterites furcatus* (LO = base nannofossil-zone CC13; Fig. 14R) throughout the sampled boundary interval (Fig. 13), and the absence of *Micula staurophora* (lowest occurrence in biozone UC10), demonstrate that the entire boundary section can be assigned to calcareous nannofossil Zone UC9c of Burnett (1998), and CC13 of Sissingh (1977) and Perch-Nielsen (1985). This assignment was formerly recognized by Lees (2008) and confirmed by Püttmann (in Voigt et al., 2020).

The LO of *Broinsonia parca* subsp. *expansa* (Fig. 14D), together with *Zeugrhabdotus biperforatus* (Fig. 14II), has been recorded from the basal *M. scupini* Zone Marl MG at Salzgitter-Salder (Lees, 2008, table 1; Voigt et al., 2020 fig. 6), 38 m below the base of our study section. The HO of *Helicolithus turonicus* (Fig. 14O), proposed by Lees (2008) as a marker event located slightly above the Turonian – Coniacian boundary, is now recorded in Bed 62, about 6.5 m higher than previously identified (Fig. 13). The LO of *Micula adumbrata*, a possible ancestral form to *M. staurophora* (Young et al., 2020), was not

**Fig. 13.** Calcareous nannofossil range chart showing the relative abundance of representative taxa from the Turonian – Coniacian boundary interval at Salzgitter-Salder. Stratigraphic framework after Fig. 3. Stratigraphically significant taxa are highlighted by bold text and purple ornament. Note the *M. furcatus* maximum in the upper *C.d. erectus* Zone, and the HO of *H. turonicus* in Bed 62, mid-*C. w. hannovrensis* Zone. Yellow curves highlight abundance increases in cooler water indicator species across the Turonian – Coniacian boundary (see text, Section 5.2). Nannofossil zones: [1] Burnett et al. (1998); [2] Sissingh (1977) and Perch-Nielsen (1985).

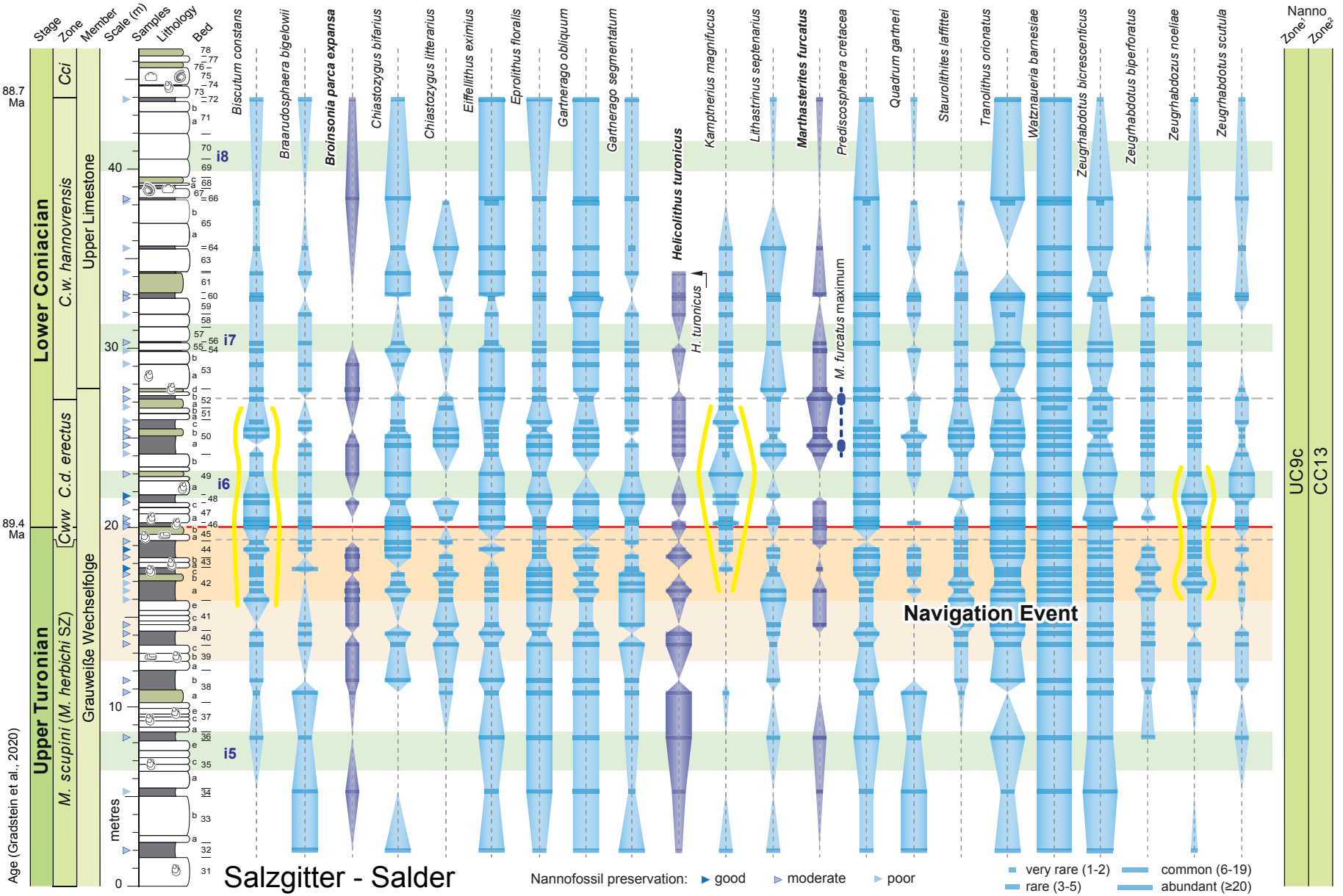
Stage
Zone
Member
Scale (m)
Samples
Lithology
Bed
Nanno Zone[1] Zone[2]
Age (Gradstein et al., 2020)
88.7 Ma
89.4 Ma
Lower Coniacian
Upper Turonian
Cci
C.w. hannovrensis
C.d. erectus
Cww
M. scupini (M. herbichi SZ)
Upper Limestone
Grauweiße Wechselfolge
metres
0
10
20
30
40
i8
i7
i6
i5
Biscutum constans
Braarudosphaera bigelowii
Broinsonia parca expansa
Chiastozygus bifarius
Chiastozygus litterarius
Eiffellithus eximius
Eprolithus floralis
Gartnerago obliquum
Gartnerago segmentatum
Helicolithus turonicus
H. turonicus
Kamptnerius magnificus
Lithastrinus septenarius
Marthasterites furcatus
M. furcatus maximum
Prediscosphaera cretacea
Quadrum gartneri
Staurolithites laffittei
Tranolithus orionatus
Watznaueria barnesiae
Zeugrhabdotus bicrescenticus
Zeugrhabdotus biperforatus
Zeugrhabdotus noeliae
Zeugrhabdotus scutula
Navigation Event
UC9c
CC13
Salzgitter - Salder
Nannofossil preservation: good moderate poor
very rare (1-2)
rare (3-5)
common (6-19)
abundant (≥20)

**Fig. 14.** Selected calcareous nannofossils from the Turonian – Coniacian boundary interval, Salzgitter-Salder. **A**. *Ahmuelerella regularis*, Bed 46 top. **B**. *Biscutum melaniae*, Bed 42c top. **C**. *Braarudosphaera bigelowii,* Bed 50 sample 59. **D**. *Broinsonia parca expansa*, Bed 44 base. **E**. *Corolithion signum*, Bed 44a top. **F**. *Cretarhabdus conicus,* Bed 42c bottom. **G**. *Cyclagelosphaera margerelii*, sample 48. **H**. *Discorhabdus ignotus*, Bed 44 middle. **I**. *Eprolithus floralis*, Bed 56. **J**. *Eprolithus moratus*, Bed 50 sample 57. **K**. *Gartnerago obliquum*, Bed 46 base. **L**. *Gartnerago segmentatum*, Bed 49a. **M**. *Helicolithus compactus*, Bed 54. **N**. *Helicolithus trabeculatus*, Bed 44 middle. **O**. *Helicolithus turonicus*, Bed 60 top. **P**. *Kamptnerius magnificus*, Bed 48 top. **Q**. *Lithastrinus septenarius*, Bed 40 top. **R**. *Marthasterites furcatus*, Bed 48 base. **S**. *Miravetesina bergenii*, Bed 44 base. **T**. *Nannoconus* cf. *regularis,* Bed 50 top. **U**. *Prediscosphaera cretacea*, Bed 40 top. **V**. *Prediscosphaera ponticula*, Bed 42a middle. **W**. *Prediscosphaera spinosa*, Bed 40 base. **X**. *Quadrum gartneri*, Bed 36. **Y**. *Quadrum intermedium*, Bed 50 sample 58. **Z**. *Rhagodiscus achlyostaurion*, Bed 40 top. **AA**. *Rhagodiscus angustus*, Bed 38b. **BB**. *Seribiscutum primitivum*, Bed 48 base. **CC**. *Tegumentum stradneri*, Bed 50 sample 59. **DD**. *Tranolithus minimus*, Bed 44 middle. **EE**. *Watznaueria barnesiae*, Bed 49a. **FF**. *Watznaueria biporta*, Bed 56. **GG**. *Zeugrhabdotus acanthus*, Bed 42a top. **HH**. *Zeugrhabdotus bicrescenticus,* Bed 46 top. **II**. *Zeugrhabdotus biperforatus*, Bed 36. Scale bar in A (5 µm) is valid for all specimens.

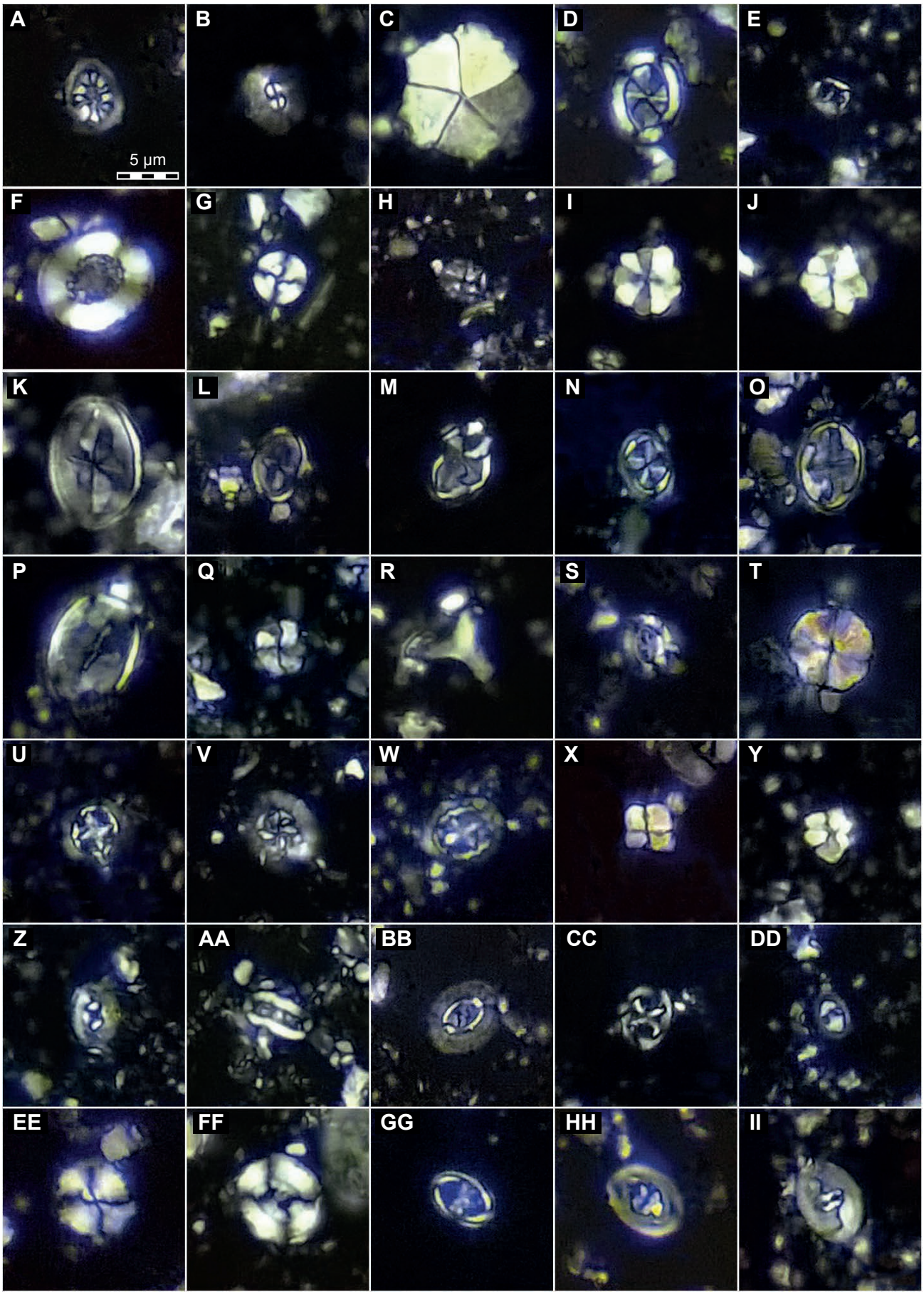
A
5 µm
B
C
D
E
F
G
H
I
J
K
L
M
N
O
P
Q
R
S
T
U
V
W
X
Y
Z
AA
BB
CC
DD
EE
FF
GG
HH
II

recorded in the studied interval, but has been documented from Bed 105, high in the lower Coniacian *C. c. crassus* Zone (Lees in Walaszczyk et al., 2020). This is stratigraphically higher than the LO of the species in the Czech Bch-1 borehole, where it appears in the mid-*C. d. erectus* Zone (Uličný et al., 2014).

*Micula staurophora* has not been observed in Salzgitter-Salder Quarry. The species appears in the basal *Inoceramus frechi / I. gibbosus* Zone at Bch-1 (Čech and Uličný, 2020), 12 m below the top of the core and immediately above the section analysed by Uličný et al. (2014) and Olde et al. (2015b). This suggests that the base of UC10 lies stratigraphically above the top of the section exposed in Salzgitter-Salder Quarry (cf. Fig. 12).

## *5.1 Calcareous nannofossil abundance*

A total of 119 different nannofossil taxa were recorded from the boundary interval sample suite (Appendix B, Supplementary data Table 2). The median species richness is 36 different taxa per sample, with a minimum of 6 species in Bed 52 and a maximum of 56 species in Bed 42c. The nannofossil assemblages are dominated by *Watznaueria barnesiae* (Fig. 14EE), *Tranolithus orionatus* and *Zeugrhabdotus bicrescenticus* (Fig. 13). Further common to abundant taxa with continuous occurrences are *Gartnerago obliquum* (Fig. 14K), *Prediscosphaera cretacea* (Fig. 14U) and *Eiffellithus eximius*. These taxa are characterized by rather large and robust coccoliths. The rarity of delicate taxa, and overgrowth observed on individual coccoliths, suggest a slight diagenetic overprint of the nannofossil assemblages. Therefore, the palaeoecological signal provided by the calcareous nannofossils is interpreted with caution.

## *5.2 Relative abundance trends*

The overall high abundances of *Watznaueria barnesiae* and *Tranolithus orionatus,* and the absence of major fluctuations in the nannofossil assemblage compositions observed throughout the studied Turonian – Coniacian boundary interval reflect generally stable, warm and oligotrophic to mesotrophic surface water conditions (Lees et al., 2004; Linnert and Mutterlose, 2015). The taxon *Biscutum constans*, associated with mesotrophic to eutrophic and likely cooler waters, is generally rare in Salzgitter-Salder compared to more

near-shore deposits in NW Germany (Linnert and Mutterlose, 2015; Püttmann and Mutterlose, 2019).

Slightly increased abundances of *B. constans* occur around the Turonian – Coniacian boundary interval in beds 42 – 50, which coincide with an increase of *Zeugrhabdotus noeliae* between beds 42 – 48 (Fig. 13). Both species likely have an affinity to eutrophic, cooler water conditions (Linnert and Mutterlose, 2015). A similar trend is displayed by the species *Kamptnerius magnificus* (Fig. 14P) in beds 46 – 50, a taxon that has also been associated with cooler sea-surface conditions (Thierstein, 1981; Thibault and Gardin, 2006; Thibault et al., 2015, 2016; Guerra et al., 2016). Besides the relatively stable conditions reflected by the overall nannofossil assemblage, the relative increase of *B. constans*, *Z. noeliae*, and *K. magnificus* points to a possible phase of cooling and elevated nutrient levels across the Turonian – Coniacian boundary interval. This increase immediately preceeds and overlaps with the influx in peridinioid dinocysts in Bed 50 and the *M. furcatus* maximum in beds 50 – 52. It is notable that the abundance peak in the three nannofossil taxa spanning the stage boundary coincides with the dinocyst diversity maximum (Fig. 7).

## *5.3 Correlation of NW European Turonian – Coniacian boundary sections by calcareous nannofossil events*

### 5.3.1 Słupia Nadbrzeżna

The Turonian – Coniacian boundary section exposed at Słupia Nadbrzeżna is correlated to beds 38 – 49 at Salzgitter-Salder (Voigt et al., 2020) and is considered here to lie entirely within nannofossil-zones UC9c and CC13, despite discontinuous records of some marker taxa, including *M. furcatus* (Lees, 2008). The HO of *H. turonicus* is located directly above the proposed boundary but the species occurs rarely and sporadically in the section.

### 5.3.2 Bohemian Cretaceous Basin Bch-1 borehole

Integrated stratigraphic data, including a biozonation based on calcareous nannofossils, was provided by Uličný et al. (2014) for the Bch-1 borehole. Both the Navigation CIE and the LO of *Cremnoceramus deformis erectus* are located at the lower part of nannofossil zone UC9c,

between the LO of *Broinsonia parca expansa* in the mid-*M. scupini* Zone and the LO of *M. staurophora* in the basal *Inoceramus frechi / I. gibbosus* Zone (Čech and Uličný, 2020).

In contrast to Salzgitter-Salder, the *M. furcatus* acme is more extensive in the Bch-1 core, covering a 74 m thick interval from a short distance above the LO of B*. parca expansa* in the mid-*M. scupini* Zone to the mid-*C. c. inconstans* Zone (Čech and Uličný, 2020). The *M. furcatus* acme event includes the LO of *M. adumbrata* in the lower *C. w. hannovrensis* Zone (Čech and Uličný, 2020) which is stratigraphically considerably lower than the LO of the species recorded at Salzgitter-Salder in the *C. c. crassus* Zone. A *M. furcatus* acme is developed more widely in the Turonian – Coniacian boundary interval of the Bohemian Cretaceous Basin and Outer Flysch Carpathians of the Czech Republic (Švábenická and Bubík, 2014). However, further quantitative analysis is necessary to precisely define the *M. furcatus* acme and evaluate its stratigraphic reliability using data from additional sections.

### 5.3.3 Trunch borehole

The Turonian – Coniacian boundary interval of the Trunch borehole discussed here (Fig. 11), with palynological data derived from Pearce et al. (2020), was placed entirely within nannofossil-zone CC13 by Burnett (in McArthur et al., 1993), allowing for the large uncertainty ascribed to the position of the CC12/13 boundary (±11 m) caused by the low sampling resolution. Detailed nannofossil records remain unpublished.

## 6 General discussion

Sikora et al. (2004) argued that the low-diversity dinocyst flora dominated of *P. infusorioides* was typical of very shallow water. We do not agree with this interpretation. The motile stage of *P. infusorioides* was probably a heterotroph, and the taxon responded principally to surface water fertility. It can be found in shallow-water settings if there was a high terrestrial nutrient input, but the very low relative abundance of terrestrial palynomorphs in the assemblages at Salzgitter-Salder, on average <3% (Supplementary data Table 1), precludes a significant terrestrial influence. Contrary to the view of Sikora et al. (2004), assemblages that yield high abundances of *P. infusorioides* at Salzgitter-Salder are far from being monospecific. Indeed, diversity remains moderately high throughout, despite very

wide fluctuations in both the absolute and relative abundance of *P. infusorioides* (Figs. 6, 7). The assertion that "*High-diversity, high-abundance events that include relatively abundant deep-water taxa (i.e.* Pterodinium *spp.)*" is also not substantiated. The nannofossil assemblages lack the high relative abundances of *B. constans* and other features that characterise shallow-water deposits in the region (cf. Püttmann and Mutterlose, 2019).

No relationship is apparent between dinocyst abundance or diversity parameters and the 100 kyr productivity cycles derived from sediment stacking patterns and spectral analysis of stable-isotope time-series (compare Fig. 3; Voigt et al., 2020). This contrasts with the middle to lower upper Turonian of the Bohemian Cretaceous Basin Bch-1 core where a correlation between levels of increased dinocyst species richness and flooding surfaces has been observed (Olde et al., 2015b). This was attributed to periods of rapid sea-level rise causing influxes of more diverse 'outer shelf' assemblages, with the addition of shallower-water species, postulated to have been carried into the central basin by hypopycnal flows. In the case of the Lower Saxony Basin, the organic plankton appear insensitive to flooding events. Calcareous nannofossils also show no clear relationship to the cycles.

## 7 Conclusions

Detailed study of the palynology of the Turonian – Coniacian boundary interval at Salzgitter-Salder Quarry, combined with stratigraphic and taxonomic revision of dinocyst records from the nearby Konrad 101 borehole at Salzgitter-Beddingen, provide a biostratigraphic framework for the proposed Coniacian GSSP at Salzgitter-Salder Quarry. Key elements are:

(1) A succession of dinocyst events characterise the upper Turonian, from base to summit: LO of *Cribroperidinium wilsonii* (upper *I. perplexus* Zone); LO of *Raetiaedinium truncigerum* (lower *M. striatoconcentricus – M. labiatoidiformis* Zone); LO of *Oligosphaeridium pulcherrimum* and influx of *Sepispinula ambigua* (base *M. scupini* Zone); LO of *Chatangiella ditissima* and acme of *Senoniasphaera turonica* (low *M. scupini* Zone), HO of *S. turonica* (mid-*M. scupini* Zone). The HO of *Cyclonephelium membraniphorum* coincides with the First Appearance Datum (FAD) of *C. d. erectus* in Salzgitter-Salder Quarry Bed 46 marking the base of the Coniacian Stage.

(2) The peridinioid cyst *Palaeohystrichophora infusorioides* dominates most assemblages through the stage boundary interval of the study sections but displays a minimum in the uppermost Turonian (summit of the *M. herbichi* Subzone and *C. w. walterdorfensis* Zone), within the interval of the $\delta^{13}C$ minimum that marks the Navigation carbon isotope event (CIE).
(3) A renewed influx, then acme of *P. infusorioides* with associated P/G ratio maximum occur in the lower Coniacian *C. w. hannovrensis* Zone.

A revised correlation of Lower Saxony Basin Salzgitter Quarry and Konrad 101 borehole sections with stratigraphically equivalent successions in the Bohemian Cretaceous Basin (Bch-1 borehole) and eastern England (Trunch borehole), indicates that the *P. infusorioides* and P/G acme is located a short distance above the level of the Beeding CIE. The stratigraphic position of the Beeding CIE in Lower Saxony and the Bohemian Cretaceous Basin is revised downwards to equate to the level of the i7 CIE.

The P/G acme marks an oceanic marine productivity pulse in the Bohemian, Lower Saxony and southern North Sea basins indicative of water mass reorganisation coincident with early Coniacian eustatic sea-level rise. There is no evidence of an increased terrestrial nutrient supply at this time.

Semi-quantitative analysis of calcareous nannofossils through the boundary interval at Salzgitter-Salder Quarry allows to identify three nannofossil events close to the stage boundary:

(1) *Helicolithus turonicus* has its highest occurrence in Bed 62 of the lower Coniacian *C. w. hannovrensis* Zone. The species is common throughout beds 36 to 44, slightly below the base Coniacian in Bed 46.
(2) *Marthasterites furcatus*, which has its LO at the base of the *M. scupini* Zone, occurs across the Turonian–Coniacian boundary but is common only in beds 50a and 52, slightly above the base Coniacian. A comparable but stratigraphically more extended *M. furcatus* acme has been reported from the Bohemian Cretaceous Basin and the Outer Carpathian deposits of the Czech Republic.

(3) A slight increase in the relative abundances of *Biscutum constans*, *Zeugrhabdotus noeliae* and *Kamptnerius magnificus* is recognized spanning the summit of the *M. herbichi* Subzone to upper *C. d. erectus* Zone, beds 42 to 50, coincident with a dinocyst diversity maximum. These taxa have been interpreted previously to have an association with cool-water, nutrient enriched conditions. Detailed quantitative data for Salzgitter-Salder and other sections are required to validate this relative increase as an additional marker for the Turonian – Coniacian boundary interval.

## Acknowledgements

Malcolm Jones (Palynological Laboratory Services Limited, PLS) is thanked for the preparation of the palynological samples. Support by Evolution Applied Limited to MAP and Equinor Energy AS (previously Statoil ASA) to IJ (contract 4502311303) is gratefully acknowledged. IW received financial support from National Science Centre (NCN) Grant no. 2018/31/B/ST10/01820. Paul Dodsworth, Birgit Niebuhr and Nicolas Thibault are thanked for their careful reviews and suggestions for improving the manuscript.

## Appendix A. List of palynological taxa

A complete list of organic-walled dinoflagellate cyst taxa and associated palynomorphs identified in our study of Turonian – Coniacian boundary section at Salzgitter-Salder Quarry is provided below. The classification of Fensome et al. (1993) is followed here, with references cited therein. The taxonomy of Fensome et al. (2019a) is employed and taxa are cited as they appear in that work, with additions from Pearce (2018) and Pearce and Williams (2018). Species marked with an asterisk (*) are illustrated on the Salzgitter-Salder range chart (Fig. 4). Stratigraphically significant species and selected other taxa are illustrated in Fig. 5.

*Division:* DINOFLAGELLATA (Bütschli, 1885) Fensome et al., 1993
*Subdivision:* DINOKARYOTA Fensome et al., 1993
*Class:* DINOPHYCEAE Pascher, 1914
*Subclass:* Dinophysiphycidae Möhn 1984 ex Fensome et al. 1993b
*Order:* Nannoceratopsiales Piel and Evitt 1980
*Family:* Nannoceratopsiaceae Gocht, 1970b
*Nannoceratopsis pellucida* Deflandre, 1939a

*Subclass:* PERIDINIPHYCIDAE Fensome et al., 1993
*Order:* GONYAULACALES Taylor, 1980
*Suborder:* CLADOPYXIINEAE Fensome et al., 1993
*Family:* CLADOPYXIACEAE Cladopyxiaceae Stein, 1883
*Microdinium*? *crinitum* Davey, 1969
*Microdinium setosum* Sarjeant, 1966b
*Microdinium* sp.A FitzPatrick 1992
*Microdinium* spp. Cookson and Eisenack, 1960

*Family:* PAREODINIACEAE Gocht, 1957
*Subfamily:* PAREODINIOIDEAE (Autonym)
*Protobatioladinium* spp. Nøhr-Hansen, 1986

*Family:* UNCERTAIN

*Rhiptocorys veligera* (Deflandre, 1937) Lejeune-Carpentier and Sarjeant, 1983

*Suborder:* GONYAULACINEAE (Autonym)

*Family:* GONYAULACACEAE Lindemann, 1928

*Subfamily:* CRIBROPERIDINIOIDEAE Fensome et al., 1993

*Apteodinium deflandrei* (Clarke and Verdier, 1967) Lucas-Clark, 1987

*Apteodinium* spp. Eisenack, 1958a

*Cribroperidinium* spp. Neale and Sarjeant, 1962

*Cribroperidinium wilsonii* (Yun, 1981) Poulsen, 1996

*Florentinia buspina* (Davey and Verdier, 1976) Duxbury, 1980

*Florentinia clavigera* (Deflandre, 1937b) Davey and Verdier, 1973

*Florentinia deanei* (Davey and Williams, 1966b) Davey and Verdier, 1973

*Florentinia ferox* (Deflandre, 1937) Duxbury, 1980

*Florentinia laciniata* Davey and Verdier, 1973

*Florentinia radiculata* (Davey and Williams, 1966a) Davey and Verdier, 1973

*Florentinia* spp. Davey and Verdier, 1973

*Florentinia*? *torulosa* (Davey and Verdier, 1976) Lentin and Williams, 1981

*Subfamily:* GONYAULACOIDEAE (Autonym)

*Achomosphaera granulata* Mao Shaozhi, 1989

**Achomosphaera ramulifera* (Deflandre, 1937) Evitt, 1963

**Achomosphaera regiensis* Corradini, 1973

*Achomosphaera sagena* Davey and Williams, 1966a

*Hystrichosphaeropsis ovum* Deflandre, 1935

**Hystrichostrogylon membraniphorum* Agelopoulos, 1964

*Impagidinium* spp. Stover and Evitt, 1978

*Psaligonyaulax deflandrei* Sarjeant, 1966

**Pterodinium cingulatum* subsp. *cingulatum* (Wetzel, 1933) Below, 1981

*Pterodinium cingulatum* subsp. *granulatum* (Clarke and Verdier, 1967) Lentin and Williams, 1981

*Spiniferites jarvisii* Pearce, 2010

**Spiniferites membranaceus* (Rossignol, 1964) Sarjeant, 1970

*Spiniferites porosus* (Manum and Cookson, 1964) Harland, 1973

*Spiniferites pseudofurcatus* (Klumpp, 1953) Sarjeant, 1970

**Spiniferites ramosus* subsp. *gracilis* (Davey and Williams, 1966b) Lentin and Williams, 1973

*Spiniferites ramosus* subsp. *granomembranaceus* (Davey and Williams, 1966a) Lentin and Williams, 1973

**Spiniferites ramosus* subsp. *granosus* (Davey and Williams, 1966b) Lentin and Williams, 1973

**Spiniferites ramosus* subsp. *ramosus* (Ehrenberg, 1838) Mantell, 1854

*Spiniferites ramosus* subsp. *reticulatus* (Davey and Williams, 1966a) Lentin and Williams, 1973

**Spiniferites* spp. Mantell, 1850

**Spiniferites twistringiensis* (Maier, 1959) Fensome et al., 1990

*Turnhosphaera hypoflata* (Yun Hyesu, 1981) Slimani, 1994

*Subfamily:* LEPTODINIOIDEAE Fensome et al., 1993

*Kleithriasphaeridium loffrense* Davey and Verdier, 1976

*Kleithriasphaeridium mantellii* (Davey and Williams 1966a) Fensome et al., 2016b

*Kleithriasphaeridium readei* (Davey and Williams, 1966b) Davey and Verdier, 1976

**Oligosphaeridium complex* (White, 1842) Davey and Williams, 1966b

**Oligosphaeridium pulcherrimum* (Deflandre and Cookson, 1955) Davey and Williams, 1966a

*Rhynchodiniopsis* spp. Deflandre, 1935

*Subfamily:* UNCERTAIN

*Callaiosphaeridium asymmetricum* (Deflandre and Courteville, 1939) Davey and Williams, 1966a

*Cometodinium*? *comatum* Srivastava, 1984

*Cometodinium obscurum* Deflandre and Courteville, 1939

*Cometodinium* spp. Deflandre and Courteville, 1939

*Coronifera hebospina* (Yun Hyesu, 1981) Peyrot, 2011

*Coronifera striolata* (Deflandre, 1937) Stover and Evitt, 1978 sensu Schiøler, 1992

*Hystrichodinium pulchrum* Deflandre, 1935

*Pervosphaeridium pseudhystrichodinium* (Deflandre, 1937) Yun, 1981

*Pervosphaeridium truncatum* (Davey, 1969) Below, 1982

**Scriniodinium campanula* Gocht, 1959

*Sentusidinium euteichum* (Davey, 1969) Wood et al., 2016

*Sentusidinium explanatum* (Bujak in Bujak et al., 1980) Wood et al., 2016

*Sentusidinium ringnesiorum* (Manum and Cookson, 1964) Wood et al., 2016

**Sentusidinium* spp. Sarjeant and Stover, 1978

*Surculosphaeridium longifurcatum* (Firtion, 1952) Davey et al., 1966

*Trichodinium castanea* Deflandre, 1935 ex Clarke and Verdier, 1967

*Family:* AREOLIGERACEAE Evitt, 1963

*Canningia glomerata* (Clarke and Verdier, 1967) Fensome et al., 2019b

*Canningia reticulata* Cookson and Eisenack, 1960

*Canningia spongireticulata* Prössl, 1990

*Circulodinium distinctum* (Deflandre and Cookson, 1955) Jansonius, 1986

*Cleistosphaeridium latoaculeum* (Yun, 1981) Fensome et al., 2019b

**Cyclonephelium membraniphorum* Cookson and Eisenack, 1962

*Senoniasphaera filoreticulata* (Slimani, 1994) Fensome et al., 2019b

*Senoniasphaera* spp. Clarke and Verdier, 1967

**Tenua colliveri* (Cookson and Eisenack, 1960) Helby, 1987

*Suborder:* CERATIINEAE Fensome et al., 1993

*Family:* CERATIACEAE Willey and Hickson, 1909

**Odontochitina costata* Alberti, 1961

**Odontochitina operculata* (Wetzel, 1933) Deflandre and Cookson, 1955

*Xenascus australensis* Cookson and Eisenack, 1969

*Xenascus blastema* (Davey, 1970) Stover and Helby, 1987a

*Xenascus ceratioides* (Deflandre, 1937) Lentin and Williams, 1973

*Xenascus* spp. Cookson and Eisenack, 1969

*Suborder:* GONIODOMINEAE Fensome et al., 1993

*Family:* GONIODOMACEAE Lindemann, 1928

*Subfamily:* PYRODINIOIDEAE Fensome et al., 1993

*Dinopterygium alatum* Cookson and Eisenack, 1962) Fensome et al., 2009

*Dinopterygium cladoides* Deflandre, 1935

*Dinopterygium konradense* Prössl, 1990

*Dinopterygium* spp. Deflandre, 1935

*Fetchamium prolixispinosum* (Davey and Williams, 1966a) Pearce and Williams, 2018

*Hystrichosphaeridium bowerbankii* Davey and Williams, 1966b

*Hystrichosphaeridium conispiniferum* Yun Hyesu, 1981

*Hystrichosphaeridium recurvatum* (White, 1842) Lejeune-Carpentier 1940

*Hystrichosphaeridium* spp. Deflandre, 1937b

**Hystrichosphaeridium tubiferum* subsp. *tubiferum* (Ehrenberg, 1838) Deflandre, 1937

*Suborder:* UNCERTAIN

*Family:* UNCERTAIN

*Atopodinium haromense* Thomas and Cox, 1988

*Batiacasphaera* spp. Drugg, 1970b

*Caligodinium aceras* (Manum and Cookson, 1964) Lentin and Williams, 1973

*Caligodinium amiculum* Drugg, 1970b

*Cassiculosphaeridia reticulata* Davey, 1969a

*Chlamydophorella discreta* Clarke and Verdier, 1967

*Chlamydophorella nyei* Cookson and Eisenack, 1958

*Dapsilidinium laminaspinosum* (Davey and Williams, 1966b) Lentin and Williams, 1981

*Dapsilidinium* spp. Bujak et al., 1980

*Desmocysta plekta* Duxbury, 1983

*Desmocysta* spp. Duxbury, 1983

*Ellipsodinium rugulosum* Clarke and Verdier, 1967

*Exochosphaeridium arnace* Davey and Verdier, 1973

*Exochosphaeridium majus* (Clarke and Verdier, 1967) Peyrot, 2011

**Exochosphaeridium phragmites* Davey et al., 1966

*Exochosphaeridium* spp. Davey et al., 1966

*Heterosphaeridium difficile* (Manum and Cookson, 1964) Ioannides, 1986

*Heterosphaeridium heteracanthum* (Deflandre and Cookson, 1955) Eisenack and Kjellström, 1972

*Heterosphaeridium heteracanthum* (Deflandre and Cookson, 1955) Eisenack and Kjellström, 1972 sensu Pearce et al., 2003

*Membranilarnacia polycladiata* Cookson and Eisenack in Eisenack, 1963

**Membranilarnacia wilsonii* Pearce, 2010

*Montanarocysta aemiliana* Corradini, 1973

*Neosphaerodictyon filosum* Slimani, 2003

*Raetiaedinium truncigerum* (Deflandre, 1937) Kirsch, 1991

*Tanyosphaeridium xanthiopyxides* Wetzel, 1933b ex Deflandre, 1937b) Stover and Evitt, 1978

*Trigonopyxidia ginella* (Cookson and Eisenack, 1960) Downie and Sarjeant, 1965

*Wallodinium luna* (Cookson and Eisenack, 1960a) Lentin and Williams, 1973

*Order:* PERIDINIALES Haeckel, 1894

*Suborder:* PERIDINIINEAE (Autonym)

*Family:* PERIDINIACEAE Ehrenberg, 1831

*Subfamily:* PALAEOPERIDINIOIDEAE (Vozzhennikova, 1961) Bujak and Davies, 1983

**Palaeohystrichophora infusorioides* Deflandre, 1935

*Palaeoperidinium pyrophorum* (Ehrenberg, 1838) Sarjeant, 1967b

**Subtilisphaera* spp. Jain and Millepied, 1973

*Subfamily:* DEFLANDREOIDEAE Bujak and Davies, 1983

**Chatangiella ditissima* (McIntyre, 1975) Lentin and Williams, 1976

*Chatangiella granulifera* (Manum, 1963) Lentin and Williams, 1976

*Chatangiella islae* Pearce et al., 2019

*Chatangiella* spp. Vozzhennikova, 1967

*Chatangiella tripartita* (Cookson and Eisenack, 1960a) Lentin and Williams, 1976

*Isabelidinium cooksoniae* (Alberti, 1959) Lentin and Williams, 1977

*Isabelidinium glabrum* (Cookson and Eisenack, 1969) Lentin and Williams, 1977a

*Isabelidinium* spp. Lentin and Williams, 1977a

*Spinidinium* spp. Cookson and Eisenack, 1962b

*Trithyrodinium sabulum* Mao Shaozhi and Norris, 1988

*Subfamily:* OVOIDINIOIDEAE (Norris, 1978) Bujak and Davies, 1983

*Leberidocysta chlamydata* (Cookson and Eisenack, 1962) Stover and Evitt, 1978

*Leberidocysta defloccata* (Davey and Verdier, 1973) Stover and Evitt, 1978

*Class:* UNCERTAIN

*Disphaeria macropyla* Cookson and Eisenack, 1960

*Downiesphaeridium armatum* (Deflandre, 1937) Islam, 1993

*Downiesphaeridium* spp. Islam, 1993

*Downiesphaeridium*? *aciculare* (Davey, 1969) Islam, 1993

*Impletosphaeridium banterwickense* Pearce, 2018

*Impletosphaeridium* spp. Morgenroth, 1966a

**Sepispinula ambigua* (Deflandre, 1937) Masure in Fauconnier and Masure, 2004

Additional palynomorphs:

*Afropollis operculatus* Doyle et al., 1982 (angiosperm pollen)

angiosperm pollen (undiff. simple tricolpate and tricolporates)

*Araucariacites australis* Cookson, 1947 (gymnosperm pollen)

*Auritulinasporites* spp. Nilsson, 1958 (spore)

*Biretisporites* spp. Delcourt and Sprumont, 1955 (spore)

Bisaccate gymnosperm pollen

*Callialasporites dampieri* (Balme, 1957) Dev, 1961 (gymnosperm pollen)

*Cerebropollenites macroverrucosus* (Thiergart, 1949) Schultz, 1967 (gymnosperm pollen)

*Cerebropollenites thiergartii* Schultz, 1967 (gymnosperm pollen)

*Chasmatosporites hians* Nilsson, 1958 (spore)

*Cicatricosisporites* spp. Potonié and Gelletich, 1933 (spore)

*Cingulatisporites* spp. Thomson in Thomson and Pflug, 1953 (spore)

*Converrucosisporites* spp. Potonié and Kremp, 1954 (spore)

*Crassosphaera* spp. Cookson and Manum, 1960 (Prasinophyceae)

*Cyathidites minor* Couper, 1958 (spore)

*Cymatiosphaera* spp. Wetzel, 1933 (Prasinophyceae)

*Densosporites* spp. Berry 1937 (spore)

*Echinatisporis* spp. Krutzsch 1959 (spore)

*Exesipollenites scabratus* Pocock 1970 (gymnosperm pollen )

*Fromea fragilis* (Cookson and Eisenack, 1962) Stover and Evitt, 1978 (acritarch)

Fromea laevigata (Drugg, 1967) Stover and Evitt, 1978 (acritarch)

fungal hyphae

fungal spore

*Granulatisporites* spp. Ibrahim 1933 (spore)

*Inaperturopollenites* spp. Pflug and Thomson in Thomson and Pflug 1953 (pollen)

*Incertae sedis*

*Laevigatosporites* spp. Ibrahim 1933 (spore)

*Leiosphaeridia* spp. Eisenack, 1958c (Prasinophyceae)

*Micrhystridium* spp. Deflandre, 1938 (acritarch)

Microforaminferal-test-lining

*Nummus similis* (Cookson and Eisenack, 1960b) Burger, 1980b (acritarch)

*Ovoidites* spp. Potonié, 1966 (Zygnemataceous zygospore)

*Palambages morulosa* Wetzel, 1961 (colonial marine alga)

*Paralecaniella indentata* (Deflandre and Cookson, 1955) Cookson and Eisenack, 1970 (acritarch)

*Pediastrum* spp. Meyen, 1829 (Chlorophyceae)

*Pterospermella australiensis* (Deflandre and Cookson, 1955) Eisenack et al., 1973 (Prasinophyceae)

*Pterospermella* spp. Eisenack, 1972 (Prasinophyceae)

*Rugubivesiculites rugosus* Pierce 1961 (bisaccate gymnosperm pollen)

*Tasmanites* spp. Newton, 1875 (Prasinophyceae)

undifferentiated zooclasts

*Veryhachium* spp. Denuff, 1954 (acritarch)

## Appendix B. List of calcareous nannofossil taxa

A complete list of calcareous nannofossil taxa identified in our study of the Turonian – Coniacian boundary section at Salzgitter-Salder Quarry is provided below, in alphabetical order. The classification of Burnett et al. (1998) is followed here, with references cited therein. Species marked with an asterisk (*) are illustrated on the Salzgitter-Salder range chart (Fig. 13). Stratigraphically significant species and selected other taxa are illustrated in Fig. 14.

*Acuturris scotus* (Risatti, 1973) Wind & Wise in Wise & Wind, 1977
*Ahmuellerella octoradiata* (Górka, 1957) Reinhardt & Górka, 1967
*Ahmuellerella regularis* (Górka, 1957) Reinhardt & Górka, 1967
*Amphizygus brooksii* Bukry, 1969
*Arkhangelskiella confusa* Burnett, 1997
*Bilapillus wadeae* Lees, 2007
**Biscutum constans* (Górka, 1957) Black in Black & Barnes, 1959
*Biscutum ellipticum* (Górka, 1957) Grün in Grün & Allemann, 1975
*Biscutum hattneri* Wise, 1983
*Biscutum melaniae* (Górka, 1957) Reinhardt, 1969
**Braarudosphaera bigelowii* (Gran & Braarud, 1935) Deflandre, 1947
*Broinsonia cenomanica* (Black, 1973) Bown, 2001
*Broinsonia enormis* (Shumenko, 1968) Manivit, 1971
*Broinsonia furtiva* (Bukry, 1969) Hattner & Wise, 1980
*Broinsonia matalosa* (Stover, 1966) Burnett in Gale et al., 1996
**Broinsonia parca expansa* (Wise & Watkins in Wise, 1983)
*Bukrylithus ambiguus* Black, 1971
*Calciosolenia fossilis* (Deflandre in Deflandre & Fert, 1954) Bown in Kennedy et al., 2000
*Calculites cyclops* Lees, 2007
*Calculites ovalis* (Stradner, 1963) Prins & Sissingh in Sissingh, 1977
*Calculites obscurus* (Deflandre, 1959) Prins & Sissingh, 1977
*Calculites turonicus* Lees, 2007
**Chiastozygus bifarius* Bukry, 1969
**Chiastozygus litterarius* (Górka, 1957) Manivit, 1971

*Chiastozygus synquadriperforatus* Bukry 1969

*Chiastozygus trabalis* (Górka, 1957) Burnett, 1997

*Corollithion signum* Stradner, 1963

*Cretarhabdus conicus* Bramlette & Martini, 1964

*Cribrosphaerella circular* (Risatti, 1973) Lees, 2007

*Cribrosphaerella ehrenbergii* (Arkhangelsky, 1912) Deflandre in Piveteau, 1952

*Cyclagelosphaera margerelii* Noël, 1965

*Cylindralithus biarcus* (Bukry, 1969)

*Cylindralithus coronatus* Bukry, 1969

*Cylindralithus sculptus* Bukry, 1969

*Cylindralithus serratus* Bramlette & Martini, 1964

*Discorhabdus ignotus* (Górka, 1957) Perch-Nielsen, 1968

*Eiffellithus casulus* Shamrock in Shamrock & Watkins, 2009

**Eiffellithus eximius* (Stover, 1966) Perch-Nielsen, 1968

*Eiffellithus gorkae* Reinhardt, 1965

*Eiffellithus turriseiffelii* (Deflandre in Deflandre & Fert, 1954) Reinhardt, 1965

**Eprolithus floralis* (Stradner, 1962) Stover, 1966

*Eprolithus moratus* (Stover, 1966) Burnett, 1998

*Eprolithus octopetalus* Varol, 1992

*Flabellites oblongus* (Bukry, 1969) Crux in Crux et al., 1982

**Gartnerago obliquum* (Stradner, 1963) Noël, 1970

**Gartnerago segmentatum* (Stover, 1966) Thierstein, 1974

*Grantarhabdus coronadventis* (Reinhardt, 1966) Grün in Grün & Allemann, 1975

*Haquius circumradiatus* (Stover, 1966) Roth, 1978

*Helicolithus anceps* (Górka, 1957) Noël, 1970

*Helicolithus compactus* (Bukry, 1969) Varol & Girgis, 1994

*Helicolithus trabeculatus* (Górka, 1957) Verbeek, 1977

**Helicolithus turonicus* Varol & Girgis, 1994

**Kamptnerius magnificus* Deflandre, 1959

**Lithastrinus septenarius* Forchheimer, 1972

*Lithraphidites carniolensis* Deflandre, 1963

*Loxolithus armilla* (Black in Black & Barnes, 1959) Noël, 1965

*Lucianorhabdus arcuatus* Forchheimer, 1972

*Lucianrhabdus maleformis* Reinhardt, 1966

*Lucianorhabdus quadrifidus* Forchheimer, 1972

*Manivitella pemmatoidea* (Deflandre in Manivit, 1965) Thierstein, 1971

**Marthasterites furcatus* Deflandre in Deflandre & Fert, 1954) Deflandre, 1959

*Microrhabdulus ambiguus* Black, 1971

*Microrhabdulus belgicus* Hay & Towe, 1963

*Microrhabdulus decoratus* Deflandre, 1959

*Microrhabdulus helicoideus* Deflandre, 1959

*Micula staurophora* (Gardet, 1955) Stradner, 1963

*Miravetesina bergenii* Lees, 2007

*Nannoconus elongatus* Brönnimann, 1955

*Nannoconus regularis* Deres & Achéritéguy, 1980

*Placozygus fibuliformis* (Reinhardt, 1964) Hoffmann, 1970

*Prediscosphaera columnata* (Stover, 1966) Perch-Nielsen, 1984

**Prediscosphaera cretacea* (Arkhangelsky, 1912) Gartner, 1968

*Prediscosphaera ponticula* Bown & Hampton in Bown, 2005

*Prediscosphaera spinosa* (Bramlette & Martini, 1964) Gartner, 1968

**Quadrum gartneri* (Prins & Perch-Nielsen in Manivit et al., 1977)

*Quadrum intermedium* Varol, 1992

*Quadrum octobrachium* Varol, 1992

*Radiolithus planus* Stover, 1966

*Reinhardtites anthophorus* (Deflandre, 1959) Perch-Nielsen, 1968

*Repagulum parvidentatum* (Deflandre & Fert, 1954) Forchheimer, 1972

*Retecapsa angustiforata* Black, 1971

*Retecapsa crenulata* (Bramlette & Martini, 1964) Grün in Grün & Allemann, 1975

*Retecapsa ficula* (Stover, 1966) Burnett, 1997

*Retecapsa surirella* (Deflandre & Fert, 1954) Grün in Grün & Allemann, 1975

*Rhagodiscus achlyostaurion* (Hill, 1976) Doeven, 1983

*Rhagodiscus angustus* (Stradner, 1963) Reinhardt, 1971

*Rhagodiscus asper* (Stradner, 1963) Reinhardt, 1967

*Rhagodiscus reniformis* Perch-Nielsen, 1973

*Rhagodiscus splendens* (Deflandre, 1953) Verbeek, 1977

*Rotelapillus crenulatus* (Stover, 1966) Perch-Nielsen, 1984

*Seribiscutum primitivum* (Thierstein, 1974) Filewicz et al. in Wind & Wise, 1983

*Staurolithites crux* (Deflandre & Fert, 1954) Caratini, 1963

*Staurolithites dentatus* (Bukry, 1969) Burnett, 1997

*Staurolithites dicandidula* (Bergen in Bralower & Bergen, 1998) Thibault, 2010

*Staurolithites ellipticus* (Gartner, 1968) Lambert, 1987

*Staurolithites flavus* Burnett, 1997

**Staurolithites laffittei* Caratini, 1963

*Staurolithites minutus* Burnett, 1997

*Stoverius achylosus* (Stover, 1966) Perch-Nielsen, 1986

*Tegumentum stradneri* Thierstein in Roth & Thierstein, 1972

*Tetrapodorhabdus decorus* (Deflandre in Deflandre & Fert, 1954) Wind & Wise, 1983

*Tranolithus gabalus* Stover, 1966

*Tranolithus minimus* (Bukry, 1969) Perch-Nielsen, 1984

**Tranolithus orionatus* (Reinhardt, 1966a) Reinhardt, 1966b

**Watznaueria barnesiae* (Black in Black & Barnes, 1959) Perch-Nielsen, 1968

*Watznaueria biporta* Bukry, 1969

*Watznaueria fossacincta* (Black, 1971) Bown in Bown & Cooper, 1989

*Watznaueria ovata* Bukry, 1969

*Zeugrhabdotus acanthus* Reinhardt, 1965

**Zeugrhabdotus bicrescenticus* (Stover, 1966) Burnett in Gale et al., 1996

**Zeugrhabdotus biperforatus* (Gartner, 1968) Burnett, 1997

*Zeugrhabdotus diplogrammus* (Deflandre in Deflandre & Fert, 1954) Burnett in Gale et al., 1996

*Zeugrhabdotus embergeri* (Noël, 1959) Perch-Nielsen, 1984

*Zeugrhabdotus erectus* (Deflandre in Deflandre & Fert, 1954) Reinhardt, 1965

*Zeugrhabdotus howei* Bown in Kennedy et al., 2000

*Zeugrhabdotus kerguelenensis* Watkins, 1992

**Zeugrhabdotus noeliae* Rood et al., 1971

**Zeugrhabdotus scutula* (Bergen, 1994) Rutledge & Bown, 1996

*Zeugrhabdotus trivectis* Bergen, 1994

## References

Amenábar, C.R., Montes, M., Nozal, F., Santillana, S.N., 2020. Dinoflagellate cysts of the La Meseta Formation (middle to late Eocene), Antarctic Peninsula: implications for biostratigraphy, palaeoceanography and palaeoenvironment. Geological Magazine 157, 351–366.

Århus, N., 1991. Dinoflagellate cyst stratigraphy of some Aptian and Albian sections from North Greenland, south-eastern Spitsbergen and the Barents Sea. Cretaceous Research 12, 209–225.

Bailey, H.W., Gale, A.S., Mortimore, R.N., Swiecicki, A., Wood, C.J., 1983. The Coniacian – Maastrichtian stages of the United Kingdom, with particular reference to southern England. Newsletters on Stratigraphy 12, 29–42.

Baldschuhn, R., Kockel, F., 1998. Der Untergrund von Hannover und seiner Umgebung. Bericht der Naturhistorischen Gesellschaft Hannover 140, 5–98.

Birkelund, T., Hancock, J.M., Hart, M.B., Rawson, P.F., Remane, J., Robaszynski, F., Schmid, F., Surlyk, F., 1984. Cretaceous stage boundaries - proposals. Bulletin of the Geological Society of Denmark 33, 3–20.

Blakey, R., 2012. Paleogeography of Europe series, Cretaceous ca. 75 Ma. Colorado Plateau Geosystems (now DeepTimeMaps$^{TM}$), Flagstaff AZ.

Bräutigam, F., 1962. Zur Stratigraphie und Paläontologie des Cenomans und Turons im nordwestlichen Harzvorland. Unpublished PhD thesis, Technische Hochschule Braunschweig, Braunschweig, p. 261.

Burnett, J.A., Gallagher, L.T., Hampton, M.J., 1998. Upper Cretaceous, in: Bown, P.R. (Ed.), Calcareous Nannofossil Biostratigraphy. Kluwer, Dordrecht, pp. 132–199.

Čech, S., Uličný, D., 2020. The Turonian–Coniacian stage boundary in an expanded siliciclastic succession: integrated stratigraphy in deltaic through offshore facies, Bohemian Cretaceous Basin. Cretaceous Research 117, 104576 p. 29 https://doi.org/10.1016/j.cretres.2020.104576.

Clarke, R.F.A., Verdier, J.P., 1967. An investigation of microplankton assemblages from the Chalk of the Isle of Wight, England. Verhandelingen der Koninklijke Nederlandse Akademie van Wetenschappen Afdeling Natuurkunde Eerste Reeks 24, 1–96.

Cooper, D.A., Cooper, R.W., Stevens, J.B., Stevens, M.S., Cobban, W.A., Walaszczyk, I., 2017. The Boquillas Formation of the Big Bend National Park, Texas, USA, a reference Cenomanian through Santonian (Upper Cretaceous) carbonate succession at the southern end of the Western Interior Seaway. Acta Geologica Polonica 67, 547–565.

Costa, L., Davey, R.J., 1992. Dinoflagellates of the Cretaceous System, in: Powell, A.J. (Ed.), A Stratigraphic Index of Dinoflagellate Cysts. Chapman and Hall, London, pp. 99–153.

Cramer, B.S., Jarvis, I., 2020. Carbon isotope stratigraphy, in: Gradstein, F., Ogg, J.G., Ogg, G. (Eds.), The Geologic Time Scale 2020, Vol. 1. Elsevier, Amsterdam, pp. 309–343.

Dahmer, D.-D., Ernst, G., 1986. Upper Cretaceous event stratigraphy in Europe, in: Walliser, O. (Ed.), Global Bio-Events. Springer, Berlin, pp. 353–362.

Dahmer, D.-D., Hilbrecht, H., Ernst, G., 1986. Neue Erkenntnisse zur Multistratigraphie, Sedimentologie und Palökologie der Oberkreide von Niedersachsen und Westfalen unter besonderer Berücksichtigung des Cenoman bis Coniac. Exkursionsführer der Geländetagung „Oberkreide NW-Deutschland", der Subkommission für Kreidestratigraphie 4–8 Oktober 1986 [unpublished]

Dale, B., Fjellså, A., 1994. Dinoflagellate cysts as paleoproductivity indicators: state of the art, potential and limits, in: Zahn, R., Pedersen, T.F., Kaminiski, M., Lebeyrie, L. (Eds.), Carbon Cycling in the Glacial Ocean: Constraints on the Ocean's Role in Global Change. Springer, Berlin, Heidelberg, pp. 521–537.

de Vernal, A., Marret, F., 2007. Chapter nine. Organic-walled dinoflagellate cysts: tracers of sea-surface conditions. Developments in Marine Geology 1, 371–408.

Dodsworth, P., 2000. Trans-Atlantic dinoflagellate cyst stratigraphy across the Cenomanian–Turonian (Cretaceous) Stage boundary. Journal of Micropalaeontology 19, 69–84.

Dodsworth, P., 2004. The palynology of the Cenomanian – Turonian (Cretaceous) boundary succession at Aksudere in Crimea, Ukraine. Palynology 28, 129–141.

Dodsworth, P., Eldrett, J.S., 2019. A dinoflagellate cyst zonation of the Cenomanian and Turonian (Upper Cretaceous) in the Western Interior, United States. Palynology 43, 701–723.A

Dodsworth, P., Eldrett, J.S., Hart, M.B., 2020. Cretaceous Oceanic Anoxic Event 2 in eastern England: further palynological and geochemical data from Melton Ross. Proceedings of the Yorkshire Geological Society 63, 88 – 123.

Eldrett, J.S., Minisini, D., Bergman, S.C., 2014. Decoupling of the carbon cycle during Ocean Anoxic Event 2. Geology 42, 567–570.

Eldrett, J.S., Dodsworth, P., Bergman, S.C., Wright, M., Minisini, D., 2017. Water-mass evolution in the Cretaceous Western Interior Seaway of North America and equatorial Atlantic. Climate of the Past 13, 855–878.

Ernst, G., Schmid, F., 1975. Stand der geologischen Forschungsarbeiten in den Oberkreide-Mulden zwischen Misburg und Lehrte. Berichte der Naturhistorischen Gesellschaft 119, 113–126.

Ernst, G., Wood, C.J., 1995. Die tiefere Oberkreide des subherzynen Niedersachsens. Terra Nostra 5/95, 41–84.

Ernst, G., Schmid, F., Klischies, G., 1979. Multistratigraphische Untersuchungen in der Oberkreide des Raumes Braunschweig-Hannover, in: Wiedmann, J. (Ed.), Aspekte der Kreide Europas. IUGS Series A6, pp. 11–46.

Ernst, G., Schmid, F., Seibertz, E., 1983. Event-Stratigraphie im Cenoman und Turon von NW Deutschland. Zitteliana 10, 531–554.

Eshet, Y., Almogilabin, A., Bein, A., 1994. Dinoflagellate cysts, paleoproductivity and upwelling systems - a Late Cretaceous example from Israel. Marine Micropaleontology 23, 231–240.

Esper, O., Zonneveld, K.A.F., 2007. The potential of organic-walled dinoflagellate cysts for the reconstruction of past sea-surface conditions in the Southern Ocean. Marine Micropaleontology 65, 185–212.

Estebenet, M.S.G., Paolillo, M.A., Guler, M.V., 2019. Marine Cretaceous organic-walled dinoflagellate cysts from the Austral-Magallanes Basin. Latin American Journal of Sedimentology and Basin Analysis 26, 75–98.

Fensome, R.A., Taylor, F.J.R., Norris, G., Sarjeant, W.A.S., Wharton, D.I., Williams, G.L., 1993. A classification of living and fossil dinoflagellates. Micropaleontological Press, Special Publication 7, p. 351.

Fensome, R.A., Williams, G.L., MacRae, R.A., 2019a. The Lentin and Williams Index of Fossil Dinoflagellates 2019 Edition. American Association of Stratigraphic Palynologists Contribution Series 50, 1–1173.

Fensome, R.A., Williams, G.L., Wood, S.E.L., Riding, J.B., 2019b. A review of the areoligeracean dinoflagellate cyst *Cyclonephelium* and morphologically similar genera. Palynology 43 (supplement 1), 1–71.

Fisher, R.A., Corbet, A.S., Williams, C.B., 1943. The relation between the number of species and the number of individuals in a random sample of an animal population. Journal of Animal Ecology 12, 42–58.

FitzPatrick, M.E.J., 1992. Turonian Dinoflagellate Cyst Assemblages from Southern England, Department of Geology. Unpublished PhD thesis, Polytechnic South West, Plymouth, p. 373.

FitzPatrick, M.E.J., 1995. Dinoflagellate cyst biostratigraphy of the Turonian (Upper Cretaceous) of southern England. Cretaceous Research 16, 757–791.

Foucher, J.-C., 1971. Microfossiles des silex Coniaciens de la falaise du Boise-de-Cise (Somme). Cahiers de Micropaléontologie 8, 1–13.

Foucher, J.-C., 1975. Dinoflagellés et acritarches des silex crétacé du Bassin de Paris: une synthèse stratigraphique. Annales Université et de l'ARERS (Association Régionale pour l'Étude et la Recherche Scientifiques), Reims 1–2, 8–11.

Foucher, J.-C., 1976. Les Dinoflagellés des silex et la stratigraphie du Crétacé supérieur français. Revue de Micropaléontologie 18, 213–220.

Foucher, J.-C., 1980. Dinoflagellés et acritarches, in: Robaszynski, F., Amédro, F., Foucher, J.-C., Gaspard, D., Magniez-Jannin, F., Manivit, H., Sornay, J. (Eds.), Synthèse Biostratigraphique de l'Aptien au Santonien du Boulonnais a Partir de Sept Groupes Paléontologiques: Foraminifères, Nannoplancton, Dinoflagellés et Macrofaunes. Revue de Micropaléontologie 22, 195–321.

Foucher, J.-C., 1981. Kystes de Dinoflagellés du Crétacé moyen européen: Proposition d'une échelle biostratigraphique pour le domaine nord-occidental. Cretaceous Research 2, 331–338.

Foucher, J.-C., 1983. Distribution des kystes de Dinoflagellés dans le Crétacé moyen et supérieur du Bassin de Paris. Cahiers de Micropaléontologie 4, 23–41.

Gedl, P., 2007. Dinocysts from Upper Cretaceous deep-water marine variegated facies (Malinowa Shale Formation), Pieniny Klippen Belt, Poland: example from the Potok Trawne creek, in: Birkemajer, K. (Ed.), Geology of the Pieniny Klippen Belt and the Tatra

Mts, Carpathians. Institute of Geological Sciences, Polish Academy of Sciences, Warsaw, pp. 139–152.

Gerardi, J., 1986. Bohrung Konrad 101, Teil I : Geologischer Bericht, Teil II: Schichtenverzeichnis. Bundesanstalt für Geowissenschaften und Rohstoffe (BGR), Hannover [unpublished].

Gradstein, F.M., Ogg, J.G., Schmitz, M.D., Ogg, G.M., 2020. The Geologic Time Scale 2020. Vol. 1 and 2. Elsevier, Amsterdam, pp. 1357.

Guerra, R.M., Concheyro, A., Wise, S.W.J., Fauth, G., 2016. Late Campanian–Maastrichtian *Kamptnerius magnificus* acme in the South Atlantic section of the Southern Ocean, ODP Holes 690C and 700B. Micropaleontology 62, 213–219.

Hancock, J.M., Kauffman, E.G., 1979. The great transgressions of the Late Cretaceous. Journal of the Geological Society London 136, 175–186.

Haq, B.U., 2014. Cretaceous eustasy revisited. Global and Planetary Change 113, 44–58.

Ibrahim, M.I.A., Tahoun, S.S., Zobaa, M.K., Oboh-Ikuenobe, F.E., Kholeif, S.E., 2020. Late Cretaceous palynology and paleoenvironment of the Razzak-3 well, North Western Desert, Egypt. Arabian Journal of Geosciences 13, 870. https://doi.org/10.1007/s12517-020-05705-z.

Ifrim, C., Wiese, F., Stinnesbeck, W., 2014. Inoceramids and biozonation across the Turonian–Coniacian boundary (Upper Cretaceous) at El Rosario, Coahuila, northeastern Mexico. Newsletters on Stratigraphy 47, 211–246.

Jarvis, I., Carson, G.A., Cooper, M.K.E., Hart, M.B., Leary, P.N., Tocher, B.A., Horne, D., Rosenfeld, A., 1988a. Microfossil assemblages and the Cenomanian – Turonian (late Cretaceous) oceanic anoxic event. Cretaceous Research 9, 3–103.

Jarvis, I., Carson, G.A., Hart, M.B., Leary, P.N., Tocher, B.A., 1988b. The Cenomanian – Turonian (late Cretaceous) anoxic event in SW England: evidence from Hooken Cliffs near Beer, SE Devon. Newsletters on Stratigraphy 18, 147–164.

Jarvis, I., Gale, A.S., Jenkyns, H.C., Pearce, M.A., 2006. Secular variation in Late Cretaceous carbon isotopes: A new $\delta^{13}C$ carbonate reference curve for the Cenomanian–Campanian (99.6–70.6 Ma). Geological Magazine 143, 561–608.

Jarvis, I., Trabucho-Alexandre, J., Gröcke, D.R., Uličný, D., Laurin, J., 2015. Intercontinental correlation of organic carbon and carbonate stable isotope records: evidence of climate

and sea-level change during the Turonian (Cretaceous). The Depositional Record 1, 53–90.

Jenkyns, H.C., Gale, A.S., Corfield, R.M., 1994. Carbon- and oxygen-isotope stratigraphy of the English Chalk and Italian Scaglia and its palaeoclimatic significance. Geological Magazine 131, 1–34.

Joo, Y.J., Sageman, B.B., 2014. Cenomanian to Campanian carbon isotope chemostratigraphy from the Western Interior Basin, U.S.A. Journal of Sedimentary Research 84, 529–542.

Kauffman, E.G., Kennedy, W.J., Wood, C.J., 1996. The Coniacian stage and substage boundaries, in: Rawson, P.F., Dhondt, A.V., Hancock, J.M., Kennedy, W.J. (Eds.), Proceedings "Second International Symposium on Cretaceous Stage Boundaries" Brussels 8–16 September 1995. l'Institut Royal des Sciences Naturelles de Belgique, pp. 81–94.

Kirsch, K.-H., 1991. Dinoflagellatenzysten aus der Oberkreide des Helvetikums und Nordultrahelvetikums von Oberbayern. Münchner geowissenschaftliche Abhandlungen A 22, 1–306.

Lamolda, M.A., Mao, S.Z., 1999. The Cenomanian–Turonian boundary event and dinocyst record at Ganuza (northern Spain). Palaeogeography Palaeoclimatology Palaeoecology 150, 65–82.

Leandro, L.M., Santos, A., Carvalho, M.d.A., Fauth, G., 2020. Middle to late Miocene Caribbean dinoflagellate assemblages and palynofacies (DSDP Leg 15 Site 153). Marine Micropaleontology 160, 101898, p. 13.

Lees, J.A., 2008. The calcareous nannofossil record across the Late Cretaceous Turonian/Coniacian boundary, including new data from Germany, Poland, the Czech Republic and England. Cretaceous Research 29, 40–64.

Lees, J.A., Bown, P.R., Young, J.R., Riding, J.B., 2004. Evidence for annual records of phytoplankton productivity in the Kimmeridge Clay Formation coccolith stone bands (Upper Jurassic, Dorset, UK). Marine Micropaleontology 52, 29–49.

Lignum, J., 2009. Cenomanian (Upper Cretaceous) palynology and chemostratigraphy: dinoflagellate cysts as indicators of palaeoenvironmental and sea-level change. Unpublished PhD thesis, Kingston University London, Kingston upon Thames, UK, p. 582.

Lignum, J., Jarvis, I., Pearce, M.A., 2008. A critical assessment of standard processing methods for the preparation of palynological samples. Review of Palaeobotany and Palynology 149, 133–149.

Linnert, C., Mutterlose, J., 2015. Boreal early Turonian calcareous nannofossils from nearshore settings - implications for paleoecology. Palaios 30, 728–742.

Mao, S., Mohr, B., 1992. 20. Late Cretaceous dinoflagellate cysts (?Santonian–Maestrichtian) from the southern Indian Ocean (Hole 748C), in: Wise, S.W.Jr, Schlich, R. (Eds.), Central Kerguelen Plateau. Proceedings of the Ocean Drilling Program, Scientific Results 120, 307–341.

Masure, E., Aumar, A.-M., Vrielynck, B., 2013. Worldwide palaeogeography of Aptian and Late Albian dinoflagellate cysts: implications for sea-surface temperature gradients and paleoclimate, in: Lewis, J.M., Marret, F., Bradley, L. (Eds.), Biological and Geological Perspectives of Dinoflagellates. The Micropalaeontological Society Special Publication, London, pp. 97–125.

McArthur, J.M., Thirlwall, M.F., Gale, A.S., Kennedy, W.J., Burnett, J.A., Mattey, D., Lord, A.R., 1993. Strontium isotope stratigraphy for the Late Cretaceous: a new curve, based on the English Chalk, in: Hailwood, E.A., Kidd, R.B. (Eds.), High Resolution Stratigraphy. Geological Society Special Publication 70, 195–209.

Mohr, B.A.R., Gee, C.T., 1992. Late Cretaceous palynofloras (sporomorphs and dinocysts) from the Kerguelen Plateau, southern Indian Ocean (Sites 748 and 750). Proceedings of the Ocean Drilling Program, Scientific Results 120, 281–306.

Morter, A.A., Gallois, R.W., Clark, R.D., 1975. Record of the IGS Trunch borehole. Institute of Geological Sciences, London, p. 207.

Mutterlose, J., Wood, C.J., Ernst, G., 1998. The Lower and Upper Cretaceous of the Hannover-Braunschweig area (NW Germany), in: Mutterlose, J., Bornemann, A., Rauer, S., Spaeth, C., Wood, C.J. (Eds.), Key Localities of the Northwest European Cretaceous. Ruhr-Universität Institut für Geologie, Bochum, pp. 39–51.

Niebuhr, B., Wiese, F., Wilmsen, M., 2001. The cored Konrad 101 borehole (Cenomanian – Lower Coniacian, Lower Saxony): calibration of surface and subsurface log data for the lower Upper Cretaceous of northern Germany. Cretaceous Research 22, 643–674.

Niebuhr, B., Hiss, M., Kaplan, U., Tröger, K.-A., Voigt, S., Voigt, T., Wiese, F., Wilmsen, M., 2007. Lithostratigraphie der norddeutschen Oberkreide. Schriftenreihe der Deutschen Gesellschaft für Geowissenschaft 55, 1–136.

Nøhr-Hansen, H., 1993. Dinoflagellate cyst stratigraphy of the Barremian to Albian, Lower Cretaceous, north-east Greenland. Grønlands Geologiske Undersøgelse Bulletin 166, 1–171.

Nøhr-Hansen, H., 1996. Upper Cretaceous dinoflagellate cyst stratigraphy, onshore West Greenland. Grønlands Geologiske Undersøgelse Bulletin 170, 1–104.

Nøhr-Hansen H, Piasecki S, and Alsen P., 2020. A Cretaceous dinoflagellate cyst zonation for NE Greenland. Geological Magazine 157, 1658–1692.

Oboh-Ikuenobe, F.E., Benson, D.G., Scott, R.W., Holbrook, J.M., Evetts, M.J., Erbacher, J., 2007. Re-evaluation of the Albian–Cenomanian boundary in the US Western Interior based on dinoflagellate cysts. Review of Palaeobotany and Palynology 144, 77–97.

Olde, K., Jarvis, I., Pearce, M.A., Uličný, D., Tocher, B.A., Trabucho-Alexandre, J., Gröcke, D., 2015a. A revised northern European Turonian (Upper Cretaceous) dinoflagellate cyst biostratigraphy: integrating palynology and carbon isotope events. Review of Palaeobotany and Palynology 213, 1–16.

Olde, K., Jarvis, I., Uličný, D., Pearce, M.A., Trabucho-Alexandre, J., Čech, S., Gröcke, D.R., Laurin, J., Švábenická, L., Tocher, B.A., 2015b. Geochemical and palynological sea-level proxies in hemipelagic sediments: A critical assessment from the Upper Cretaceous of the Czech Republic. Palaeogeography, Palaeoclimatology, Palaeoecology 435, 222–243.

Olde, K., Jarvis, I., Pearce, M.A., Walaszczyk, I., Tocher, B.A., 2016. Organic-walled dinoflagellate cyst records from a prospective Turonian – Coniacian (Upper Cretaceous) GSSP, Słupia Nadbrzeżna, Poland. Cretaceous Research 65, 17–24.

Pearce, M.A., 2018. Additional new organic-walled dinoflagellate cysts from two onshore UK Chalk boreholes. Journal of Micropalaeontology 37, 73–86.

Pearce, M.A., Williams, G.L., 2018. *Fetchamium prolixispinosum* gen. et comb. nov (division Dinoflagellata). Journal of Micropalaeontology 37, 17–20.

Pearce, M.A., Jarvis, I., Swan, A.R.H., Murphy, A.M., Tocher, B.A., Edmunds, W.M., 2003. Integrating palynological and geochemical data in a new approach to palaeoecological

studies: Upper Cretaceous of the Banterwick Barn Chalk borehole, Berkshire, UK. Marine Micropaleontology 47, 271–306.

Pearce, M.A., Jarvis, I., Tocher, B.A., 2009. The Cenomanian–Turonian boundary event, OAE2 and palaeoenvironmental change in epicontinental seas: New insights from the dinocyst and geochemical records. Palaeogeography Palaeoclimatology Palaeoecology 280, 207–234.

Pearce, M.A., Lignum, J.S., Jarvis, I., 2011. *Senoniasphaera turonica* (Prössl, 1990 ex Prössl, 1992) comb. nov., senior synonym of *Senoniasphaera rotundata alveolata* Pearce et al., 2003: an important dinocyst marker for the Lower Turonian chalk of NW Europe. Journal of Micropalaeontology 30, 91–93.

Pearce, M.A., Jarvis, I., Ball, P.J., Laurin, J., 2020. Palynology of the Cenomanian to lowermost Campanian (Upper Cretaceous) Chalk of the Trunch Borehole (Norfolk, UK) and a new dinoflagellate cyst bioevent stratigraphy for NW Europe. Review of Palaeobotany and Palynology 278, 104188, p. 77.

Perch-Nielsen, K., 1985. Mesozoic calcareous nannofossils, in: Bolli, H.M., Saunders, J.B., Perch-Nielsen, K. (Eds.), Plankton Stratigraphy. Cambridge University Press, pp. 329–426.

Pestchevitskaya, E.B., Nikitenko, B.L., 2019. Barremian–Aptian assemblages of microfauna and palynomorphs from the north-west of the Yamal Peninsula (biostratigraphy and palaeofacies). Paleontological Journal 53, 812–816.

Powell, A.J., Dodge, J.D., Lewis, J., 1990. Late Neogene to Pleistocene palynological facies of the Peruvian continental margin upwelling, Leg 112. Proceedings of the Ocean Drilling Program, Scientific Results 112, 297–321.

Powell, A.J., Lewis, J., Dodge, J.D., 1992. The palynological expressions of post-Palaeogene upwelling: a review, in: Summerhayes, C.P., Prell, W.L., Emeis, K.C. (Eds.), Upwelling Systems: Evolution Since the Early Miocene. Geological Society of London Special Publication 64, 215–226.

Prauss, M., 2001. Sea-level changes and organic-walled phytoplankton response in a Late Albian epicontinental setting, Lower Saxony basin, NW Germany. Palaeogeography Palaeoclimatology Palaeoecology 174, 221–249.

Prauss, M.L., 2015. Marine palynology of the Oceanic Anoxic Event 3 (OAE3, Coniacian – Santonian) at Tarfaya, Morocco, NW Africa - transition from preservation to production controlled accumulation of marine organic carbon. Cretaceous Research 53, 19–37.

Prince, I.M., Jarvis, I., Tocher, B.A., 1999. High-resolution dinoflagellate cyst biostratigraphy of the Santonian–basal Campanian (Upper Cretaceous): new data from Whitecliff, Isle of Wight, England. Review of Palaeobotany and Palynology 105, 143–169.

Prince, I.M., Jarvis, I., Pearce, M.A., Tocher, B.A., 2008. Dinoflagellate cyst biostratigraphy of the Coniacian – Santonian (Upper Cretaceous): new data from the English Chalk. Review of Palaeobotany and Palynology 150, 59–96.

Prössl, K.F., 1990. Dinoflagellaten der Kreide - Unter-Hauterive bis Ober-Turon - im Niedersächsischen Becken. Stratigraphie und Fazies in der Kernbohrung Konrad 101 sowie einiger anderer Bohrungen in Nordwestdeutschland. Palaeontographica B 218, 93–191.

Püttmann, T., Mutterlose, J., 2019. Calcareous nannofossils from a Late Cretaceous nearshore setting. Journal of Nannoplankton Research, Special Issue 4, 82–88.

Rasemann, G., 1984. Stratigraphie der Salzgitterer Struktur zwischen Osterlinde und Salder unter besonderer Berücksichtigung der Oberkreide (Turon–Coniac). Unpublished diploma thesis, FU Berlin, Berlin, p. 197.

Reichart, G.-J., Brinkhuis, H., 2003. Late Quaternary *Protoperidinium* cysts as indicators of paleoproductivity in the northern Arabian Sea. Marine Micropaleontology 49, 303–315.

Roth, P.H., 1978. Cretaceous nannoplankton biostratigraphy and oceanography of the northwestern Atlantic Ocean, in: Benson, W.E., Sheridan, R.E., Pastouret, L., Enos, P., Freeman, T., Murdmaa, I.O., Worstell, P., Gradstein, F., Schmidt, R.R., Weaver, F.M., Stuermer, D.H. Initial Reports of the Deep Sea Drilling Project 44, 731–760.

Sarjeant, W.A.S., Lacalli, T., Gaines, G., 1987. The cysts and skeletal elements of dinoflagellates: speculations on the ecological causes for their morphology and development. Micropaleontology 33, 1–36.

Schiøler, P., 1992. Dinoflagellate cysts from the Arnager Limestone Formation (Coniacian, Late Cretaceous), Bornholm, Denmark. Review of Palaeobotany and Palynology 72, 1–25.

Scott, R.W., Oboh-Ikuenobe, F.E., Benson, D.G., Holbrook, J.M., Alnahwi, A., 2018. Cenomanian–Turonian flooding cycles: US Gulf Coast and Western Interior. Cretaceous Research 89, 191–210.

Shannon, C.E., 1948. A mathematical theory of communication. Bell System Technical Journal 27, 379–423, 623–656.

Sikora, P.J., Howe, R.W., Gale, A.S., Stein, J.A., 2004. Chronostratigraphy of proposed Turonian–Coniacian (Upper Cretaceous) stage boundary stratotypes: Salzgitter-Salder, Germany, and Wagon Mound, New Mexico, USA, in: Beaudoin, A.B., Head, M.J.H. (Eds.), Palynology and Micropalaeontology of Boundaries. Geological Society London Special Publications 230, 207–242.

Simon, E., Owen, E.F., 2001. A first step in the revision of the genus *Cretirhynchia* PETTITT, 1950. Bulletin de l'Institut Royal Sciences Naturelles de Belgique Sciences de la Terre 71, 53–118.

Sissingh, W., 1977. Biostratigraphy of Cretaceous nannoplankton. Geologie en Mijnbouw 56, 37–65.

Sluijs, A., Pross, J., Brinkhuis, H., 2005. From greenhouse to icehouse; organic-walled dinoflagellate cysts as paleoenvironmental indicators in the Paleogene. Earth-Science Reviews 68, 281–315.

Stoll, H.M., Schrag, D.P., 2000. High-resolution stable isotope records from the Upper Cretaceous rocks of Italy and Spain: Glacial episodes in a greenhouse planet? Geological Society of America Bulletin 112, 308–319.

Stover, L.E., Brinkhuis, H., Damassa, S.P., Verteuil, L.D., Helby, R.J., Monteil, E., Partridge, A.D., Powell, A.J., Riding, J.B., Smelror, M., Williams, G.L., 1996. Mesozoic–Tertiary dinoflagellates, acritarchs and prasinophytes., in: Jansonius, J., McGregor, D.C. (Eds.), Palynology: Principles and Applications (Volume 2). American Association of Stratigraphic Palynologists Foundation, College Station TX, pp. 641–750.

Švábenická, L., Bubík, M., 2014. Biostratigraphical correlations of the calcareous nannofossil *Marthasterites furcatus* in the Bohemian Cretaceous Basin and Outer Flysch Carpathians, Czech Republic. Cretaceous Research 51, 386–398.

Svobodová, M., Švábenická, L., Skupien, P., Hradecká, L., 2011. Biostratigraphy and paleoecology of the Lower Cretaceous sediments in the Outer Western Carpathians (Silesian Unit, Czech Republic). Geological Carpathica 62, 309–332.

Tahoun, S.S., Ied, I.M., 2019. A Cretaceous dinoflagellate cyst palynozonation of northern Egypt. Palynology 43, 394–410.

Tahoun, S.S., Deaf, A.S., Ied, I.M., 2018. The use of cyclic stratigraphic pattern of peridinioid and gonyaulacoid dinoflagellate cysts in differentiating potential thick monotonous carbonate reservoirs: A possible ecostratigraphic tool under test. Marine and Petroleum Geology 96, 240–253.

Takashima, R., Nishi, H., Yamanaka, T., Hayashi, K., Waseda, A., Obuse, A., Tomosugi, T., Deguchi, N., Mochizuki, S., 2010. High-resolution terrestrial carbon isotope and planktic foraminiferal records of the Upper Cenomanian to the Lower Campanian in the Northwest Pacific. Earth and Planetary Science Letters 289, 570–582.

Takashima, R., Nishi, H., Yamanaka, T., Orihashi, Y., Tsujino, Y., Quidelleur, X., Hayashi, K., Sawada, K., Nakamura, H., Ando, T., 2019. Establishment of Upper Cretaceous bio- and carbon isotope stratigraphy in the northwest Pacific Ocean and radiometric ages around the Albian/Cenomanian, Coniacian/Santonian and Santonian/Campanian boundaries. Newsletters on Stratigraphy 52, 341–376.

Thibault, N., Gardin, S., 2006. Maastrichtian calcareous nannofossil biostratigraphy and paleoecology in the Equatorial Atlantic (Demerara Rise, ODP Leg 207 Hole 1258A). Revue de Micropaléontologie 49, 199–214.

Thibault, N., Anderskouv, K., Bjerager, M., Boldreel, L.O., Jelby, M.E., Stemmerik, L., Surlyk, F., 2015. Upper Campanian–Maastrichtian chronostratigraphy of the Skaelskor-1 core, Denmark: correlation at the basinal and global scale and implications for changes in sea-surface temperatures. Lethaia 48, 549–560.

Thibault, N., Harlou, R., Schovsbo, N.H., Stemmerik, L., Surlyk, F., 2018. Late Cretaceous (late Campanian–Maastrichtian) sea-surface temperature record of the Boreal Chalk Sea. Climate of the Past 12, 429–438.

Thierstein, H.R. 1981. Late Cretaceous nannoplankton and the change at the Cretaceous-Tertiary boundary. SEPM Special Publication 32, 355–394.

Tocher, B.A., Jarvis, I., 1987. Dinoflagellate cysts and stratigraphy of the Turonian (Upper Cretaceous) chalk near Beer, southeast Devon, England, in: Hart, M.B. (Ed.), Micropalaeontology of Carbonate Environments. British Micropalaeontological Society Series, Ellis Horwood, Chichester, pp. 138–175.

Tocher, B.A., Jarvis, I., 1994. Dinoflagellate cyst distribution from the Lower Turonian (Upper Cretaceous) of Ports, Indre-et-Loire. Bulletin d'Information des Géologues du Bassin de Paris 31, 13–23.

Tocher, B.A., Jarvis, I., 1995. Dinocyst distributions and stratigraphy of two Cenomanian – Turonian boundary (Upper Cretaceous) sections from the western Anglo-Paris Basin. Journal of Micropalaeontology 14, 97–105.

Torricelli, S., 2000. Lower Cretaceous dinoflagellate cyst and acritarch stratigraphy of the Cismon APTICORE (Southern Alps, Italy). Review of Palaeobotany and Palynology 108, 213–266.

Uličný, D., Jarvis, I., Gröcke, D.R., Čech, S., Laurin, J., Olde, K., Trabucho-Alexandre, J., Švábenická, L., Pedentchouk, N., 2014. A high-resolution carbon-isotope record of the Turonian stage correlated to a siliciclastic basin fill: Implications for mid-Cretaceous sea-level change. Palaeogeography, Palaeoclimatology, Palaeoecology 405, 42–58.

Van Helmond, N.A.G.M., Sluijs, A., Reichart, G.-J., Sissingh Damsté, J.S., Slomp, C.P., Brinkhuis, H., 2014. A perturbed hydrological cycle during Oceanic Anoxic Event 2. Geology 42, 123–126.

Van Helmond, N.A.G.M., Sluijs, A., Papadomanolaki, N.M., Plint, A.G., Grocke, D.R., Pearce, M.A., Eldrett, J.S., Trabucho-Alexandre, J., Walaszczyk, I., van de Schootbrugge, B., Brinkhuis, H., 2016. Equatorward phytoplankton migration during a cold spell within the Late Cretaceous super-greenhouse. Biogeosciences 13, 2859–2872.

Voigt, S., Hilbrecht, H., 1997. Late Cretaceous carbon isotope stratigraphy in Europe: correlation and relations with sea level and sediment stability. Palaeogeography Palaeoclimatology Palaeoecology 134, 39–59.

Voigt, S., Püttmann, T., Mutterlose, J., Bornemann, A., Jarvis, I., Pearce, M.A., Walaszczyk, I., 2020. Reassessment of the Salzgitter-Salder section as a potential stratotype for the Turonian–Coniacian boundary: stable carbon isotopes and cyclostratigraphy constrained by calcareous nannofossils and palynology. Newsletters on Stratigraphy, p. 20 https://dx.doi.org/10.1127/nos/2020/0615.

Voigt, T., Reicherter, K., Von Eynatten, H., Littke, R., Voigt, S., Kley, J., 2008. Sedimentation during basin inversion., in: Littke, R., Beyer, U., Gajewski, D., Nelskamp, S. (Eds.), Dynamics of complex sedimentary basins. The example of the Central European Basin System. Springer, Berlin, Heidelberg, pp. 211–228.

Walaszczyk, I., Cobban, W.A., 1998. The Turonian – Coniacian boundary in the United States Western Interior. Acta Geologica Polonica 48, 495–507.

Walaszczyk, I., Cobban, W.A., 2000. Inoceramid faunas and biostratigraphy of the Upper Turonian – Lower Coniacian of the Western Interior of the United States. Special Papers in Palaeontology 64, 1–118.

Walaszczyk, I., Wood, C.J., 1998. Inoceramids and biostratigraphy at the Turonian/Coniacian boundary; based on the Salzgitter-Salder Quarry, Lower Saxony, Germany, and the Słupia Nadbrzeżna section, Central Poland. Acta Geologica Polonica 48, 395–434.

Walaszczyk, I., Wood, C.J., 2008. Turonian–Coniacian boundary; definition, recognition and stratotype problems. Proceedings of the 33rd International Geological Congress, Oslo 2008, August 6–14, 3315.

Walaszczyk, I., Wood, C.J., Lees, J.A., Peryt, D., Voigt, S., Wiese, F., 2010. The Salzgitter-Salder Quarry (Lower Saxony, Germany) and Słupia Nadbrzeżna river cliff section (central Poland): a proposed candidate composite Global Boundary Stratotype Section and Point for the Coniacian Stage (Upper Cretaceous). Acta Geologica Polonica 60, 445–477.

Walaszczyk, I., Lees, J.A., Peryt, D., Cobban, W.A., Wood, C.J., 2012. Testing the congruence of the macrofossil versus microfossil record in the Turonian–Coniacian boundary succession of the Wagon Mound-Springer composite section (NE New Mexico, USA). Acta Geologica Polonica 62, 581–594.

Walaszczyk, I., Čech, S., Crampton, J., Dubicka, Z., Ifrim, C., Jarvis, I., Lodowski, D., Pearce, M.A., Peryt, D., Schiøler, P., Todes, J., Uličný, D., Voigt, S., Wiese, F., submitted. Formal proposal for the Global Boundary Stratotype Section and Point (GSSP) of the Coniacian Stage at Salzgitter-Salder (Germany) and its auxiliary sections. Coniacian Working Group of the Subcommission on Cretaceous Stratigraphy.

Wendler, I., 2013. A critical evaluation of carbon isotope stratigraphy and biostratigraphic implications for Late Cretaceous global correlation. Earth-Science Reviews 126, 116–146.

Wiese, F., 1999. Stable isotope data ($\delta^{13}C$, $\delta^{18}O$) from the Middle and Upper Turonian (Upper Cretaceous) of Liencres (Cantabria, northern Spain) with a comparison to northern Germany (Söhlde & Salzgitter-Salder). Newsletters on Stratigraphy 37, 37–62.

Wiese, F., 2009a. Additional *Prionocyclus germari* (Reuss, 1845) (Cretaceous Ammonoidea, Upper Turonian) from NW Germany. Berliner paläobiologische Abhandlungen 10, 361–371.

Wiese, F., 2009b. The Söhlde Formation (Cenomanian, Turonian) of NW Germany: shallow marine pelagic red beds, in: Hu, X. (Ed.), Cretaceous Oceanic Red Beds: Stratigraphy, Composition, Origins and Paleoceanographic and Paleoclimatic Significance. SEPM Special Publication 91, 153–170.

Wiese, F., Kröger, B., 1998. Evidence for a shallowing event in the Upper Turonian (Cretaceous) *Mytiloides scupini* Zone of northern Germany. Acta Geologica Polonica 48, 265–284.

Wiese, F., Wood, C.J., Kaplan, U., 2004a. 20 years of event stratigraphy in NW Germany; advances and open questions. Acta Geologica Polonica 54, 639–656.

Wiese, F., Wood, C.J., Wray, D.S., 2004b. New advances in the stratigraphy and geochemistry of the German Turonian (Late Cretaceous) tephro-stratigraphic framework. Acta Geologica Polonica 54, 657–671.

Wiese, F., Hiss, M., Kaplan, U., Voigt, S., 2007. Erwitte-Formation, in: Niebuhr, B., Hiss, M., Kaplan, U., Tröger, K.-A., Voigt, S., Voigt, T., Wiese, F., Wilmsen, M. (Eds.), Lithostratigraphie der norddeutschen Oberkreide. Schweizerbart, Stuttgart, pp. 47–48.

Williams, G.L., 1977. Dinocysts: their palaeontology, biostratigraphy and palaeoecology, in: Ramsey, A.T.S. (Ed.), Oceanic Micropalaeontology. Academic Press, London, pp. 1231–1325.

Williams, G.L., Bujak, J.P., 1985. Mesozoic and Cenozoic dinoflagellates, in: Bolli, H.M., Saunders, J.B., Perch-Nielsen, K. (Eds.), Plankton Stratigraphy. Cambridge Earth Science Series, Cambridge, pp. 847–964.

Williams, G.L., Stover, L.E., Kidson, E.J., 1993. Morphology and stratigraphic ranges of selected Mesozoic–Cenozoic dinoflagellate taxa in the Northern Hemisphere. Geological Survey of Canada Paper 92-10, p. 139.

Williams, G.L., Brinkhuis, H., Pearce, M.A., Fensome, R.A., Weegink, J.W., 2004. Southern Ocean and global dinoflagellate cyst events compared: index events for the Late Cretaceous–Neogene. Proceedings of the Ocean Drilling Program, Scientific Results 189, 1–98.

Wilmsen, M., Dölling, B., Hiss, M., Niebuhr, B., 2019. The lower Upper Cretaceous of the south-eastern Munsterland Cretaceous Basin, Germany: facies, integrated stratigraphy and inter-basinal correlation. Facies 65:13, p. 29 https://doi.org/10.1007/s10347-018-0552-1.

Wood, C.J., Ernst, G., 1998. Turonian – Coniacian of Salzgitter-Salder, in: Mutterlose, J., Bornemann, A., Rauer, S., Spaeth, C., Wood, C.J. (Eds.), Key Localities of the Northwest European Cretaceous. Ruhr-Universität Institut für Geologie, Bochum, pp. 94–102.

Wood, C.J., Ernst, G., Rasemann, G., 1984. The Turonian – Coniacian stage boundary in Lower Saxony (Germany) and adjacent areas: the Salzgitter-Salder Quarry as a proposed international standard section. Bulletin of the Geological Society of Denmark 33, 225–238.

Wood, C.J., Morter, A.A., Gallois, R.W., 1994. Appendix 1. Upper Cretaceous stratigraphy of the Trunch borehole. TG23SE8., in: Arthurton, R.S., Booth, S.J., Morigi, A.N., Abbott, M.A.W., Wood, C.J. (Eds.), Geology of the Country around Great Yarmouth. Memoir for 1:50,000 Sheet 162 (England and Wales) with an Appendix on the Trunch Borehole by Wood and Morter. HMSO, London, pp. 105–110.

Wood, C.J., Walaszczyk, I., Mortimore, R.N., Woods, M.A., 2004. New observations on the inoceramid biostratigraphy of the higher part of the Upper Turonian and the Turonian – Coniacian boundary transition in Poland, Germany and the UK. Acta Geologica Polonica 54, 541–549.

Wray, D.S., 1995. Origin of clay-rich beds in Turonian chalks from Lower Saxony, Germany - a rare-earth element study. Chemical Geology 119, 161–173.

Wray, D.S., 1999. Identification and long-range correlation of bentonites in Turonian–Coniacian (Upper Cretaceous) chalks of northwest Europe. Geological Magazine 136, 361–371.

Wray, D.S., Wood, C.J., 1998. Distinction between detrital and volcanogenic clay-rich beds in Turonian–Coniacian chalks of eastern England. Proceedings of the Yorkshire Geological Society 52, 95–105.

Wray, D.S., Wood, C.J., Ernst, G., Kaplan, U., 1996. Geochemical subdivision and correlation of clay-rich beds in Turonian sediments of northern Germany. Terra Nova 8, 603–610.

Young, J.R., Bown, P.R., Lees, J.A., 2020. Nannotax3 website. International Nannoplankton Association, http://www.mikrotax.org/Nannotax3.